available at www.sciencedirect.com

ScienceDirect

www.elsevier.com/locate/molonc

Review

Imaging and cancer: A review

Leonard Fass[a,b,*]

[a]GE Healthcare, 352 Buckingham Avenue, Slough, SL1 4ER, UK
[b]Imperial College Department of Bioengineering, London, UK

ARTICLE INFO

Article history:
Received 6 March 2008
Received in revised form
28 April 2008
Accepted 29 April 2008
Available online 10 May 2008

Keywords:
Imaging
Cancer
Diagnosis
Staging
Therapy
Tracers
Contrast

ABSTRACT

Multiple biomedical imaging techniques are used in all phases of cancer management. Imaging forms an essential part of cancer clinical protocols and is able to furnish morphological, structural, metabolic and functional information. Integration with other diagnostic tools such as in vitro tissue and fluids analysis assists in clinical decision-making. Hybrid imaging techniques are able to supply complementary information for improved staging and therapy planning. Image guided and targeted minimally invasive therapy has the promise to improve outcome and reduce collateral effects. Early detection of cancer through screening based on imaging is probably the major contributor to a reduction in mortality for certain cancers. Targeted imaging of receptors, gene therapy expression and cancer stem cells are research activities that will translate into clinical use in the next decade. Technological developments will increase imaging speed to match that of physiological processes. Targeted imaging and therapeutic agents will be developed in tandem through close collaboration between academia and biotechnology, information technology and pharmaceutical industries.

1. Introduction

Biomedical imaging, one of the main pillars of comprehensive cancer care, has many advantages including real time monitoring, accessibility without tissue destruction, minimal or no invasiveness and can function over wide ranges of time and size scales involved in biological and pathological processes. Time scales go from milliseconds for protein binding and chemical reactions to years for diseases like cancer. Size scales go from molecular to cellular to organ to whole organism.

The current role of imaging in cancer management is shown in Figure 1 and is based on screening and symptomatic disease management.

The future role of imaging in cancer management is shown in Figure 2 and is concerned with pre-symptomatic, minimally invasive and targeted therapy. Early diagnosis has been the major factor in the reduction of mortality and cancer management costs.

Biomedical imaging (Ehman et al., 2007) is playing an ever more important role in all phases of cancer management (Hillman, 2006; Atri, 2006). These include prediction (de Torres et al., 2007), screening (Lehman et al., 2007; Paajanen, 2006; Sarkeala et al., 2008), biopsy guidance for detection (Nelson et al., 2007), staging (Kent et al., 2004; Brink et al., 2004; Shim et al., 2004), prognosis (Lee et al., 2004), therapy planning (Fermé et al., 2005; Ciernik et al., 2003), therapy guidance

* *Corresponding author*. Tel.: +44 7831 117132; fax: +44 1753 874578.
E-mail address: leonard.fass@med.ge.com
1574-7891/$ – see front matter © 2008 Federation of European Biochemical Societies. Published by Elsevier B.V. All rights reserved.
doi:10.1016/j.molonc.2008.04.001

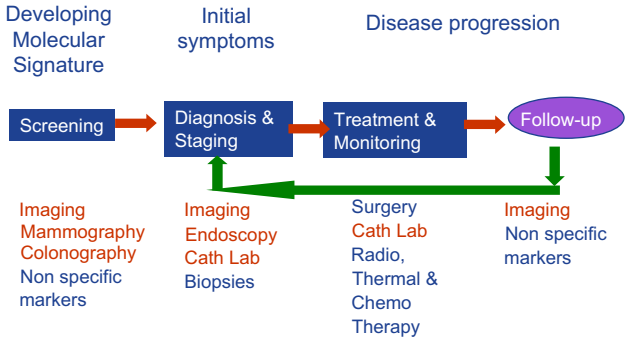

Figure 1 – Current role of imaging in cancer management.

(Ashamalla et al., 2005), therapy response (Neves and Brindle, 2006; Stroobants et al., 2003; Aboagye et al., 1998; Brindle, 2008) recurrence (Keidar et al., 2004) and palliation (Belfiore et al., 2004; Tam and Ahra, 2007).

Biomarkers (Kumar et al., 2006) identified from the genome and proteome can be targeted using chemistry that selectively binds to the biomarkers and amplifies their imaging signal. Imaging biomarkers (Smith et al., 2003) are under development in order to identify the presence of cancer, the tumour stage and aggressiveness as well as the response to therapy.

Various pharmaceutical therapies are under development for cancer that are classed as cytotoxic, antihormonal, molecular targeted and immunotherapeutic. The molecular targeted therapies lend themselves to imaging for control of their effectiveness and include signal transduction inhibitors, angiogenesis inhibitors, apoptosis inducers, cell cycle inhibitors, multi-targeted tyrosine kinase inhibitors and epigenetic modulators.

In order to obtain the health benefit from understanding the genome and proteome requires spatial mapping at the whole body level of gene expression and molecular processes within cells and tissues. Molecular imaging in conjunction with functional and structural imaging is fundamental to achieve this result. Various targeted agents for cancer markers including epidermal growth factor receptor (EGFR) receptors, $\alpha_v\beta_3$ integrin, vascular endothelial growth factor (VEGF), carcinoembryonic antigen (CEA), prostate stimulating membrane antigen (PSMA), MC-1 receptor, somatostatin receptors, transferrin receptors and folate receptors have been developed.

In vitro, cellular, preclinical and clinical imaging are used in the various phases of drug discovery (Figure 3) and integrated in data management systems using IT (Hehenberger et al., 2007; Czernin et al., 2006; Frank and Hargreaves, 2003; Tatum and Hoffman, 2000).

In vitro imaging techniques such as imaging mass spectrometry (IMS) can define the spatial distribution of peptides, proteins and drugs in tumour tissue samples with ultra high resolution. This review will mainly consider the clinical imaging techniques.

The development of minimally invasive targeted therapy and locally activated drug delivery will be based on image guidance (Carrino and Jolesz, 2005; Jolesz et al., 2006; Silverman et al., 2000; Lo et al., 2006; Hirsch et al., 2003).

Most clinical imaging systems are based on the interaction of electromagnetic radiation with body tissues and fluids. Ultrasound is an exception as it is based on the reflection, scattering and frequency shift of acoustic waves. Ultrasound also interacts with tissues and can image tissue elasticity. Cancer tissues are less elastic than normal tissue and ultrasound elastography (Hui Zhi et al., 2007; Lerner et al., 1990; Miyanaga et al., 2006; Pallwein et al., 2007; Tsutsumi et al., 2007) shows promise for differential diagnosis of breast cancer, prostate cancer and liver fibrosis.

Endoscopic ultrasound elastography (Săftoiu and Vilman, 2006) has potential applications in imaging of lymph nodes, pancreatic masses, adrenal and submucosal tumours to avoid fine needle aspiration biopsies.

Ultrasound can be used for thermal therapy delivery and is also known to mediate differential gene transfer and expression (Tata et al., 1997).

The relative frequencies of electromagnetic radiation are shown in Figure 4. High frequency electromagnetic radiation using gamma rays, X-rays or ultraviolet light is ionizing and can cause damage to the human body leading to cancer (Pierce et al., 1996). Dosage considerations play an important part in the use of imaging based on ionizing radiation especially for paediatric imaging (Brix et al., 2005; Frush et al., 2003; Byrne and Nadel, 2007; Brenner et al., 2002; Slovis, 2002). Future

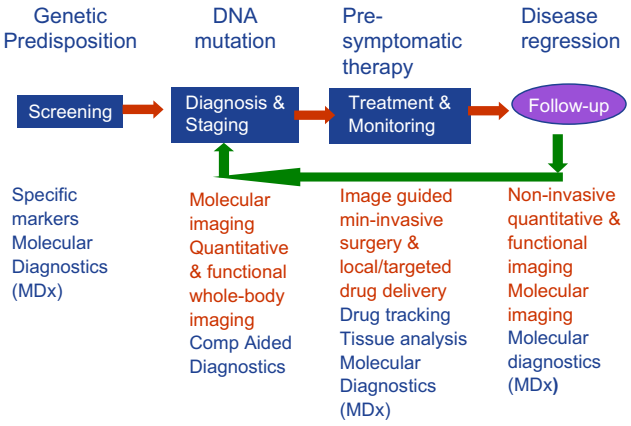

Figure 2 – Future role of imaging in cancer management.

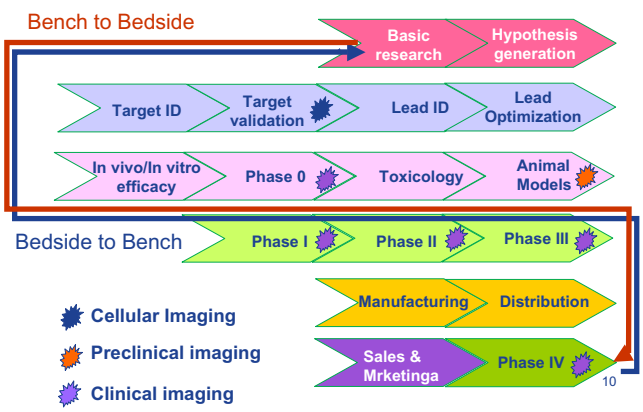

Figure 3 – Imaging in the drug discovery process.

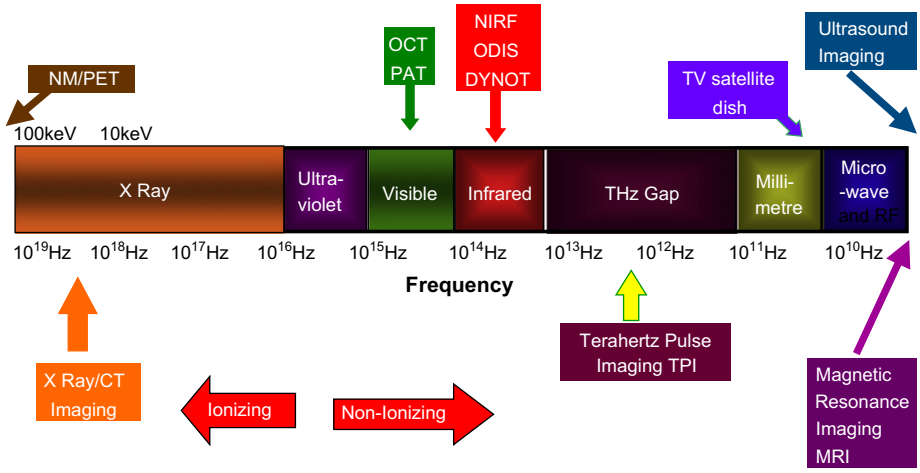

Figure 4 – Frequency spectrum of electromagnetic radiation imaging technologies.

systems may need to integrate genetic risk, pathology risk and scan radiation risk in order to optimize dose during the exam.

Non-ionizing electromagnetic radiation imaging techniques such as near infrared spectroscopy, electrical impedance spectroscopy and tomography, microwave imaging spectroscopy and photoacoustic and thermoacoustic imaging have been investigated mainly for breast imaging (Poplack et al., 2004, 2007; Tromberg et al., 2000; Pogue et al., 2001; Franceschini et al., 1997; Grosenick et al., 1999).

Imaging systems vary in physical properties including sensitivity, temporal and spatial resolution. Figure 5 shows the relative sensitivity of different imaging technologies.

PET and nuclear medicine are the most sensitive clinical imaging techniques with between nanomole/kilogram and picomole/kilogram sensitivity.

X-Ray systems including CT have millimole/kilogram sensitivity whereas MR has about 10 μmol/kg sensitivity.

Clinical optical imaging has been mainly limited to endoscopic, catheter-based and superficial imaging due to the absorption and scattering of light by body tissues and fluids. Preclinical fluorescence and bioluminescence-based optical imaging systems (D'Hallewin MA, 2005; He et al., 2007) are in routine use in cancer research institutions. Future developments using Raman spectroscopy and nanoparticles targeted to tumour biomarkers are showing promise.

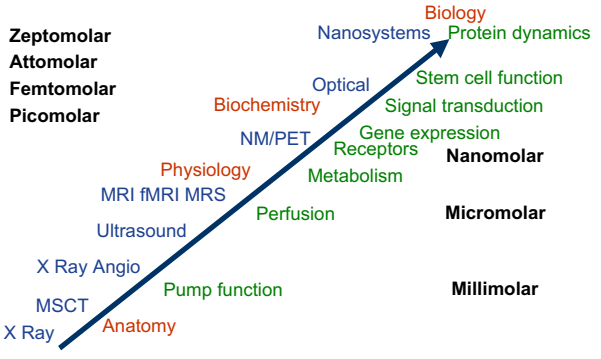

Figure 5 – Relative sensitivity of imaging technologies.

The concept of only using tumour volume as a measure of disease progression has been shown to be inadequate as it only can show a delayed response to therapy and no indication of metabolism and other parameters. This has led to the use of multiple imaging techniques in cancer management. The development of a hybrid imaging system such as PET/CT (Beyer et al., 2002) that combines the metabolic sensitivity of PET and the temporal and spatial resolution of CT.

As a result there has been an increased use of imaging of biomarkers to demonstrate metabolism, cell proliferation, cell migration, receptor expression, gene expression, signal transduction, hypoxia, apoptosis, angiogenesis and vascular function. Measurements of these parameters can be used to plan therapy, to give early indications of treatment response and to detect drug resistance and disease recurrence. Figure 6 shows the principle of biomarker imaging with different imaging technologies.

Imaging biomarkers are being developed for the selection of cancer patients most likely to respond to specific drugs and for the early detection of response to treatment with the aim of accelerating the measurement of endpoints. Examples are the replacement of patient survival and clinical endpoints with early measurement of responses such as glucose metabolism or DNA synthesis.

With combined imaging systems such as PET/CT, SPECT/CT and in the future the combination of systems using for example PET and MR and ultrasound and MR, there will be a need to have standardization in order to follow longitudinal studies of response to therapy.

Cancer is a multi-factorial disease and imaging needs to be able to demonstrate the various mechanisms and phases of pathogenesis.

The use of different modalities, various imaging agents and various biomarkers in general will lead to diagnostic orthogonality by combining independent and uncorrelated imaging technologies. The combination of information using results from these different tools, after they are placed in a bioinformatical map, will improve the sensitivity and specificity of the diagnostic process.

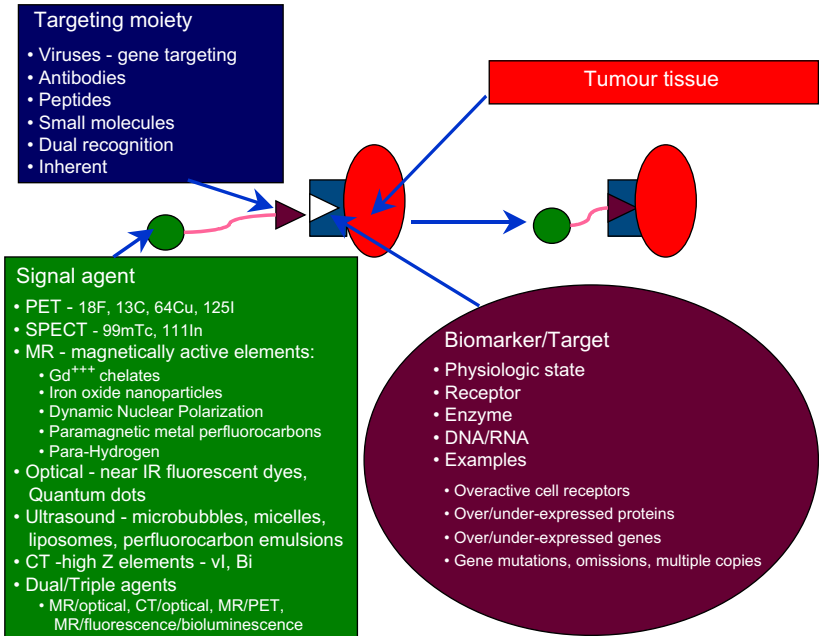

Figure 6 – Biomarker imaging.

The integration and combination of such information is considered to be the future both as part of the validation of the individual technologies but also as part of the diagnostic process, especially for disease prediction, early disease detection and early therapy response.

2. Image contrast

Imaging systems produce images that have differences in contrast. The differences in contrast can be due to changes in physical properties caused by the endogenous nature of the tissue or by the use of exogenous agents.

Endogenous mechanisms include:

- radiation absorption, reflection and transmission
- magnetic relaxivity
- magnetic susceptibility
- water molecule diffusion
- magnetic spin tagging
- oxygenation
- spectral distribution
- temperature
- electrical impedance
- acoustic frequency shifts
- mechanical elasticity

Exogenous mechanisms include:

- radiation absorption, reflection and emission
- spin hyperpolarization
- magnetic relaxivity
- magnetic susceptibility
- magnetization transfer
- saturation transfer
- isotope spectra
- fluorescence
- bioluminescence
- perfusion
- extracellular pH
- hypoxia

Diagnostic imaging agents introduced intravenously, intra-arterially or via natural orifices will play an increasing role in cancer imaging. In particular new tracers for PET (Machulla et al., 2000; Eriksson et al., 2002) and nuclear medicine (Pappo et al., 2000; Xiaobing Tian et al., 2004) are leading the development of molecular imaging. ^{11}C-based PET tracers can also be exogenous substances found in the human body. On the other hand, ^{18}F-based PET tracers are often analogues of substances found in the human body.

Nanotechnology-based agents will be developed during the next decade for MRI (Neuwalt et al., 2004; Schellenberger et al., 2002; Harishingani et al., 2003; Li et al., 2004; Kircher et al., 2003), X-ray/CT (Srinivas et al., 2002; Rabin et al., 2006; Hainfeld et al., 2006), optical (Itoh and Osamura, 2007; Gao et al., 2005; Chan et al., 2002; Min-Ho Lee, 2006) and ultrasound imaging (Liu et al., 2006, 2007; Wheatley et al., 2006) Nanoparticles are being developed as bi-modal imaging agents (Mulder et al., 2006; Li et al., 2006) for MR/CT and MR/optical imaging.

In the subsequent sections the role of various technologies involved in clinical cancer imaging will be reviewed with an emphasis on more recent developments.

3. X-Ray-based systems including CT

Digital imaging technology is expanding the role of X-ray-based systems in the imaging of cancer as the use of picture

archiving and communications systems (PACS) becomes more widespread. The various digital imaging systems include the following.

3.1. *Flat panel computed radiography (CR) and digital radiography (DR) systems that are used for chest X-ray examinations*

CR systems using phosphor plates are more suited to portable systems although improvements in DR systems are also making them more portable.

DR and CR systems can use dual-energy (MacMahon, 2003; Gilkeson and Sachs, 2006) to separate nodules from bone. DR systems use tomosynthesis (Dobbins et al., 2003) to produce slice images. Computer aided detection/diagnosis (CAD) (Campadelli et al., 2006) is used to improve lesion detection efficiency.

Dual energy systems can use two stacked detectors separated by a copper plate and using one X-ray exposure or one detector with dual X-ray exposure. In both cases images of low and high energy X-rays are produced. As a result soft tissue images or bone and calcium images can be obtained.

Dual-energy subtraction eliminates rib shadows and allows accurate, computerized measurement of lung nodule volume. Energy subtraction images have important advantages over standard radiographic images. Intra-pulmonary lesions and bone may appear superimposed when projected in two dimensions. The soft-tissue image, with bone removed, can improve the ability to detect these lesions. The more clear margins of these lesions in the soft-tissue image can assist in lesion characterization. Calcified nodules may be distinguished from non-calcified nodules. Only calcified nodules will appear on the bone image.

Calcifications in hilar lymph nodes can also be visualized on the bone image. Rib defects including sclerotic metastases or bone islands and calcified pleural plaques can mimic soft-tissue abnormalities in standard radiographic images. These lesions may be accurately characterized on the bone image in most situations. Energy subtraction images have the potential to avoid follow-up CT scans in some cases.

Tomosynthesis has been shown to improve the detection of lung nodules (Pineda et al., 2006). 2D CAD (Samei et al., 2007) increases the detection accuracy for small nodules compared to single view CAD.

3.2. *Digital radiographic and fluorographic systems for barium and air contrast studies*

Digital imaging systems using charge coupled devices capturing light from phosphors showed increased sensitivity over film-based spot film systems in the study of gastric cancer (Iinuma et al., 2000).

3.3. *Digital C-arm flat-panel systems for interventional applications using fluoro imaging and CT image reconstruction*

C-Arm CT uses data acquired with a flat-panel detector C-arm fluoroscopic angiography system during an interventional procedure to reconstruct CT-like images from different projections and this can aid interventional techniques involving embolization (Meyer et al., 2007; Kamat et al., 2008), chemo-embolization and biopsies.

Typical anatomical areas include the thorax, pancreas, kidneys, liver (Virmani et al., 2007; Wallace et al., 2007; Wallace, 2007) and spleen. C-Arm CT could be used with 3D road mapping and navigational tools that are under development. This could lead to improvements in both safety and effectiveness of complex hepatic vascular interventional procedures. Improvements include multi-planar soft tissue imaging, pretreatment vascular road mapping of the target lesion, and the ability for immediate post-treatment assessment. Other potential advantages are a reduction in the use of iodinated contrast agents, a lower radiation dose to the patient and the operator and an increase in the safety versus benefit ratio (therapeutic index). Motion correction techniques are being developed for procedures such as liver tumour chemoembolization.

Digital C-arms are also combined with MRI, CT and ultrasound systems for various interventional procedures. Image fusion and 3D segmentation technology permits planning of the intervention including calculating optimal flow of embolizing material and to follow response. Vessel permeability is increased in angiogenesis and measures of reduction of extravascular perfusion could be a measure of response to chemoembolization.

3.4. *Full field digital mammography(GE Senographe, 1999) systems and advanced applications(Rafferty, 2007) including tomosynthesis, contrast enhancement, dual energy, stereo imaging, multi-modality fusion and CAD*

Full field digital mammography systems offer several advantages (Pisano et al., 2005) over film-based systems for breast screening. These include lower dose, improved sensitivity for dense breasts, increased dynamic range, computer-aided detection/diagnosis, softcopy review, digital archiving, telemedicine, tomosynthesis, 3-D visualization techniques and reduction in breast compression pressure.

In tomosynthesis, multiple low-dose X-rays are taken from different angles usually between $\pm 30^{\circ}$. The individual images are then assembled to give a three-dimensional image of the breast, which can be viewed as a video loop or as individual slices. A potential limitation of 2D mammograms is that normal structures in the breast – for example glandular tissue – may overlap and obscure malignancies, especially ones buried deep in the breast. This can result in cancers being missed in the scan. Sometimes the opposite happens – overlapping tissues which are quite normal can resemble tumours on the X-ray image, leading to additional patient imaging and unnecessary biopsies which cause avoidable patient anxiety and greater healthcare costs. Tomosynthesis has recently been shown to detect more breast lesions, better categorize those lesions, and produce lower callback rates than conventional mammography. Combining tomosynthesis with digital mammography can reduce false negatives and increase true positives. 3-D X-ray systems with tomosynthesis also allow less breast compression.

Another 3D method produces stereoscopic images. Stereoscopic mammograms can be created using digital X-ray images of the breast acquired at two different angles, separated

by about eight degrees. When these images are viewed on a stereo display workstation, the radiologist can see the internal structure of the breast in three dimensions and better distinguish benign and malignant lesions. Early clinical trial results (Getty et al., 2007) indicate a higher detection rate and less false positives with this technique than conventional 2D mammography. The need to increase the number of images for this procedure leads to a higher radiation dose.

Contrast-enhanced mammography (Jong, 2003), using iodinated contrast agents, is an investigational technique that is based on the principle that rapidly growing tumours require increased blood supply through angiogenesis to support growth. Contrast needs to be administered when the compression device is not active. Areas of angiogenesis will cause an accumulation of contrast agent.

Contrast-enhanced mammography with tomosynthesis (Diekmann and Bick, 2007) offers a method of imaging contrast distribution in breast tissue. The images can be evaluated by two methods. One method is to look for the image where the iodine concentration is at a maximum, typically 1 min post-injection. High-uptake regions indicate active tissue growth and may indicate malignant tissues. The kinetic analysis method is able to follow iodine contrast agent flow in and out of a tissue area. Malignant cancers often exhibit a rapid wash-in and wash-out of iodine, while benign tissues have a slow iodine uptake over the duration of study over a time frame of 5 min. This is similar to what is seen on perfusion imaging with MRI using gadolinium-based contrast agents.

Tomosynthesis combined with contrast-enhanced mammography may offer advantages in detecting primary and secondary lesions as well as the possibility to monitor therapy.

Dual energy contrast mammography (Lewin et al., 2003) could increase detectability of breast lesions at a lower radiation dose (Kwan et al., 2005) compared to non-contrast enhanced mammography but needs to be evaluated versus contrast enhanced MRI.

Dual energy techniques can remove the structural noise, and contrast media, that enhance the region surrounding the tumour and improve the detectability of the lesions.

CAD is being developed to help identify lesions especially in locations where it is difficult to obtain a second reading. CAD has an advantage in identifying microcalcifications but less so for breast masses. It appears to work better in the hands of experienced breast cancer experts who can differentiate benign lesions such as surgical scars from malignant lesions.

The sensitivity of CAD is consistently high for detection of breast cancer on initial and short-term follow-up digital mammograms. Reproducibility is significantly higher for true-positive CAD marks than for false positive CAD marks (Kim et al., 2008).

Recent results from a very large-scale study of 231,221 mammograms have indicated CAD enhances performance of a single reader, yielding increased sensitivity with only a small increase in recall rate (Gromet, 2008).

Dual modality systems based on combined X-ray/ultrasound systems promise increased sensitivity and specificity (Kolb et al., 2002). This is due to the lack of sensitivity of mammography in imaging young dense breasts where the surrounding fibroglandular tissue decreases the conspicuity of lesions. Addition of screening ultrasound significantly increases detection of small cancers and depicts significantly more cancers and at smaller size and lower stage than does a physical examination, which detects independently extremely few cancers. Mammographic sensitivity for breast cancer declines significantly with increasing breast density and is independently higher in older women with dense breasts. Full field digital mammography systems have a better detection sensitivity for dense breasts than film-based systems.

Hormonal status has no significant effect on the effectiveness of screening independent of breast density.

Cone beam CT systems using flat panel detectors are being developed for CT mammography with the advantage of higher sensitivity, improved tissue contrast and no breast compression (Ning et al., 2006).

The American Cancer Society has recently revised its recommendations, stating that women should continue screening mammography as long as they are in good health.

Future systems using CMOS active pixel sensors (APS) in a large area, low noise, wide dynamic range digital X-ray detector could enable simultaneous collection of the transmitted beam and scattered radiation. This could be used to obtain biologically relevant scatter signatures from breast cancer tissue (Bohndiek et al., 2008).

3.5. *Multi-slice CT systems including 4D acquisition and reconstruction with applications in lung cancer screening, virtual colonography, radiotherapy planning and therapy response monitoring*

Multi-slice CT systems with large area matrix detectors and high power X-ray tubes are able to cover large scan volumes during breath hold acquisitions in the thorax, abdomen and brain.

CT often incidentally identifies lung nodules during exams for other lesions in the thorax. There is a need to distinguish benign from malignant nodules as on average 50% are benign. Dynamic contrast enhanced CT (Swensen and Functional, 2000; Minami, 2001; Kazuhiro et al., 2006) has been proposed to identify malignant lung nodules having increased vascularity due to angiogenesis. CT lung cancer screening (Swensen et al., 2003; Henschke et al., 2006, 2007; Henschke, 2007) is used with low dose CT combined with lung nodule analysis software (Figure 7). Lung nodule size, shape and doubling times (Reeves, 2007) are parameters of interest. Benign nodules typically have a round shape and smooth, sharply defined borders. Malignant nodules often have an oval shape, lobulated, irregular borders with spiculations. Advanced lung analysis software is used to help classify nodules (Volterrani et al., 2006). Juxtapleural nodules are more difficult to classify.

CAD is being developed especially for lung (Suzuki et al., 2005; Shah, 2005; Enquobahrie et al., 2007) and colon cancer (Kiss et al., 2001) screening using CT.

CT virtual colonography (Yee et al., 2001) has been assessed and shown to yield similar results to optical colonoscopy for clinically important polyps larger than 10 mm in size and can, in the same examination, also provide information on changes in adjacent anatomy such as aortic aneurysms and metastases in the lymph nodes and the liver (Hellstrom

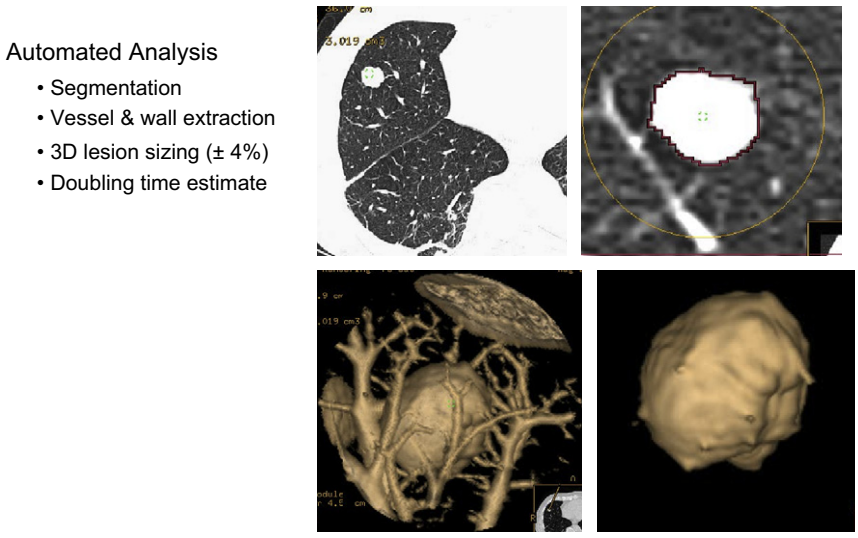

Figure 7 – Advanced lung analysis lesion sizing from 3D CT.

et al., 2004; Xiong et al., 2005). CT virtual colonography is considered suitable for elderly patients. The use of fecal tagging may permit the use of virtual colonography with limited bowel preparation (Jensch et al., 2008).

A recent study (Taylor et al., 2008) has shown that CAD is more time efficient when used concurrently in virtual colonography studies rather than when used as a second reader, with similar sensitivity for polyps 6 mm or larger. When CAD is used as a second reader the sensitivity is maximized, particularly for smaller lesions. CAD is also indicated to help identify flat lesions.

Whole body CT screening is controversial due to dose and cost issues and can lead to a large number of false negatives requiring follow-up studies (Furtado et al., 2005).

Four-dimensional CT (3D plus movement synchronization) acquisition is used for image modulated radiotherapy (IMRT) applications in the thorax so that the tumour is kept in the centre of the radiation field. Four-dimensional technology allows following of the tumour at every point throughout the breathing cycle. It is possible to focus on the tumour, sparing surrounding healthy tissue. Four-dimensional IMRT (Suh et al., 2007) decreases both the size of the margin and the size of the radiation field using linear accelerators with dynamic multi-leaf collimators (DMLC).

CT perfusion imaging is based on the linear relation between the CT attenuation values (expressed by Hounsfield units) and the concentration of contrast agent. CT perfusion imaging is used to determine therapy response (Dugdale et al., 1999; Kim et al., 2007; Fournier et al., 2007).

A CT perfusion study showing changes in hepatic tumour perfusion after anti-angiogenic therapy is shown in Figure 8.

In the future 4D CT with large detector arrays will be used to study volumetric perfusion imaging that could show the effects of anti-angiogenic therapy to reduce the amount of permeable blood vessels in organs such as the liver.

The openness of the CT gantry makes it suitable for interventional procedures but dose considerations for the personnel must be taken into account (Teeuwisse et al., 2001).

CT guided interventional procedures include: radiofrequency ablation of bone metastases (Simon and Dupuy, 2006), hepatic metastases and HCC (Ghandi et al., 2006) and renal tumours (Zagoria et al., 2004), guided brachytherapy (Pech et al., 2004; Ricke et al., 2004), alcohol injection in metastases (Gangi et al., 1994), nerve block for pain palliation (Vielvoye-Kerkmeer, 2002; Mercadante et al., 2002) guided biopsies (Maskell et al., 2003; Heilbrun et al., 2007; Suyash et al., 2008; Zudaire et al., 2008) and transcatheter arterial chemoembolization (Hayashi et al., 2007).

PET/CT is more frequently used to guide biopsy by highlighting the metabolically active region (von Rahden et al., 2006).

Needle artifacts can limit the performance of fluoroscopic CT guided biopsies of small lung lesions (Stattaus et al., 2007). Pneumothorax is a complication of transbronchial lung biopsies especially for small lesions (Yamagami et al., 2002) and can lead to empyema (Balamugesh et al., 2005) in the pleural cavity (purulent pleuritis) requiring drainage. Other complications include haemorrhage/haemoptysis, systemic air embolization and malignant seeding along the biopsy tract.

Future developments in X-ray imaging include new multitube systems based on field emitters using carbon nanotubes. These could be used for inverted geometry systems where multiple X-ray beams are directed onto a detector.

Other work is looking at imaging scattered radiation instead of the traditional X-ray transmission/absorption methods. Spectral imaging with energy sensitive detectors will enable separation of different density objects such as iodine contrast agents and calcifications.

4. Magnetic resonance systems

Magnetic resonance is used in cancer detection, staging, therapy response monitoring, biopsy guidance and minimally invasive therapy guidance. Imaging techniques that have been

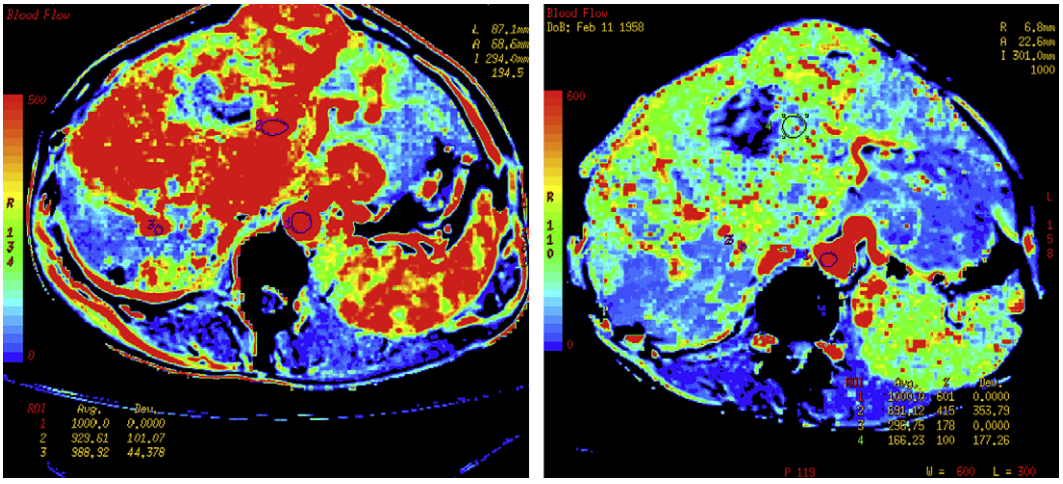

Figure 8 – Pre- and post-anti-angiogenic therapy CT perfusion maps (study courtesy of D. Buthiau, O. Rixe, J. Bloch, J.B. Méric, J.P. Spano, D. Nizri, M. Gatineau, D. Khayat).

developed to image cancer are based on relaxivity-based imaging with and without contrast agents, perfusion imaging using contrast agents, diffusion weighted imaging, endogenous spectroscopic imaging, exogenous spectroscopic imaging with hyperpolarized contrast agents, magnetic resonance elastography and blood oxygen level determination (BOLD) imaging.

Nuclear magnetic resonance (NMR) spectroscopy had existed for over 30 years before the possibility to distinguish tumour tissue from T1 and T2 relaxation time measurements in vitro was the catalyst that started the development of magnetic resonance imaging MRI systems (Damadian, 1971). MRI of the human body became possible only after the application of local gradient fields (Lauterbur, 1973).

4.1. *MRI of breast cancer*

Breast cancer was one of the first to be examined using MRI (Ross et al., 1982). After more than 10 years of clinical use breast MR is now starting to be accepted as a complementary technique on a par with mammography and ultrasound. This has happened through the development of surface coils, advanced gradient coils, parallel imaging, contrast agents and new fast imaging sequences that have greatly improved MRI of the breast. Dedicated breast imaging tables provide complete medial and lateral access to the breast, enabling unimpeded imaging and intervention including biopsies. New surface coils allow the simultaneous imaging of both breasts to indicate involvement of the contralateral breast.

The move to higher field strengths with 3 T MRI systems has been aided by parallel imaging that can reduce the effect of T1 lengthening, reduce susceptibility artifacts and avoid too high specific absorption rate (SAR) values. Breast MRI has a higher sensitivity for the detection of breast cancer than mammography or ultrasound.

Due to cost reasons, access, and high false positives MRI is not yet considered a screening exam for breast cancer except for special cases. As a result of not utilizing ionizing radiation, breast MRI has been recommended in the repeated screening of high-risk patients who have increased risk of radiation induced DNA mutations. These include individuals with the BRCA1 or BRCA2 gene mutation. It is used to screen women with a family history of breast cancer, women with very dense breast tissue, or women with silicone implants that could obscure pathology in mammography. It is also useful to look for recurrence in patients with scar tissue. The American Cancer Society has given a strong endorsement for MRI, to detect lymph node involvement and contralateral disease extension in breast cancer.

Staging is probably the most important use of breast MRI because it can show chest wall involvement, multi-focal tumours, lymph node metastases and retraction of the skin. It has a better performance in imaging invasive lobular carcinoma than other methods.

Magnetic resonance imaging appears to be superior to mammography and ultrasound for assessing pathological response and a low rate of re-operation for positive margins (Bhattacharyya et al., 2008). This indicates an important role for MRI in aiding the decision to undergo breast conserving surgery or mastectomy.

Contrast enhanced MRI has permitted dynamic studies of wash-in and wash-out. Gadolinium is strongly paramagnetic and can change the magnetic state of hydrogen atoms in water molecules. Tissues, with a high contrast agent uptake in T1-weighted images appear bright. High concentrations of gadolinium chelates induce local changes in the local magnetic field due to susceptibility effects. The effect is maximized during the first pass of a bolus of contrast agent after rapid intravenous injection. On gradient echo T2*-weighted images this causes a darkening of the image in areas of tissue that are highly perfused.

Perfusion imaging based on dynamic contrast enhanced MRI can demonstrate the presence of malignant microcalcifications seen on mammography and can be used in the evaluation of equivocal microcalcifications before stereotactic vacuum assisted biopsy (Takayoshi et al., 2007). Dynamic contrast MRI with gadolinium-based contrast agents is used to evaluate neo-angiogenesis (Folkman, 1992) and has been

shown to correlate with histopathology (Leach, 2001), microvessel density (Buckley et al., 1997; Buadu et al., 1996) and response to chemotherapy (Padhani et al., 2000a,b).

Signal intensity/time graphs are obtained for each enhancing lesion at the site of maximal enhancement. Three types of curves can be distinguished (Kuhl et al., 1999):

- Type I curves demonstrate continuous enhancement and are usually associated with benign lesions.
- Type II curves exhibit a rapid uptake of contrast followed by a plateau and can be indicative of both benign and malignant lesions.
- Type III curves demonstrate a rapid uptake of contrast with rapid wash-out and are most often related to malignant lesions.

Rapid uptake and wash-out has been attributed to the angiogenic nature of malignancies with many microvessels feeding the tumour (Morris, 2006). Figure 9 shows intensity time curves in different breast tissues.

MR perfusion imaging has the potential to monitor therapy by using agents that block angiogenesis directly and indirectly. As well as eliminating angiogenic blood vessels, it has been proposed that anti-angiogenic therapy can also transiently normalize the abnormal structure and function of tumour vasculature. Normalized blood vessels are more efficient for oxygen and drug delivery due to less permeability. Pericytes play an important role in blood vessel formation and maintenance (Bergers and Song, 2005). Pericytes (vascular smooth muscle cells) strengthen the normalized vessels. The strengthened vessels can reduce intravasation of cancer cells and consequently the risk of haematogenous metastasis. Vascular normalization can also reduce hypoxia and interstitial fluid pressure.

The American College of Radiology's Breast Imaging Reporting and Database system (BI-RADS) (American College of Radiology, 2004) provides a standard for terminology used to report MRI findings. Irregularly shaped speculated masses and heterogeneous or rim enhancement indicate malignancy. A non-mass enhancement that is asymmetrical with a segmental or regional pattern is a strong indicator of ductal carcinoma in situ (Nunes, 2001). Smooth borders or non-enhancing septa, which can be seen in a many fibroadenomas, indicate benign lesions. Small lesions measuring <5 mm (enhancing foci) are often not of clinical significance (Liberman et al., 2006).

Axillary lymph node imaging with dextran coated ultra small particle iron oxide (USPIO) contrast agents is based on the accumulation of iron oxide nanoparticles in macrophages. USPIO developed for MR imaging of the reticulo-endothelial system (liver and lymph nodes), causes a loss of signal in T2* imaging. USPIO helps to distinguish unenlarged metastatic lymph nodes from normal lymph nodes; and differentiate enlarged metastatic nodes from benign hyperplastic nodes. The combination of USPIO-enhanced MR and FDG PET achieved 100% sensitivity, specificity, PPV and NPV in lymph note detection confirmed by histopathology (Stadnik et al., 2006). USPIO has also been used to evaluate lymph node involvement in prostate cancer, colon cancer, rectal cancer and lung cancer.

4.2. *Diffusion weighted imaging*

Diffusion weighted imaging (Le Bihan et al., 1985) (DWI) has been around for over 23 years with a first application in detecting cytotoxic oedema in stroke. DWI MRI measures the diffusion of water molecules (Brownian movement) and is a promising technique for the identification of tumours and metastases and could have an application in characterizing breast lesions as benign or malignant. DWI MRI provides endogenous image contrast from differences in the motion of water molecules between tissues without the need for exogenous contrast agents. It is possible to obtain both qualitative and quantitative information related to changes at a cellular level demonstrating the influence of tumour cellularity and cell membrane integrity.

Recent advances enable the technique to be widely applied for tumour evaluation in the abdomen and pelvis and have led to the development of whole body DWI.

An inverse image of a whole body DWI acquisition of a patient with a non-Hodgkin's lymphoma having diffuse bone marrow infiltration with spread to cervical, axilla and inguinal tumoural lymph nodes is shown in Figure 10.

Tumour tissues have disrupted water molecule diffusion and a lower apparent diffusion constant (ADC) leading to

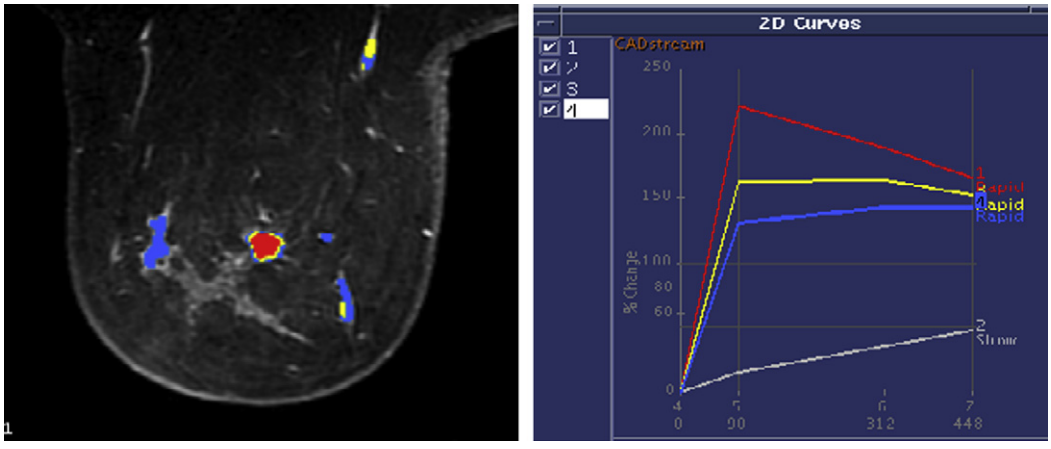

Figure 9 – MR contrast uptake intensity/time curves in the breast (courtesy of Duke University).

Figure 10 – DWI image of metastatic spread (courtesy of the Military Hospital of Laveran, France).

a high signal in DWI images. A rise in ADC indicates a positive response to therapy. The observed increase in water ADC following therapy is directly related to the number of cells killed and is thought to be due to the liberation of water into the extracellular space as a result of cell necrosis (Chenevert et al., 2000).

Measurement of ADC has been used for the assessment of metastatic breast cancer response to chemoembolization. Normal tissues had no change in their ADC values whereas tumour tissue showed an increase in ADC values after transarterial chemoembolization (Buijs et al., 2007) even when volume changes seen with contrast enhanced MRI did not show complete response based on response evaluation criteria in solid tumours (RECIST) criteria.

DWI MRI in the liver is able to see changes in hepatic metastases from neuroendocrine tumours after transarterial chemoembolization (Liapi et al., 2008).

DWI MRI could be helpful in detecting and evaluating the extent of pancreatic carcinomas. Carcinomas appear with a higher signal intensity relative to surrounding tissues. The ADC value in the tumour tissue is significantly lower compared to that of the normal pancreas and tumour-associated chronic pancreatitis (Matsuki et al., 2007a).

As bladder carcinoma ADC values are lower than those of surrounding structures, DWI MRI could be useful in evaluating invasion (Matsuki et al., 2007b).

DWI MRI has also been evaluated and compared to histology for the detection of prostate cancer. Similar to other types of cancer, the mean ADC for malignant tissue is less than non-malignant tissue but there is overlap in individual values. DWI MRI of the prostate is possible with an endorectal radiofrequency coil (Hosseinzadeh and Schwarz, 2004).

The combination of T2 imaging and DWI MRI has been shown to be better than T2 imaging alone in the detection of significant cancer of size greater than 4 mm in patients with a Gleason score of more than 6 within the peripheral zone of the prostate (Haider et al., 2000).

ADCs of lung carcinomas correlate well with tumour cellularity with some amount of overlap for different tumour types when using the Spearman rank correlation analysis. However on DWI, well-differentiated adenocarcinomas appear to have higher ADCs than those of other histologic lung carcinoma types (Matoba et al., 2007).

DWI MRI of the brain is used in combination with perfusion MRI in order to characterize brain tumours in terms of tumour type, grade and margin definition and to evaluate therapy response (Provenzale et al., 2006). High DWI MRI may be able to predict response to radiation therapy (Mardor, 2003). Tumours with a high diffusion constant corresponding to large necrotic regions have a worse response.

Palpation that assesses the stiffness of a region with respect to the surrounding tissues is used as part of the clinical detection of many breast, thyroid, prostate and abdominal pathologies. DWI MRI has been shown to be a label free method for evaluating therapy response of brain tumours in terms of non-responders and partial responders during a cycle of fractionated radiotherapy (Moffat et al., 2005). Partial responders show areas of increased ADC.

Whole-body MRI competes with scintigraphy and PET/CT in the detection of sclerotic metastases, which are common to prostate and breast cancers and multiple myeloma. PET–CT currently is used for soft-tissue metastatic disease but diffusion-weighted MRI techniques hold promise.

4.3. *MR elastography*

Magnetic resonance elastography (MRE) is an experimental method of imaging propagating mechanical waves using MRI that could emulate palpation but with quantitative stiffness information for tissue characterization (Kruse et al., 2000; Muthupillai et al., 1995) also in anatomic locations not manually accessible like the brain. It is accomplished by synchronizing motion-sensitive phase contrast MRI sequences during the application of acoustic waves. The frequency of the acoustic waves is in the range of 100 Hz to 1 kHz.

MRE creates images of propagating shear waves with variable wavelengths that are a function of the tissue shear modulus. The wavelength can be calculated by measuring the distances between black lines that show the waves in the MR image. The shear modulus and hence the stiffness of the tissue can be calculated to create a shear modulus map. There has been some experience in evaluating MRE for breast cancer (Plewes et al., 2000; Sinkus et al., 2000; McKnight et al., 2002; Xydeas et al., 2005).

In vivo MRE of the prostate gland has been show to be technically feasible in healthy volunteers (Kemper et al., 2004).

Ex vivo studies using hyperpolarized ^{3}He, a noble gas used in lung studies, have demonstrated the feasibility of performing MRE in the lung. In this case it is the gas in the alveolar spaces and not the lung parenchyma that is used to measure the shear wave propagation (McGee et al., 2007).

4.4. *MR perfusion imaging*

Perfusion imaging with MRI is used to evaluate angiogenesis and response to anti-angiogenic therapy (Su et al., 2000; Pham et al., 1998). Angiogenic blood vessels are more permeable

than normal vessels and permit the passage of contrast agents in and out of the vessels. MRI perfusion imaging can be performed using two different methods.

T1-weighted acquisitions are used for dynamic contrast enhanced imaging (Padhani and Leach, 2005; Miller et al., 2005) and are mainly used to determine leakage from permeable blood vessels as a surrogate marker for angiogenesis. Outside of the brain there can be a difficulty in distinguishing differences in vascular permeability between benign and malignant tumours using T1-weighted acquisitions (Helbich et al., 2000; Brasch and Turetschek, 2000) using standard gadolinium-based contrast agents. Efforts to overcome this issue have made in pre-clinical evaluations using higher molecular weight agents or nanoparticle agents (Turetschek et al., 2003; Su et al., 1998).

T2*-weighted acquisitions are used for dynamic susceptibility contrast imaging, mainly used to measure relative cerebral blood volume (rCBV) that corresponds to capillary density and can be used as an indicator of tumour grade (Provenzale et al., 2002).

High molecular weight contrast agents are considered more reliable in the differentiation of vascular permeability and blood volume within tumours than the low molecular weight contrast agents that are in routine use.

Direct imaging of angiogenesis has been attempted using agents that bind to proteins or receptors involved in angiogenesis. Possible targets are membrane proteins that are selectively expressed by angiogenic blood vessels. These include $\alpha_v\beta_3$ integrins, VEGF and its membrane receptors, prostate-specific membrane antigen and thrombospondin-1 receptor. Contrast agents being developed targeted to specific endothelial cell surface markers on the surface of angiogenic vessels could lead to a more precise indication of vascular response to therapy (Brindle, 2003).

4.5. *Apoptosis imaging*

Direct imaging of apoptosis has also been attempted using agents that bind to a cell surface protease that attracts phagocytes to dying cells. Annexin V has been used in optical and nuclear medicine imaging. The C2 domain of synaptotagmin, a protein, also binds to phosphatidyl serine. MRI detection of apoptotic cells, in vitro and in vivo, has been demonstrated using the C2 domain of synaptotagmin, tagged with superparamagnetic iron oxide (SPIO) particles (Zhao et al., 2001).

4.6. *Receptor imaging*

Receptor imaging has been performed using targeted SPIO. For example imaging of the tyrosine kinase Her-2/neu receptor in breast cancer cells using targeted iron oxide (Artemov et al., 2003). Streptavidin-conjugated superparamagnetic nanoparticles were used as the targeted MR contrast agent. The nanoparticles were directed to receptors prelabelled with a biotinylated monoclonal antibody and generated strong T_2 MR contrast in Her-2/neu-expressing cells. The contrast observed in the MR images was proportional to the expression level of Her-2/neu receptors determined independently with fluorescence-activated cell sorting (FACS) analysis. In these experiments, iron oxide nanoparticles were attached to the cell surface and were not internalized into the cells. This could be an advantage for potential in vivo applications of the method.

The sensitivity of MRI will limit the clinical application of direct imaging that is more promising with PET but will find applications in pre-clinical imaging.

4.7. *Stem cell tracking*

One area that is showing promise is stem cell tracking using iron oxide labelled stem cells (Rogers et al., 2006). Due to the effect of susceptibility the size of the image is larger than the physical dimensions of the cell and can be resolved by MRI.

Most of the magnetic resonance labels currently used in cell tracking are USPIO or SPIO because of their very strong negative contrast effects and their inherent lack of cell toxicity. However, as this is an indirect imaging technique the signal change is due to the amount of USPIO and SPIO and not the number of cells. As cells proliferate and the iron is divided between all the cells, the total iron content and the signal from each cell decreases. The iron from cells undergoing apoptosis or cell lysis can be internalized by macrophages resident in nearby tissue, resulting in signal wrongly attributable to cells.

USPIO and SPIO are negative contrast agents and suffer from three fundamental disadvantages. MRI cannot distinguish loss of signal from the agent from other areas of signal loss like those from artifacts or calcium. These agents are also limited by partial volume effects, in which void detection is dependent on the resolution of the image. If the void created by the agent is too small, it could be at the limits of MRI detection. Tracking cells in vivo can be difficult with a negative contrast technique.

The introduction of higher field strength MRI at 3.0 T will assist the development of this technique by helping to increase resolution.

4.8. *MR spectroscopy*

Proton magnetic resonance spectroscopy using fat and water suppression techniques can supply biochemical information about tissues. 3D MR proton spectroscopy and spectroscopic imaging (Kurhanewicz et al., 2000) have a potential role of localizing tumours and guiding biopsies in the breast, brain and prostate and detecting a response to therapy. Combining MR anatomic imaging and MR spectroscopic imaging in the same exam can localize the spatial position of metabolites.

Choline helps form phosphatidylcholine, the primary phospholipid of cell membranes and is a potential marker of cell division. It has been proposed that carcinogenesis in human breast epithelial cells results in progressive alteration of membrane choline phospholipid metabolism (Aboagye and Bhujwalla, 1999).

Increased choline levels have been detected in invasive ductal carcinomas of the breast and lymph node metastases (Yeung et al., 2002). The possibility of using the choline levels to differentiate benign from malignant tumours may decrease the number of breast biopsies and permit to monitor and predict response to chemotherapy (Bartella and Huang, 2007). Proton spectroscopy identifying the choline peak with a signal

to noise greater than 2 has a very high sensitivity and specificity for the detection of malignancy in enhancing non-mass lesions and significantly increases the positive predictive value of biopsy (Bartella et al., 2007).

A high choline peak is identified in the proton spectroscopy of a breast lesion in Figure 11.

Citrate is a normal component of prostate cells and decreases in prostate cancer due to disruption of the citrate cycle.

Prostate cancer identification with proton MR spectroscopy is based on the detection of an increased choline plus creatine to citrate ratio and a decrease in polyamines that also correlates with the Gleason score in terms of aggressiveness (Hricak, 2007).

Brain cancer exhibits high choline levels and reduced N-acetyl aspartate due to neuronal loss. Increased lactate due to anaerobic processes is observed in some tumours. Monitoring the changes in these metabolites can be used to see therapy response or malignant transformation (Nelson et al., 1997; Tedeschi et al., 1997; Wald et al., 1997).

Spectroscopy of endogenous ^{13}C (Jeffrey et al., 1991) and ^{31}P (Gillies and Morse, 2005) has been performed but its clinical application has been limited by the low signal due to the low concentration of these naturally occurring isotopes in tissues and the need for very long acquisition times.

4.9. *Spin hyperpolarization*

Signal to noise in MR imaging and spectroscopy is proportional to the product of concentration, gyromagnetic ratio and polarization. As the gyromagnetic ratio is a constant for each nucleus and concentration is limited by tolerance of the body, the main method to increase the signal to noise ratio is through an increase of polarization.

Hyperpolarization of nuclear spins can be used to greatly enhance the sensitivity of magnetic resonance spectroscopy. The injection of hyperpolarized molecules allows spectroscopic imaging of distribution and metabolism of these molecules.

Hyperpolarization can be obtained through the technique of dynamic nuclear polarization. Polarization is transferred from electrons to the nuclear spins through the excitation of electron spin resonance. This is obtained by irradiation with microwaves of a solid material doped with unpaired electrons at a low temperature of about 1.2 K in a high magnetic field of about 3.35 T. This can increase the polarization by over four orders of magnitude. Polarizations of up to 50% can be obtained (Ardenkjaer-Larsen et al., 2003).

Use of hyperpolarized agents signifies that the hyperpolarizer must be placed next to the MRI system due to the short half-life of the hyperpolarized state of the order of 1–2 min. The substances are brought rapidly to liquid state before they can be introduced into the body.

The substances that will be able to be used as hyperpolarized agents have to satisfy the criteria of a long T1 relaxation time, a clear metabolic pathway and no toxicity when used in clinical concentrations. Examples of potential substances are [^{13}C]pyruvate, [^{13}C]acetate and [^{13}C]urea.

The metabolic products of pyruvate include, lactate through reduction, alanine through transamination, bicarbonate through oxidative decarboxylation and oxyloacetate through carboxylation. Lactate is a potential marker for malignant tissue.

The possibility to follow metabolite changes as they occur requires the use of agents that have a high level of polarization. This has been demonstrated using hyperpolarized ^{13}C (Golman et al., 2006a,b; Golman and Petersson, 2006). Hyperpolarized agents show promise in monitoring therapy response.

Using a ^{13}C pyruvate agent it has been demonstrated for the first time in in-vivo preclinical studies that it is possible to spectroscopically image in tumours the exchange of the hyperpolarized ^{13}C label between the carboxyl groups of lactate and pyruvate (Day et al., 2007). This reaction is catalysed by the enzyme lactate dehydrogenase and the flux is decreased in tumours undergoing cell death induced by chemotherapy.

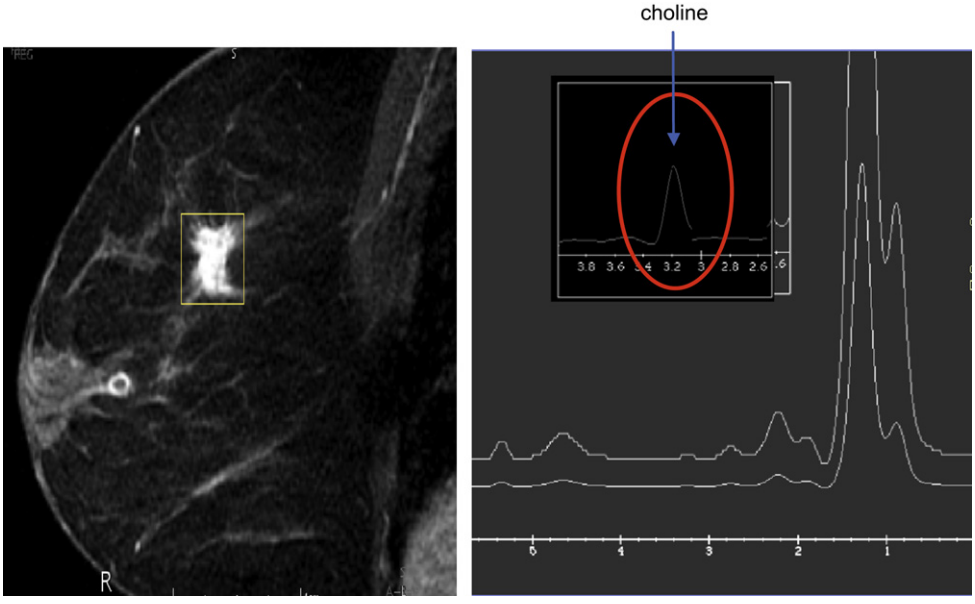

Figure 11 – MRI anatomic image and proton spectroscopy of a breast lesion.

4.10. *MR guided focused ultrasound*

MRI has great potential as a method for guidance and monitoring of minimally or non-invasive therapy. The main advantages are the 3D and 4D imaging capability, virtual real time thermometry and therapy planning and response imaging with contrast studies.

High intensity focused ultrasound (HIFU) is used to rapidly heat and destroy diseased tissue. It is a type of therapeutic ultrasound that induces hyperthermia within a time frame of a second. It should not be confused with traditional hyperthermia that heats over a time frame of an hour and to much lower therapeutic temperatures (generally $<45\,^{\circ}C$). When an acoustic wave propagates through tissue, part of it is absorbed and converted to heat. With focused beams, a very small focus can be achieved deep in tissues. At a high enough temperature, the tissue is thermally coagulated due to protein denaturization. A volume can be thermally ablated by focusing at more than one place or by scanning the focus.

High intensity focused ultrasound has been investigated for over 60 years but has only recently come into clinical use as result of image guidance using ultrasound or MRI.

HIFU approaches the criteria for optimized treatment of localized cancer as, due to the very sharp temperature profile, it can cause complete cell death in tumours without harming nearby healthy tissue. It is an extracorporeal or natural orifice technique and is a localized trackless therapy as opposed to radiotherapy.

MR guidance has many advantages including the possibility of quasi real time thermometry of the tissue to be ablated and of the surrounding tissues. There is the added advantage of 3D imaging for treatment planning with the patient in the MR system during the treatment.

It is important to avoid structures that have risk of damage such as the bowel or nerves next to the prostate or areas that can absorb an increased amount of energy and generate excess heat such as bone, surgical clips or scar tissue.

Contrast enhancement with gadolinium contrast agents identifies tumour margins for treatment planning and also shows post treatment therapy response while the patient is still in the system.

A very big advantage over radiotherapy is the ability to repeat the treatment several times if necessary.

MR guided focused ultrasound (Jolesz and Hynynen, 2002) (MRgFUS) is a closed loop thermal therapy technology that uses multiple ultrasound transducers to focus several beams onto a small area of tissue to cause highly localized heating. Heating tissue to between 55 and 80 °C will cause coagulation necrosis as a result of the denaturization of proteins that are subsequently removed by the lymphatic system leaving no scar tissue. The beam is targeted using phased array ultrasound transducers on a robotic positioning system that has 5 degrees of freedom.

Temperature measurement can be performed from changes in T1 relaxation times, diffusion coefficient or water proton resonance frequency.

One-dimensional MR elastography (Yuan et al., 2007) has recently been developed for temperature and tissue displacement measurements for the monitoring of focused ultrasound therapy.

MRgFUS technology has been approved for use in the ablation of uterine fibromas (Hindley et al., 2004) as an outpatient treatment.

Areas of development in oncology include the treatment of breast (Zippel and Papa, 2005; Gianfelice et al., 2003; Furusawa et al., 2006) prostate, liver (Kopelman et al., 2006; Okada et al., 2006), soft tissue sarcomas, kidney (Salomir et al., 2006) and brain (McDannold et al., 2003) tumours.

Figure 12 shows pre- and post-treatment contrast enhanced T1 weighted MRI maximum intensity projection (MIP) images of a breast cancer patient in a phase 2 trial for patients with an MR identified single focal lesion (up to 1.5 cm) of T1/T2, N0, M0 disease. The lack of contrast enhancement indicates treatment necrosis confirmed by histology.

Pain palliation for bone metastases (Catane et al., 2007) has the potential for fast response and has also worked in patients where fractionated radiation therapy has failed.

MRgFUS can be used together with neoadjuvant radiotherapy and chemotherapy.

Expression of tumour antigens and heat-shock protein 70 in breast cancer cells has been demonstrated after high-intensity focused ultrasound ablation indicating a potential anti-tumour response (Wu et al., 2007).

Disruption of the blood–brain barrier by trans-skull MRgFUS (Hynynen et al., 2005; Kinoshita, 2006) has demonstrated the potential of using this technique for local drug delivery to brain tumours.

The delivery of doxorubicin and increasing its anti-tumour effects has been demonstrated by exposing low-temperature heat-sensitive liposomes containing the doxyrubicin chemotherapy with HIFU exposure that causes the local release of the drug (Dromi et al., 2007). This combination therapy could lead to viable clinical strategies for improved targeting and delivery of drugs for treatment of cancer.

Future applications will include multi-drug and contrast agent delivery in locally activated multi-functional nanoparticles (Rapoport et al., 2007).

4.11. *MR guided galvanotherapy*

Preliminary results have shown that MRI guided galvanotherapy (Vogl, 2007) appears to be a safe and effective treatment for prostate cancer with the possibility to control local tumours without causing impotence or incontinence. MR compatible electrodes are inserted into the prostate and are used to pass an electric current.

5. Ultrasound

Ultrasound is one of the most common diagnostic imaging methods used in the diagnosis of tumours in the thyroid, breast, prostate, liver, pancreatic, ovarian, uterine and kidney. Volume ultrasound enhances visualization of lesions. Ultrasound is frequently used to guide biopsies.

As there is no ionizing radiation, serial follow up studies can be performed to check for recurrence using ultrasound.

Recent developments include ultrasound elastography, targeted microbubble contrast agents (Weller et al., 2005), locally

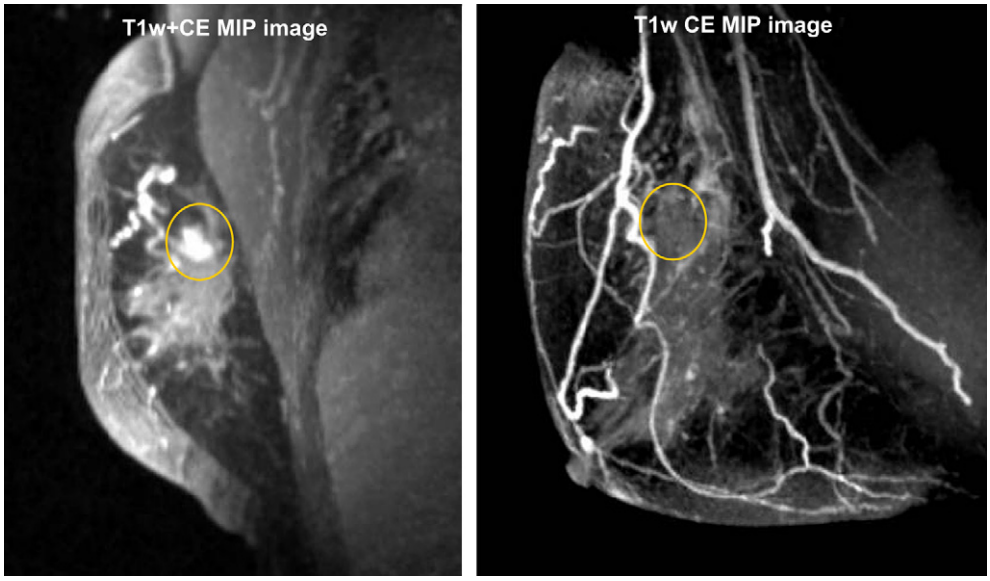

Figure 12 – Pre- and post-contrast images of a single breast cancer lesion treated by MRgFUS (images courtesy of Breastopia Namba Medical Center, Miyazaki, Japan and InSightec, Haifa, Israel).

activated ultrasound mediated drug delivery with nano and microbubbles (Gao et al., in press) and photoacoustic imaging (Xu and Wang, 2006).

5.1. *Miniaturization of ultrasound systems*

Miniaturization of ultrasound systems has made them very portable so they can be taken to the patient or even inserted into the patient through natural orifices.

Transrectal ultrasound (TRUS) is used for the diagnosis and guiding the biopsy of prostate cancer (Narayan et al., 1995). Transrectal ultrasound guided multiple systematic random biopsies are presently the method of choice for determining the presence or absence of prostate cancer (Tillmann et al., 2004).

Endoscopic ultrasound can identify lesions in mediastinum (Larson et al., 2002; Larsen et al., 2005) and is used to guide fine needle aspiration biopsy to identify primary malignancies as well as spread from lung cancer that had been previously seen on CT. It has shown a major benefit in avoiding unnecessary thoracotomies.

Endoscopic ultrasound is also used in the diagnosis of tumours of the gastrointestinal system such as oesophageal, gastric and pancreatic cancer. It is also used to obtain biopsies (Williams et al., 1999) of any focal lesions found in the upper gastrointestinal tract, lymph nodes, pancreas and perirectal tract.

The use of endoscopic interstitial high intensity focused ultrasound has been used to treat oesophageal tumours (Melodelima et al., 2006) under fluoroscopic and ultrasound guidance.

Future devices may use capacitive micromachined ultrasonic transducer (CMUT) arrays usually made on silicon substrates for non-invasive focused ultrasound ablation of lower abdominal cancers under MR guidance (Wong et al., 2006).

Endoscopic ultrasound guidance of brachytherapy using porous silicon microspheres containing phosphorus-32 introduced into the pancreas is another recent application undergoing clinical trials.

5.2. *Acoustic radiation force impulse imaging*

Acoustic radiation force impulse (ARFI) imaging (Palmeri et al., 2004) has been shown to provide information about the mechanical properties of tissues. It uses short, high-intensity, focused ultrasound to generate radiation force and uses traditional ultrasonic correlation-based methods to track the displacement of tissues. Acoustic radiation force impulse imaging exploits differences in the mechanical properties of soft tissues to outline tissue structures that may not be seen with B-Mode ultrasound. In ARFI imaging, an impulse of relative high acoustic energy is transmitted into the body to deliver a radiation force that is spatially and temporally localized at the imaging focus in a way that displaces tissue a few micrometres away from the imaging transducer. Ensembles of ultrasonic transmit-receive lines that generate data for ARFI-induced axial motion tracking with a one-dimensional cross-correlation follow each ARFI impulse.

It has the potential to be used in the endoscopic evaluation of gastrointestinal tumours.

ARFI imaging implemented on a diagnostic ultrasonic scanner has been proposed (Fahey et al., 2006) as a method to guide RF ablation procedures in the liver. This could be convenient when sonographic guidance is used for RF electrode insertion. ARFI imaging has demonstrated superior imaging of tumour boundaries of hepatic malignancies (Fahey et al., 2008).

Ultrasound microbubble contrast agent use in preclinical studies has demonstrated quantitative measures of tumour neovascularity in the glioma and breast cancer xenograft models C6 and NMU and appears to provide a non-invasive marker for angiogenesis (Ro et al., 2006).

Reflex transmission imaging (RTI) has been used to quantitatively define pigmented skin lesions such as melanoma in vivo (Rallan et al., 2006). A significant difference in attenuation is shown in skin cancer lesions. RTI could potential be synergistic with white light clinical (WLC) photography in the diagnosis of skin cancer.

Ultrasound is used as direct therapy technique in ultrasound guided high intensity focused ultrasound systems and as a method to facilitate local drug delivery and gene therapy.

5.3. *High intensity focused ultrasound*

Systems for high intensity focused ultrasound ablation of prostate cancer have been extensively evaluated (Blana et al., 2004).

Ultrasound enhanced local drug delivery into tumours has been the subject of active research (van Wamel et al., 2004; Tachibana et al., 2000; Yu et al., 2004; Rapoport et al., 2004; Nelson et al., 2002). Pretreatment with ultrasound increases the cytotoxicity of anti-cancer drugs (Paliwal et al., 2005).

Ultrasound can locally enhance systemic gene delivery into tumours (Anwer et al., 2000). Ultrasound elastography measures and displays tissue strain. Strain is the change in the dimension of tissue elements in different areas in a region of interest. Elastography uses ultrasound measurements made before and after a slight compression of tissue using a transducer. Sonoelastography (Salomir et al., 2006) uses vibrations to cause compression. The elasticity profiles of tissues are different in size to their gray scale appearance on B-mode images. Strain values can be displayed as an image and superimposed on the gray scale image. Normal soft tissue and fat typically have a smaller profile whereas tumours with harder tissue have a larger profile. Potential areas of application are in breast (Burnside et al., 2007; Itoh et al., 2006; Zhi et al., 2007), prostate (Luo et al., 2006; Lorenz et al., 2000), thyroid (Bae et al., 2007; Rago et al., 2007), liver (Săftoiu and Vilman, 2006; Masuzaki et al., 2007) and brain cancer (Scholz et al., 2005). It has been proposed that a ratio of strain image to B-mode image size of 0.75 indicates a benign breast lesion. Using this criterion it would be possible to reduce breast biopsies by 50% and have a more accurate evaluation of tumour size. The technique is most useful for lesions in the indeterminate BI-RADS categories.

6. Non-ionizing electromagnetic imaging

6.1. *Photo- and thermo-acoustic imaging*

Near-infrared spectroscopy, electrical impedance spectroscopy and tomography, microwave imaging spectroscopy and photoacoustic and thermoacoustic imaging are often referred to as electromagnetic imaging. They use non-ionizing electromagnetic radiation between the optical and RF wavelengths. MRI uses RF as well but is not normally classified as part of electromagnetic imaging.

Thermo- and photo-acoustic imaging systems use hybrid imaging techniques that are able to combine the high contrast in microwave, RF and light absorption between healthy and tumour tissues with the high resolution of ultrasound. These systems use non-ionizing radiation and are hybrid because they use both the transmission of electromagnetic energy and the reception of ultrasound waves generated by the tissues. The electromagnetic energy is deposited as a very short time impulse as uniformly as possible throughout the imaging object that causes a small amount of thermal expansion. Typical pulse widths for optical excitation are of the order of 5–10 ns. The photoacoustic technique depends precisely on the absorbed photons (Xu and Wang, 2006) for a signal and avoids the issues due to light scattering in optical imaging.

Due to increased haemoglobin and ionic water content tumour masses preferentially absorb more electromagnetic energy, heat and expand more quickly than nearby healthy tissue (Joines et al., 1994). These masses act as internal acoustic sources that create pressure waves. Ultrasound transducers surrounding the object detect the pressure waves. The transducers that are sensitive to acoustic sources throughout the imaging field of view collect the tomographic data. Optical heating with very short wavelengths is known to provide high contrast between healthy and cancerous tissue (Gusev and Karabutov, 1993; Wang and Wu, 2007). Imaging with optical pulses is limited by tissue absorption to a penetration depth of a few centimetres. Microwave and RF have more penetration. Microwave excitation has a less uniform distribution over large volumes and may be more suitable for preclinical imaging (Xu and Wang, 2006). Breast imaging has been performed using RF excitation at 434 MHz with about 1 μs pulse widths (Kruger et al., 2000). RF at this frequency is absorbed by ionic water contained in breast tumours. Laser-based near infrared excitation breast imaging systems have started clinical evaluation (Manohar et al., 2005, 2007). The potential with photoacoustic imaging in the near infrared is due to the absorption of the infrared light by haemoglobin that can indicate regions of angiogenesis in tumours (Pogue et al., 2001; Oraevsky et al., 2002).

Recent developments using an optical ultrasound mapping system based upon a Fabry–Perot polymer film sensor instead of piezoelectric detectors can give very highresolution images (Zhang et al., 2008). The system could have applications in the study of superficial microvasculature. Photoacoustic microscopy has been used for the study of subcutaneous vasculature (Zhang et al., 2006).

6.2. *Electrical impedance tomography*

Electrical impedance tomography (EIT) (Bayford, 2006) is an imaging method that has developed over the last two decades. Its future application as a clinical diagnostic technique will depend on the development of hardware for data capture and the image reconstruction algorithms especially to take into account tissue anisotropy. It was originally developed for use in geological studies and industrial processes. The main advantage of this technique is the very good temporal resolution of the order of milliseconds and the lack of ionizing radiation.

Electrical impedance tomography (EIT) determines the electrical conductivity and permittivity distribution in the interior of a body from measurements made on its surface. Conducting electrodes are attached to the skin of the subject and small currents are applied to some or all of the electrodes and the corresponding electrical potentials are measured. The

process is repeated for different configurations of the applied current.

EIT imaging in the body is based around measuring the impedance of tissues made up of cells, membranes and fluids. Cells and membranes have a high resistivity and act as small imperfect capacitors and contribute a frequency dependence. Fluids provide the resistive component of the impedance that has a frequency dependence only for liquids outside the cells. High frequencies of the order a MHz show only the resistive component due to conduction through intracellular and extracellular fluids. Low frequencies in the range of a few Hz to several kHz cause the membranes to impede the flow of current and can be used to measure dimensions, shapes and electrical properties of cells (Geddes and Baker, 1967).

Two types of imaging are possible: difference imaging and absolute imaging. Difference imaging is able to relate to changes in blood volume or cell size. Absolute imaging is more difficult as it needs to account for changes in electrode impedance and channel noise.

Prototype breast imagers have been developed (Halter et al., 2005, 2008; Cherepenin et al., 2001; Ye et al., 2006) that look for differences in bioimpedance that can differentiate malignant from benign lesions. Clinical evaluations have been performed using 3D image reconstruction. The combination with mammography tomosynthesis aids the localization for EIT imaging (Kao et al., 2007). Hand held probes are also under development (Kao et al., 2006).

Skin cancer detection is another application under development for tumour imaging (Aberg et al., 2004).

Future developments will be in the area of algorithm optimization and the applications of targeted metal nanoparticles for the imaging of cell biomarkers involved in carcinogenesis, invasion and metastasis. Metal nanoparticles are known to change the bioimpedance of cells.

6.3. *Near infrared optical tomography*

Differences in optical signatures between tissues are manifestations of multiple physiological changes associated with factors such as vascularization, cellularity, oxygen consumption, oedema, fibrosis, and remodelling.

Near-infrared (NIR) optical tomography is an imaging technique with high blood-based contrast. This is due to the fact that haemoglobin absorbs visible wavelength light up to the near infrared region. There is a window of opportunity in the near infrared because water absorbs the far infrared wavelengths.

Non-invasive NIR tomographic imaging has been used in organs like the breast because they can be transilluminated externally. A small change in vascularity creates a very large image contrast. The high contrast of NIR optical tomography is mainly due to increased light attenuation by haemoglobin relative to water in parenchymal tissue and the distinct spectral differences between the oxygenated and deoxygenated states of haemoglobin.

Breast imaging studies (Franceschini et al., 1997; Tromberg et al., 1997; Pogue et al., 2001; Ntziachristos et al., 2002) have shown high sensitivity and specificity based upon differences in vasculature due to angiogenesis in malignant tissues and several clinical trials are still proceeding.

Time domain (Intes, 2005) and frequency domain (Franceschini et al., 1997) imaging can give depth information not available with transmission imaging.

Recent evaluation with a four-wavelength time domain optical imaging system has indicated the potential to differentiate malignant from benign lesions (Rinneberg et al., 2005) with a statistically significant discrimination based on deoxy-haemoglobin content. This could potentially avoid the need for invasive biopsies of benign lesions.

Although NIR optical imaging of the breast has a limited resolution due to light scattering effects it can give spectral information (Dehghani et al., 2003) that permits functional measurements associated with haemoglobin concentration and oxygenation, water concentration, lipid content, and wavelength dependence of tissue scattering.

Oxygenation-index images and perfusion/oxygenation maps can be obtained from multi-wavelength optical data.

NIR diffuse optical tomography can distinguish cysts and solid masses (Gu et al., 2004).

Near-infrared optical tomography could also be used in endoscopy. High sampling speeds allow in vivo use for cancer detection of internal organs. Imaging of haemodynamic changes in prostate cancer (Goel et al., 2006) is a potential application. The use of a transrectal probe has been investigated for prostate imaging (Piao et al., 2007). A clinical system would require integrated imaging with transrectal ultrasound.

7. Nuclear medicine

7.1. *Applications in cancer*

Nuclear medicine systems are one of the mainstays of cancer centres both for imaging and therapy delivery. Nuclear medicine imaging has been used for over three decades in the diagnosis, treatment planning, and the evaluation of response to treatment in patients with cancer. Patient management is one of the most important applications of nuclear medicine in oncology in terms of staging of new cancer patients, restaging for treatment planning and the prediction of therapy response. Nuclear medicine can non-invasively indicate treatment response and disease recurrence so studies can be repeated because of low side effects and the low radiation absorbed doses. It is also possible to correlate nuclear medicine results with analytical laboratory data.

7.2. *Radiopharmaceutical imaging agents*

Nuclear medicine employs radiopharmaceuticals: radiolabelled ligands that have the ability to interact with molecular targets involved in the causes or treatment of cancer. These exogenous agents using radionuclides are injected intravenously and are relatively non-invasive.

Radionuclides can be α, β or γ emitters. Nuclear medicine imaging involves the use of γ radiation from radionuclides. Radioimmunotherapy uses α or β emitters.

Typical radionuclides used in nuclear medicine imaging are ^{131}I (half-life 8 days), ^{123}I (half-life 13.3 h), ^{111}In (half-life 67.3 h), ^{99m}Tc (half-life 6.02 h) ^{201}Tl (half-life 73 h) and ^{67}Ga (half-life 78 h).

SPECT agents have the advantage of a relatively long half-life. A relatively simple chemistry also permits the synthesis of ligands on site. The uptake and biodistribution of these agents depends on their pharmokinetic properties. By targeting to a disease specific biomarker it is possible to get accumulation in diseased tissue that can be imaged.

7.3. *Nuclear medicine imaging systems*

Imaging can be performed using planar gamma cameras (scintigraphy) or single photon emission computed tomography (SPECT) systems. SPECT permits 3D imaging. The resulting images give a physiological and functional response more than anatomical details. Recently SPECT/CT systems have been introduced with the advantage of improved attenuation correction of γ-rays in the body. Multi-slice CT systems are also employed in SPECT/CT for anatomic correlation.

7.4. *Bone scan*

The bone scan continues to have the most common use in oncology because of its good sensitivity and relatively low cost. Technetium-based radiopharmaceuticals such as ^{99m}Tc-MDP, ^{99m}Tc-MIBI and ^{99m}Tc(V)-DMSA are used to detect metastases. FDG PET has however superior specificity compared to the technetium bone scan especially for bone marrow metastases. There is still considerable discussion on the relative merits of each technique (Fogelman et al., 2005).

7.5. *Lymphoscintigraphy and the sentinal lymph node*

^{99m}Tc-labelled human serum albumin is used for lymphoscintigraphy to observe lymph node drainage. Its non-particulate nature allows it to pass well through the lymphatic system but it has the disadvantage of going to second tier nodes and may not remain in the sentinel lymph node (SLN).

The sentinel node is the first lymph node met by lymphatic vessels draining a tumour (Mariani et al., 2001). The absence of tumour cells in the SLN could indicate the absence of metastatic disease in other local nodes. Extensive node dissection surgery can be avoided if the sentinel node is identified and found to be free of tumour cells.

Radiocolloids are cleared by lymphatic drainage with a speed that is inversely proportional to the particle size. A particle size between 100 and 200 nm is a good compromise between fast lymphatic drainage and nodal retention of the particle. Particles larger than 300 nm migrate too slowly but are retained for a longer per time in the sentinel node. Particles less than 50 nm progress to second or third-tier nodes too quickly.

The permeability of the lymphatic system to colloidal particles is highest for particles less than 50 nm. The optimal size for imaging lymphatic drainage has been identified as between 10 and 25 nm. [^{99m}Tc]Antimony sulphide nano-colloids in this size range are no longer commercially available.

^{99m}Tc-sulphur micro or nano colloids are now used for sentinel lymph node imaging and typically have a mean particle size of 300 nm and a range from 50 to 2000 nm. They have the advantage of remaining longer in the sentinel lymph node.

Intra-operative sentinel lymph node imaging can be performed using a hand held γ-ray detector. Radiolymphoscintigraphy confirms the location of the SLN, which is determined initially with a pre-operative lymphoscintigram and intra-operative vital blue dye injection. The combination of the isotope and blue dye has a complementary effect in sentinel node localization.

Lymph node imaging (Even-Sapir et al., 2003; Mar et al., 2007; Lerman et al., 2007) is an important application of SPECT/CT.

SPECT /CT is better than planar imaging for the confirmation of the exact anatomic location of a sentinel node (van der Ploeg et al., 2007).

SLN imaging has over 99% success rate for melanoma sentinel lymph node biopsy (Rossi et al., 2006).

Poor visualization of the deep lymphatic system is an inherent limitation of lymphoscintigraphy. Web space injections between the toes can only show the superficial lymphatic system. As a result deep lymphatic channels originating posterior to the malleoli and running to the popliteal nodes and along the superficial femoral vein cannot normally be seen with lymphoscintigraphy.

SPECT/CT systems may aid in identification of nodes that are obscured by injection site activity, for deeply located and in-transit nodes (Belhocine et al., 2006).

7.6. *Immunoscintigraphy*

Immunoscintigaphy utilizes radiolabelled monoclonal antibodies to target tumour specific antigens such as CEA (Yao et al., 2007).

Capromab pendetide is a murine monoclonal antibody (7E11-C53) that reacts with prostate membrane specific antigen (PMSA). PMSA is a membrane glycoprotein that is highly expressed in prostate cancer. Immunoscintigraphy is accomplished by labelling the antibody with ^{111}In. Capromab pendetide is indicated in the evaluation of patients with newly diagnosed prostate cancer especially with an intermediate to high Gleason grade who are at risk for advanced disease. It is also indicated for the evaluation of patients who have had a prostatectomy or radiation therapy and who present with a rising PSA level. This is to determine whether further local therapy or systemic hormone therapy is indicated. SPECT/CT has advantages (Wong et al., 2005) in the imaging of capromab pedetide.

7.7. *Receptor targeting*

Transferrin receptors that are markers of tumour growth, take up ^{67}Ga. Imaging with ^{67}Ga-citrate is not used for staging because it is non-specific due to take up by inflammatory processes but could be useful in predicting therapy response and outcome (Front et al., 2000).

If ^{67}Ga imaging is ambiguous for example when looking for lung cancer in the presence of infection then ^{201}Tl in the chloride form is often used because tumours take it up and it is not normally taken up by inflamed lymph nodes.

7.8. *Neuroendocrine tumour imaging*

Radiopharmaceuticals used to image neuroendocrine tumours are either similar in molecular structure to the hormones that

the tumours synthesize or incorporated into various metabolic and cellular processes of the tumour cells.

meta-Iodobenzylguanidine (MIBG) also known as iobenguane, localizes to storage granules in adrenergic tissue of neural crest origin and is concentrated in catecholamine producing adrenal medullary tumours (Intenzo et al., 2007).

MIBG is a combination of the benzyl group of bretylium and the guanidine group of guanethidine. It structurally resembles norepinephrine and guanethidine (a neurosecretory granule depleting agent). MIBG enters neuroendocrine cells by an active uptake mechanism. It is believed to share the same transport pathway with norepinephrine and displace norepinephrine from intra-neuronal storage granules in adrenergic nerves.

As MIBG is stored in the neurosecretory granules this results in a specific concentration in contrast to cells of other tissues. Uptake is proportional to the number of neurosecretory granules within the tumour. In neuroblastomas, the agent remains within the cellular cytoplasm, free of granular storage. The retention in neuroblastomas is related to the rapid reuptake of the agent that has escaped the cell (Shulkin et al., 1998).

MIBG scintigraphy is used as a sulphate with ^{131}I or ^{123}I to image tumours of neuroendocrine origin (Ilias et al., 2003; Kumar and Shamim, 2004; Bergland et al., 2001; Kushner et al., 2003), particularly those of the sympathoadrenal system (phaeochromocytomas, paragangliomas and neuroblastomas) and other neuroendocrine tumours (carcinoids, medullary thyroid carcinoma, etc.).

Due its superior imaging characteristics, the sensitivity of ^{123}I-MIBG scintigraphy is higher than that of ^{131}I-MIBG. SPECT is also possible with ^{123}I-MIBG.

Neuroendocrine tumours are formed from tissue that embryologically develops into neurons and neuronal structures. Neuroendocrine tumours are derived from embryonic neural crest tissue found in the hypothalamus, pituitary gland, thyroid gland, adrenal medulla and the gastrointestinal tract.

The uptake–re-uptake system preserves norepinephrine in sympathetic neurons.

Octreotide, a somatostatin analogue consisting of eight amino acids, is used to perform somatostatin receptor imaging. Octreotide is labelled with ^{111}In and chelated with DTPA to make the radiopharmaceutical [^{111}In]DTPA-D-Phe-octreotide also known as [^{111}In]pentetreotide. It has a half-life in plasma of nearly 2 h. Somatostatin has a half-life of only 2–4 min due to the disruption of its molecular structure by circulating enzymes.

Somatostatin, a 14 amino acid peptide hormone, is produced in the hypothalamus and pancreas to inhibit the release of growth hormone, insulin, glucagon and gastrin. Somatostatin receptors are integral membrane glycoproteins distributed in different tissues. They are receptors on neuroendocrine originating cells. These include the somatotroph cells of the anterior pituitary gland and pancreatic islet cells. Endocrine related tumours such as neuroendocrine tumours have somatostatin receptors. These include pancreatic islet cell tumours that include gastrinomas, insulinomas, glucagonomas and vasoactive intestinal peptide (VIP-)-omas, carcinoid tumours, some pituitary tumours, small cell lung carcinomas, neuroblastomas, pheochromocytomas, paragangliomas and medullary thyroid carcinoma. Somatostatin receptors are also found in Hodgkin's and non-Hodgkin's lymphomas, Merkel cell tumours of the skin, breast cancer, meningiomas and astrocytomas.

7.9. *Radioimmunotherapy and peptide receptor radionuclide therapy*

Scintigraphy imaging is used for dosimetry measurements when performing radioimmunotherapy (RIT) or peptide receptor radionuclide therapy (PRRT).

RIT and PPRT have the possibility to specifically irradiate tumours while sparing healthy organs. Fractionated external beam irradiation (XRT), does not permit precise focusing of the beam specifically to a tumour without affecting proximal healthy organs, especially in metastatic disease. RIT and PRRT involve continuous, low-dose irradiation from tumour-targeted radionuclides. The biological effect is due to energy absorption from the radionuclide's emissions.

Cells express receptor proteins on their plasma membranes, with high affinity for regulatory peptides, such as somatostatin, bombasin and the neuropeptide NPY (Y_1). For example, NPY (Y_1) is involved in both proliferation and angiogenesis. Over expression of these receptors in many tumours is the basis for peptide receptor imaging and therapy. Radiolabelled somatostatin, bombasin and NPY (Y_1) analogues are used in scintigraphy for the visualization of receptor-positive tumours. ^{111}In-DTPA-octeotride, for example, is used for somatostatin receptor scintigraphy imaging. These analogues have also been labelled with therapeutic radionuclides (α and β) for PRRT individually or in combination for multi-receptor targeting. An example is the use of ^{90}Y-DOTATOC as a somatostatin receptor-based radionuclide therapeutic agent.

The β-particle emitters such as ^{131}I, ^{90}Y, ^{186}Re and ^{188}Re have a tissue range of several millimetres. This can create a ''crossfire'' effect so that antigen or receptor negative cells in a tumour can also be treated. β-particle therapy is preferred for large tumours. Other β-emitters that have been studied are ^{177}Lu and ^{67}Cu.

The short range, high energies and high linear energy transfer (LET) of α particles should be better suited for treatment of micrometastases or circulating tumour cells. The α-particle emitters such as ^{225}Ac (half-life 10 days), ^{211}At (half-life 7.2 h), ^{212}Bi (half-life 60.55 min) and ^{213}Bi (half-life 45.6 min) could also be more efficient and specific in killing tumour cells.

The use of two and three step pre-targeting techniques (Albertoni, 2003) based on the avidin-biotin system is showing promise in improving the performance of RIT. Further work on intra-operative pre-targeting could be an alternative to fractionated radiotherapy in SLN negative breast cancer patients under going breast conserving surgery (Paganelli et al., 2007). In a two-step technique, intra-operative injection of avidin in the tumour bed after quadrantectomy causes intravenously (IV) administered radioactive biotin labelled with ^{90}Y to home in onto the target site. Dosimetric and pharmacokinetic studies with ^{111}In-DOTA-biotin give scintigraphic images at different time points provided evidence of a fast and stable uptake of labelled DOTA-biotin at the site of the operated breast. Chelation with DOTA inhibits the release of ^{90}Y that would otherwise build up in bone. ^{111}In is a γ-ray emitting isotope that can

be imaged by scintigraphy and mimics the dosimetry of ^{90}Y that cannot be imaged. The scintigraphic images are acquired over a 48-h period after injection.

7.10. Scintimammography

Future developments in nuclear medicine will be in the area of development of specialized imaging systems. One example where further development of specialized gamma cameras will be of use is in breast and axillary node imaging using scintimammography. This is due to the need to avoid scatter from extramammary sources that plays an important role in breast imaging with radiotracers, and is the dominant effect when imaging near the chest wall is used for mammoscintigraphy. Conventional gamma cameras, also known as large field of view cameras, have been used to image radiopharmaceuticals for scintimammography. These cameras have a large inactive area at the edge of the detector that prevents the camera from imaging breast tissue adjacent to the chest wall. As a result scintimammography using a conventional gamma camera is typically performed either with the patient supine and the camera positioned to take a lateral view of the breast, or in the prone position that permits the breast to hang freely. Compression of the breast is not possible, thus decreasing the sensitivity for detecting smaller lesions. Dedicated breast specific gamma camera imaging (BSGI) systems (Coover et al., 2004; Rhodes et al., 2005; Brem et al., 2005; O'Connor MK et al., 2007) have been developed to reduce the limitations of conventional scintimammography. These cameras have a small field of view that increases the resolution and gives improved flexibility of movement compared to conventional gamma cameras. Some systems allow positioning similar to that of an X-ray mammogram with the possibility of applying compression to the breast during imaging. Improvement in this technology has renewed interest in scintimammography as a potential primary screening technique. It would be important to develop a biopsy system to be used with breast specific gamma cameras. ^{99m}Tc-sestamibi is a second-line diagnostic test after mammography approved to assist in the evaluation of breast lesions in patients with an abnormal mammogram of breast mass (Sampalis et al., 2003; Khalkhali et al., 2002). False positives can be caused by uptake of the radiotracer in the chest as a result of physiological activity in the auricular aspect of the right atrium (Civelek et al., 2006). A recent study (Brem et al., 2007) has shown a breast specific gamma camera imaging system has comparable sensitivity and greater specificity than MRI (Sweeney and Sacchini, 2007) for the detection of breast cancer in patients with equivocal mammograms. The smallest cancer detected by BSGI was 3 mm. Current recommendations for the use of scintimammography are:

1. As a general adjunct to mammography to differentiate between benign and malignant breast lesions in patients with palpable masses or suspicious mammograms
2. In patients referred for biopsy when lesions are considered to have a low probability of malignancy
3. In patients with probably benign findings on mammography but who are recommended for close follow-up (e.g., repeat mammography in 3–6 months)
4. In patients who have dense breast tissue on mammography who are considered difficult to evaluate on mammography
5. For detection of axillary lymph node metastases in patients with confirmed breast cancer.

7.11. Angiogenesis imaging

Cell adhesion molecules, such as integrins, have a major role in angiogenesis and metastasis. The integrin $\alpha_v\beta_3$ recognizes the RGD (Arg-Gly-Asp) sequence. ^{99m}Tc RGD peptides (Fani et al., 2006; Liu, 2007; Zhang and Cheng, 2007) have been developed for scintigraphy imaging of angiogenesis and have potential for early detection of breast cancer and following response to anti-angiogenic therapy (Jung et al., 2006).

There is a developing interest in using scintigraphy to follow drug delivery using nanoparticles as drug delivery systems (Liu and Wang, 2007). Pre-clinical studies can use radiolabelling to evaluate the biodistribution of carbon functionalized nanotubes (CNT). Future drug delivery systems may use carbon CNT to transport and translocate therapeutic molecules. It is possible to functionalize CNT with bioactive nucleic acids, peptides, proteins, and drugs for delivery to tumour cells. Functionalized CNT have increased solubility and biocompatibility, display low toxicity and are not immunogenic.

7.12. Multi-drug resistance imaging

Radiopharmaceutical agents with lipophilic or cationic properties signal the presence or absence of P-glycoprotein. ^{99m}Tc-MIBI, ^{99m}Tc-tetrofosmin, ^{99m}Tc-Q58, and several ^{11}C PET agents share these characteristics but ^{99m}Tc MIBI has shown the most promise. In the absence of P-glycoprotein the lipophilicity of ^{99m}Tc-MIBI enables it to translocate across the cell membrane and its cationic charge allows it to concentrate inside the cell and be sequestered in the mitochondria. The agent uptake is consequently high.

In the presence of P-glycoprotein ^{99m}Tc-MIBI acts like a therapeutic agent and is pumped out of the cell. The uptake is low and quantifiable and the radiopharmaceutical can measure the effectiveness of drugs designed to treat multi-drug resistance.

8. PET and PET/CT

8.1. PET radioisotopes

PET cancer imaging utilizes positron-emitting radioisotopes, created in a cyclotron, like ^{18}F, ^{11}C, ^{64}Cu, ^{124}I, ^{86}Y, ^{15}O and ^{13}N or in a generator like ^{68}Ga.

The most widely used isotope is ^{18}F due to the practicality of transport with a half-life of 109.8 min. Various tracers labelled with ^{18}F, ^{11}C and ^{68}Ga and imaged with a PET/CT system are shown in Figure 13.

Some of these tracers are in development and used for research. The research tracers are not products and may never become commercial products.

The only two FDA approved tracers for oncology imaging are [^{18}F]2 fluoro-D-deoxyglucose (^{18}F-FDG) a substrate for

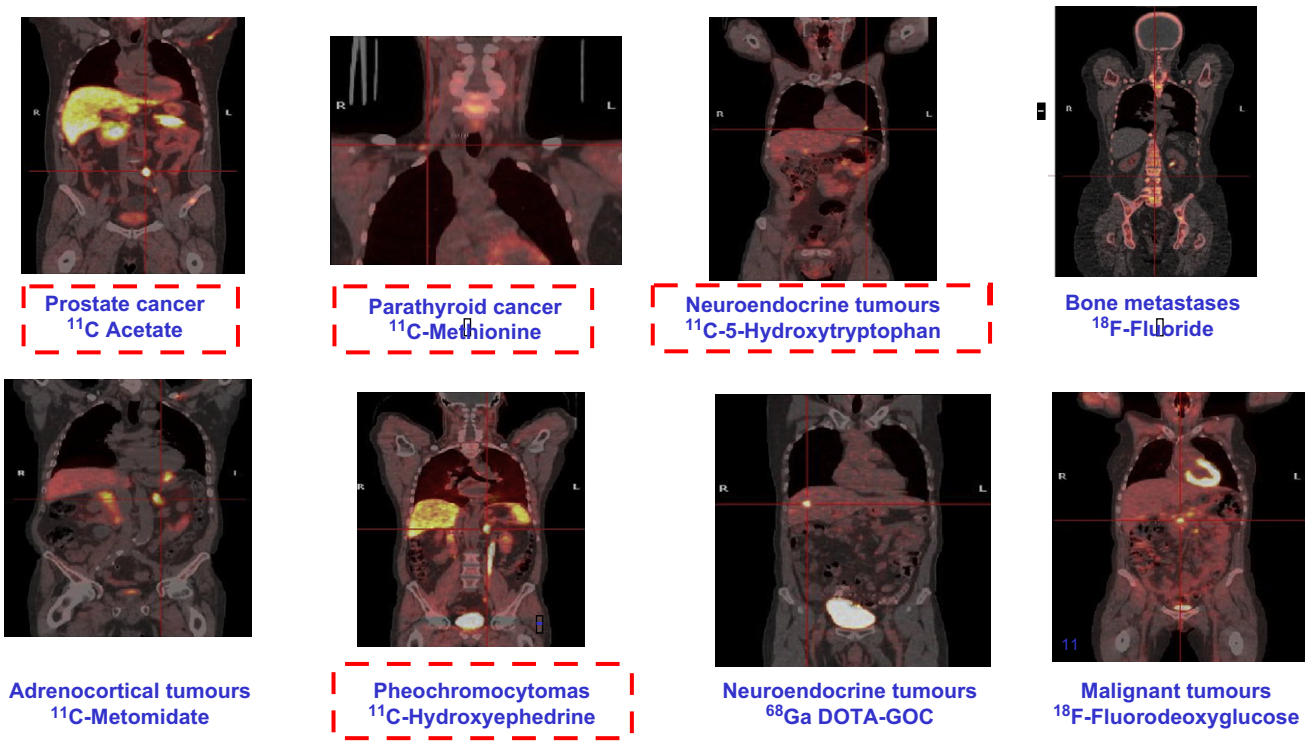

Figure 13 – Examples of PET tracers in oncology where endogenous substances are framed (courtesy of Imanet Uppsala).

hexokinase in glucose metabolism and [^{18}F]fluoride ions such as ^{18}F-NaF_2 that are incorporated in the hydroxyapatite crystals in bone for bone imaging.

The unique perspective of ^{11}C chemistry is that many tracers based on ^{11}C are endogenous compounds in the human body such as the amino acids methionine and hydroxytryptophan, the neurotransmitter hydyroxyephedrine and the energy substrate /fatty acid acetate. Other compounds such as ^{18}F-FDG and ^{18}F-FDOPA are analogues of endogenous substances.

Manmade drug-based tracers are of great interest. [^{11}C]Metomidate (1*H*-imidazole-5-carboxylic acid, 1-[(1*R*)-1-phenylethyl]-methyl ester hydrochloride), a vetinary sedative and an inhibitor of 11β-hydroxylase is an example of synthetic drug like tracers that are connecting tracer development to the imaging of proteins involved in disease processes.

Vorozole (6-[(4-chlorophenyl)-(1,2,4-triazol-1-yl)methyl]-1-methyl-benzotriazole) is an imidazole-based inhibitor of aromatase that was initially developed as a therapy for breast cancer. [*N*-methyl-^{11}C]Vorozole, a high-affinity aromatase-binding radiotracer is being developed for use in imaging ovarian and breast cancer.

Another synthetic drug-based tracer is ^{18}F-RGD peptide (arginine-glycine-aspartic acid) is an example of an integrin binding agent currently being investigated for angiogenesis imaging. This tripeptide motif can be found in proteins of the extracellular matrix. Integrins link the intracellular cytoskeleton of cells with the extracellular matrix by recognizing this RGD motif. Without attachment to the extracellular matrix, cells normally undergo anoikis a form of apoptosis that is induced by anchorage-dependent cells detaching from the surrounding extracellular matrix (ECM). Soluble RGD peptides induce apoptosis and might be used as drugs against angiogenesis, inflammation and cancer metastasis since small soluble peptides containing the RGD motif inhibit cell attachment and consequently induce apoptosis.

FDG is also related to an endogenous substrate but it is an analogue. Oncological applications of ^{18}F-FDG approved in the US are shown in Figure 14.

All other tracers under investigation except [^{18}F]fluoride are used for research purposes in clinical and pre-clinical imaging.

An example of an ^{18}F-based research tracer is ^{18}F-FHBG (9-(4-[^{18}F]fluoro-3-hydroxymethylbutyl)guanine) that is used as a reporter probe for the herpes simplex virus type 1 thymidine kinase (HSV1-tk) gene, which is transfected into malignant cells in experimental suicide gene therapy. ^{18}F-FHBG has also been used for the imaging of human mesenchymal stem cells (hMSCs) expressing HSV1-tk (Hung et al., 2005).

^{11}C is potentially a much more interesting radioisotope but its use so far has been limited due its short half-life of 20.4 min. There is however the potential to make smaller and less costly cyclotrons and for developments in carbon chemistry and in particular the use of [^{11}C]carbon monoxide as a versatile and useful precursor in labelling chemistry (Långström et al., 2007).

^{124}I (half-life 4.2 days) has been used to label agents for apoptosis imaging such as annexin V, new tumour targeting agents such as phospho-lipid ether (PLE) and antibody fragments where the physical half-life of ^{124}I matches the biological half-life of the antibody fragments.

^{68}Ga (half-life 68.1 min) prepared in a generator shows a lot of promise for the labelling of peptides and antibodies for targeted imaging. It has also the potential to be used to label

Indications	Diagnosis	Initial Staging	Treatment Monitoring	Re-Staging
Breast		x*	x	x
Cervical		x**		
Colorectal	x	x		x
Esophagus	x	x		x
Head & neck	x	x		x
Lung, non-small	x	x		x
Lymphoma	x	x		x
Melanoma	x	x*		x
Solitary Pulmonary Nodule	x			
Thyroid				x * * *

*Does not cover initial staging for axillary lymph nodes for breast cancer and regional lymph nodes for melanoma

**Patient must have prior CT or MRI negative for extrapelvic metastatic disease

*** Thyroid cancer must be of follicular cell origin and been previously treated by thyroidectomy and radioiodine ablation

Figure 14 – US covered PET indications in oncology.

cancer stem cells (CSCs). Cancer stem cells can originate from mutations in normal somatic stem cells that deregulate their physiological programs. Mutations could also target more committed progenitor cells and mature cells that are re-programmed to acquire stem-like functions.

^{64}Cu (half-life 12.7 h) may have a use in specialized imaging such as the identification of areas of hypoxia or measurement of blood flow with ^{64}Cu ATSM (copper-diacetyl-bis(N^4-methyl-thiosemicarbazone) and [^{64}Cu]copper-pyruvaldehyde-bis(N^4-methylthiosemicarbazone (^{64}Cu-PTSM) or for the labelling of antibodies, peptides and nanoparticles that have been conjugated to DOTA.

$^{15}O_2$ (half-life 2.03 min) is used as [^{15}O]H_2O to measure tissue perfusion and blood flow in response to anti-angiogenic therapy. Due the very short half-life this radioisotope has to be used directly from a cyclotron.

^{13}N (half-life 9.97 min) is used as [^{13}N]ammonia (^{13}N-NH_3) to measure blood flow to determine the grade of brain tumours and identify benign brain lesions. This isotope also has to be used directly from a cyclotron.

^{74}As (half-life 17.8 days) is being used to label antibodies because of its long half-life.

8.2. *FDG PET*

PET and in particular PET/CT promise to have a big impact on the management of cancer patients. Currently most cancer imaging is based on the tracer ^{18}F-FDG that is an analogue of glucose. It is transported across the plasma membrane into cells by the glucose transport proteins such as glut 1 and glut 3 down a concentration gradient through a process of facilitated transport. Glut 1 and glut 3 are over expressed in tumour cell membranes. Hexokinase in the cell phosphorylates the ^{18}F-FDG into the 6-phospho form. As glut transporters do not transport the phosphorylated form it remains in the cell whereas normal glucose is removed. 6-Phospho-^{18}F-FDG cannot be further metabolized and therefore accumulates in cells. With the development of ultra-fast PET systems in the future it would be interesting to be able to perform dynamic studies of glucose metabolism using a [^{11}C]glucose tracer.

In tumours, ^{18}F-FDG PET uptake correlates with the rate of glycolysis that is far greater in neoplastic tissues than in the normal tissues from which the neoplasia develops (Larson et al., 1999). In order to evaluate the usefulness of ^{18}F-FDG-based PET imaging in cancer management the National Oncological PET Registry has been set up in the USA (Hillner et al., 2007). ^{18}F-FDG uptake is believed to be related to the underlying cancer biology and to predict aggressive tumour behaviour and treatment response. ^{18}F-FDG PET is being validated as a true surrogate that could be used in evaluating treatment response of tumours in place of classic endpoints such as those based on RECIST (Therasse et al., 2000)that are not completely satisfactory. For example in correlation with time to failure (TTF), ^{18}F-FDG PET, is competitive with CT optimized bi-dimensional measurements of no growth from baseline to 1 month as an early prognostic indicator of response to imatinib mesylate in patients with a gastrointestinal stromal tumour (GIST) (Holdsworth et al., 2007). The use ^{18}F-FDG PET to evaluate chemotherapy response of patients with non-small cell lung cancer correlates with patient outcome (de Geus-Oei et al., 2007).

The common measurement used by PET is the standard uptake value (SUV) (Huang, 2000). The SUV is defined by tumour activity per dose injected per body mass. It is proportional to the glucose metabolic rate within the normal range of serum glucose concentration. The metabolic response is defined by the percentage change of post-therapy SUV from the pre-therapy SUV. The rate-limiting step for FDG uptake and retention in most tissues is phosphorylation rather than transport.

The maximum standardized uptake value has been shown to predict prognosis in some cancers. These include lung cancer (Downey et al., 2004), oesophageal cancer (Rizk et al., 2006) and thyroid cancer (Robbins et al., 2006). The SUV value can also help differentiate between indolent and aggressive lymphomas (Schoder et al., 2005).

There are multiple examples of the use of ^{18}F-FDG PET to predict treatment response in several cancers such as non-Hodgkin's lymphoma (Juweid et al., 2005), oesophageal cancer (Downey et al., 2003; Kato et al., 2007), colorectal cancer (Cascini et al., 2006; de Geus-Oei et al., 2008) and breast cancer (McDermott et al., 2007; Tardivon et al., 2006; Rousseau et al., 2006; Su et al., 2006) as well as lung cancer (Wong et al., 2007).

The use of 4D PET/CT imaging with respiratory compensation in the thorax improves the accuracy of SUV measurements. Incorporating metabolic change by PET into concomitant size change by CT is more sensitive and accurate in predicting local control than CT alone. Delayed imaging can avoid the inflammatory effects of post radiation therapy.

In patients with locally advanced adenocarcinomas of the oesophago-gastric junction, relative changes in tumour FDG uptake are better predictors for treatment outcome after pre-operative chemotherapy than absolute SUVs (Wieder et al., 2007). Metabolic changes within the first 2 weeks of therapy are at least as efficient for prediction of histopathologic response and patient survival as later changes.

The potential underlying mechanisms causing changes in ^{18}F-FDG uptake as an indicator of early response after therapy have been reviewed (Linden et al., 2006a).

8.3. Acetate and choline PET imaging

Not all cancers are visualized well with ^{18}F-FDG PET. [^{11}C]Acetate or [^{18}F]acetate are activated to acetyl-CoA in both the cytosol and mitochondria by acetyl-CoA synthetase. [^{11}C]Acetate has been used as a tracer for renal, pancreatic, liver, lung and prostate tumours. [^{11}C]Acetate PET could be useful to diagnose pulmonary nodules with ground-glass opacity images that are not identified by FDG PET (Nomori et al., 2005).

Well-differentiated HCC tumours are detected by [^{11}C]acetate and ^{18}F-FDG detects poorly differentiated types. The two tracers are complementary for liver imaging (Ho et al., 2003).

Visualization of prostate cancer with ^{18}F-FDG as the radiopharmaceutical is limited by the low uptake of FDG in the tumour and by radioactivity excreted into the bladder. Serum testosterone levels influence glucose and acetate metabolism in the prostate. Acetate is converted into fatty acids by the enzyme fatty acid synthetase (FAS) that is over expressed in cancer cells and [^{11}C]acetate is also mainly incorporated into intracellular phosphatidylcholine membrane microdomains that play a key role in tumour growth and metastasis. [^{11}C]Acetate has been utilized for early detection of recurrence of prostate cancer after prostatectomy when salvage radiotherapy may still have a chance of success (Sandblom et al., 2006). [^{11}C]Acetate PET has been shown to have a higher sensitivity than ^{18}F-FDG PET for detection of recurrent prostate cancer and metastases (Oyama et al., 2003). A limitation of [^{11}C]acetate PET imaging of the prostate is that SUVs for normal prostate and benign prostate overlap significantly with those for prostate cancer (Kato et al., 2002).

It is thought that the malignant transformation of cells is associated with the induction of choline kinase activity, with increased demand on phospholipids attributed to proliferation and that choline modulates the signalling process of cell proliferation and differentiation (Zeisel, 1993).

Prostate cancer has a phospholipid metabolism. ^{11}C labelled choline a substrate for choline kinase in choline metabolism is potentially useful as it is incorporated in the cell membrane phospholipids through phosphorylcholine synthesis as phosphatidylcholine that is up-regulated in cancer.

[^{11}C]Choline is readily taken up in prostate cancer by both the primary tumour and the lymph node metastases. There is almost no uptake in the bladder due to low and delayed renal excretion. Positive [^{11}C]choline PET–CT in the prostatic fossa indicates local recurrence after radical prostatectomy but negative PET–CT is not correlated with the absence of tumour (Wiegel, 2007). A correlation has been shown between PSA levels and potential need for an [^{11}C]choline study to identify recurrence (Vormola et al., 2007). A disadvantage of [^{11}C]choline is that it will not distinguish between benign prostate hyperplasia (BPH) and prostate cancer.

[^{11}F]Choline has been investigated for staging and restaging of prostate cancer (Husarik et al., 2008) but initial results were disappointing due to the difficulty in detecting small metastases. [^{11}F]Choline may have an application in imaging of bone metastases from prostate cancer (Beheshti et al., 2007) particularly in the bone marrow and in early sclerotic and lytic changes of the bone when [^{18}F]fluoride imaging is negative. [^{18}F]Fluoride normally identifies dense sclerotic lesions but not ultra-dense sclerotic lesions.

Other potential areas of application of [^{11}C]choline PET–CT include the brain, the thorax and the bones. Bronchoalveolar carcinoma has a very low uptake of FDG so that inflammation may lead to over estimation of aggressiveness.

^{18}F-FDG is not useful for the diagnoses or therapy control of brain tumours due to the high uptake by normal brain tissue and the accumulation as a result of radiotherapy induced inflammation in tumour tissues. [^{11}C]Choline PET and MRI may provide an accurate method to identify high-grade gliomas (Ohtani et al., 2001).

8.4. Neuroendocrine tumour targeted tracers

Neuroendocrine tumours (NETs) are able to express cell membrane neuroamine uptake mechanism and/or specific receptors such as somatostatin receptors. The most common gastrointestinal neuroendocrine tumours, arising from enterochromaffin cells of the gastrointestinal tract are carcinoids. They are clinically less aggressive than the more common intestinal adenocarcinoma and typically occur as well-circumscribed round submucosal lesions.

FDG PET is not very useful for imaging gastropancreatic neuroendocrine tumours. Only tumours with high proliferative activity and low differentiation show an increased FDG uptake.

PET molecules under evaluation are also showing promise in the imaging of neuroendocrine tumours. These molecules include:

- [^{11}C]5-hydroxytryptophan (^{11}C-5-HTP), a serotonin precursor
- [^{11}C]hydroxyephedrine (^{11}C-HED), a catecholamine analogue
- [^{11}C]epinephrine (^{11}C-EPI), a catecholamine analogue
- [^{11}C]metomidate (^{11}C-MTO),11β-hydroxylase inhibitor
- [^{11}C]etomidate (^{11}C-ETO), 11β-hydroxylase inhibitor
- [^{18}F]metomidate (^{18}F-FMTO), 11β-hydroxylase inhibitor
- [^{18}F]etomidate (^{18}F-FETO), 11β-hydroxylase inhibitor
- [^{11}C]L-dihydroxyphenylalanine (^{11}C-L-DOPA), amine precursor
- [^{18}F]dihydroxyphenylalanine (^{18}F-DOPA), amine precursor
- 6-[^{18}F]dopamine (^{18}F-DA), norepinephrine transporter substrate
- [^{68}Ga]DOTA-octreotide, somatostatin receptor SSTR-III binding
- [^{68}Ga]DOTA-NOC, somatostatin receptors SSTR-II, III, V binding
- [^{68}Ga]DOTATATE, somatostatin receptor SSTR-II binding
- [^{68}Ga]DOTATOC, somatostatin receptor SSTR-II binding

Carcinoid tumours produce serotonin via precursors tryptophan and 5-hydroxytryptophan (5-HTP). Serotonin is synthesized from the amino acid tryptophan by hormone-producing enterochromaffin cells in the gut and bronchi. Serotonin increases the dilation of blood vessels and platelet aggregation. Serotonin is metabolized in the liver to 5-HIAA

(5- hydroxyindole acetic acid) and eventually ends up in the urine.

The ^{11}C-labelled amine precursors ^{11}C-5-HTP (Eriksson et al., 2002) and ^{11}C-L-DOPA have been developed for PET imaging of these tumours. ^{11}C-5-HTP has a higher uptake in endocrine pancreatic tumours. ^{11}C-5-HTP PET is better than CT and somatostatin receptor scintigraphy for tumour visualization. Small, previously overlooked lesions can be diagnosed by ^{11}C-5-HTP PET. There is a strong correlation during treatment between changes in the transport rate constant at repeated PET and those of urinary 5-hydroxyindole acetic acid (U-HIAA). This indicates the possible use of ^{11}C-5-HTP PET also for therapy monitoring. The pre-medication of patients with carbidopa ((2*S*)-3-(3,4-dihydroxyphenyl)-2-hydrazinyl-2-methyl-propanoic acid) orally before PET blocks the aromatic amino acid decarboxylase enzyme. As a result the decarboxylation rate of ^{11}C-5-HTP decreases, leading to a 300% higher tumour uptake and 600% less urinary radioactivity concentration and a reduction of streak artefacts.

^{11}C-HED is a catecholamine analogue and its uptake reflects catecholamine transport and storage and neuronal reuptake. Phaeochromocytomas are chromaffin cell tumours that produce catecholamines. ^{11}C-HED has depicted both phaeochromocytomas and neuroblastomas with high sensitivity, specificity and accuracy (Trampal et al., 2004).

The catecholamine analogue ^{11}C-EPI has also been used to localize phaeochromocytomas (Shulkin et al., 1995).

Dopamine is a better substrate for the norepinephrine transporter than most other amines, including norepinephrine. ^{18}F-DA a sympathoneuronal imaging agent is a highly specific for the localization of adrenal and extra-adrenal phaeochromocytomas, including metastatic lesions (Ilias et al., 2003).

Imaging of malignant phaeochromocytomas by ^{68}Ga-DOTATATE may be indicated for therapy with ^{90}Y-labelled DOTATATE (Win et al., 2007).

^{68}Ga-DOTATOC uptake in neuroendocrine tumours is mainly dependent on receptor binding and fractional blood volume. Pharmacokinetic data analysis can help to separate blood background activity from the receptor binding that may help to optimize planning of ^{90}Y-DOTATOC therapy (Koukouraki et al., 2006).

MTO is an inhibitor of 11β-hydroxylase, an important enzyme in the biosynthesis of cortisol and aldosterone in the adrenal cortex. Due to the binding of MTO to the 11β-hydroxylase activity, the differential diagnosis of adrenocortical carcinomas versus other adrenal tumours such as phaeochromocytomas is possible using ^{11}C-MTO also in the presence of extended necrosis (Hennings et al., 2006). ^{18}F-FETO has also shown promise in imaging for adrenocortical imaging (Wadsak et al., 2006).

8.5. *Cancer related processes*

PET molecules are under development to image processes influencing cancer progression and treatment response such as proliferation, transport, blood flow, angiogenesis, apoptosis and hypoxia. These processes are inter-related as for example in the case of hypoxia.

8.6. *Hypoxia imaging*

Hypoxia activates various agents including Hypoxia-inducible factor-1 (HIF-1α and HIF-1β), activation protein-1 (AP-1) and heat shock proteins (HSP). These agents affect the behaviour of genes that control angiogenesis (HIF-1 upregulates the mRNA of VEGF), cell cycle regulation and apoptosis. In combination, they encourage cancer cells to divide and metastasize more rapidly through anaerobic glycolysis that is a transcription factor for HIF-1.

Hypoxia reduces the cancer-killing power of radiotherapy, chemotherapy, photodynamic therapy and surgical therapy. Oxygen is an important mediator of radiation-induced DNA damage. As a result low pO_2 levels in the tumour significantly impede the ability of radiation to kill tumour cells by as much as 300%. Hypoxia can vary regionally and over time. As a result radiotherapy plans based on a static image of hypoxia may be misleading. In general chronic rather than transient hypoxia is the dominant component. Chronic hypoxia is probably due to a large distance between tumour cells and blood vessels. Transient hypoxia may be due to blood flow variations.

Compounds for PET imaging of hypoxia that include fluorinated nitroimidazole nucleoside analogues ^{18}F-FMISO (Kob et al., 1992; Rajendran et al., 2006) (fluoromisonidazole) and [^{18}F](1-(5-fluoro-5-deoxy-alpha-D-arabinofuranosyl)-2-nitroimidazole) (^{18}F-FAZA) (Grosu et al., 2005; Beck et al., 2007), [^{18}F]fluoroerythronitroimidazole (^{18}F-FETNIM) (Lehtio et al., 2003), [^{18}F][2-(2-nitro-1*H*-imidazol-1-yl)-*N*-(2,2,3,3,3-pentafluoropropyl) acetamide] (^{18}F-EF5) (Evans et al., 2006) and [^{64}Cu]Cu-diacetyl-bis (N^4-methylthiosemicarbazone (^{64}Cu-ATSM) (Yuan et al., 2006) are being evaluated for hypoxia imaging.

^{18}F-FMISO binds covalently to intracellular macromolecules upon reduction at low oxygen levels. In the presence of oxygen, the molecule is re-oxygenated to its lower reactivity parent compound that is eliminated from the tissue (Thorwarth et al., 2005). ^{18}F-FMISO has shown promise for predicting response to radiotherapy in patients with head and neck cancer and non-small cell lung cancer (Eschmann et al., 2005).

Slow specific accumulation and clearance from normoxic tissues will limit the clinical use of ^{18}F-MISO. ^{18}F-FAZA and ^{18}F-FETNIM have faster clearance due to reduced lipophilicity (Lehtio et al., 2001; Sorger et al., 2003). ^{18}F-FETNIM and ^{18}F-FMISO have similar intra-tumoural uptake but ^{18}F-FMISO has more uptake in normal tissues than ^{18}F-FETNIM (Grönroos et al., 2004). ^{18}F-FAZA has been used for clinical imaging of head and neck cancer patients (Souvatzoglou et al., 2007).

8.7. *DNA proliferation and protein synthesis imaging*

As a consequence of tumour therapy, changes in DNA proliferation occur more rapidly than changes in glucose metabolism. DNA proliferation imaging is possible through the use of the nucleoside analogues [2-^{11}C]thymidine (Wells et al., 2004), [^{18}F1-(2′-deoxy-2′-fluoro-beta-D-arabinofuranosyl)thymine (^{18}F-FMAU) (Sun et al., 2005) and [^{18}F]3′-deoxy-3′-[^{18}F]fluorothymidine) (Barthel et al., 2003; Herrmann et al., 2007). Glucuronidation of ^{18}F-FLT and ^{18}F-FMAU leads to high background radioactivity and limits their use in the liver.

Cytosolic S-phase-specific thymidine kinase 1 (TK1) regulates the uptake of ^{18}F-FLT. ^{18}F-FLT has potential as a marker for monitoring anti-proliferative therapy in tumours and shows more reduction in uptake than ^{18}F-FDG after chemotherapy. In the evaluation of brain tumours, ^{18}F-FLT (Chen et al., 2005) has more sensitivity, more correlation with proliferation markers (Ki-67) and is a better predictor of progression and survival than ^{18}F-FDG. ^{18}F-FDG has the disadvantage of high uptake by normal brain tissue so ^{18}F-FLT is better than ^{18}F-FDG in determining the grade of gliomas.

Due to increased protein synthesis amino acid uptake in tumour tissue is higher than that in normal tissue. Amino acids have a small involvement in inflammatory cell metabolism compared to glucose. As a result amino acid-based PET radiopharmaceuticals have the potential to be more specific than ^{18}F-FDG (Kubota et al., 1989). Most amino acid PET studies have been made with [methyl-^{11}C]L-methionine (^{11}C-MET).

^{11}C-MET has also more sensitivity than ^{18}F-FLT in the detection of gliomas and is better suited for imaging the extent of gliomas than ^{18}F-FDG, because it is transported specifically into the tumours but only very slightly into normal brain tissue (Jacobs et al., 2005).

The disadvantage of ^{11}C-MET is that methionine is involved in several metabolic pathways such as transmethylation and polyamine synthesis. The accumulation of non-protein metabolites in tumour tissue makes it difficult to quantify protein synthesis (Jager et al., 2001).

L-[1-^{11}C]Tyrosine (^{11}C-TYR) is a carboxyl-labelled amino acid that has the potential to determine protein synthesis rates (Bolster et al., 1986; Willemsen et al., 1995) in tumour tissue due to its irreversible main metabolic pathway producing $^{11}CO_2$.

^{11}C-TYR PET has been used for the visualization and protein synthesis rate assessment of laryngeal and hypopharyngeal carcinomas (De Boer et al., 2002). Head and neck cancer is a difficult area for ^{18}F-FDG PET due to the presence of inflammatory regions.

8.8. Angiogenesis imaging

RGD peptides bind to $\alpha_v\beta_3$ integrins that are specifically expressed on proliferating endothelial cells and tumour cells and have been developed for the imaging of angiogenesis with MRI USPIO contrast agents, ultrasound microbubble contrast agents, fluorescence imaging agents, scintigraphy tracers and PET tracers. RGD peptides have been labelled with tracers such as ^{18}F (Chen et al., 2004a; Beer et al., 2006), ^{64}Cu (Chen et al., 2004b) and ^{125}I (Chen et al., 2004c). Due its 68-min half-life ^{68}Ga is very suitable for labelling peptides and could be used to label RGD peptides in the future. ^{68}Ge/^{68}Ga generators with microwave acceleration are being developed for preparing high purity ^{68}Ga that are GMP compliant with a high specific radioactivity of ^{68}Ga (Velikyan et al., 2004).

Angiogenesis imaging with dimeric ^{18}F-RGD peptides has improved performance versus momomeric ^{18}F-RGD peptides for the quantitative PET imaging of tumour integrin $\alpha_v\beta_3$ expression (Zhang et al., 2006b). The dimeric RGD peptide has nearly an order of magnitude higher integrin-binding affinity than the monomeric analogue. This may be due to the receptor binding of one RGD domain greatly enhancing the local concentration of the other RGD domain near the receptor. This could cause a faster rate of receptor binding or a slower rate of dissociation from the radiolabelled RGD dimer. As a result there is a slower wash-out. A dimeric RGD peptide–paclitaxel conjugate model has been developed for integrin-targeted anti-angiogenic drug delivery (Chen et al., 2005).

Vascular endothelial growth factor (VEGF) is the most important regulator of angiogenesis and VEGF has been labelled with ^{64}Cu for PET imaging (Cai et al., 2006; Backer et al., 2007).

Angiogenesis and lymphangiogenesis are both regulated by the VEGF receptors.

8.9. Blood flow imaging

The short half-life tracers $^{15}O_2$-H_2O and ^{13}N-NH_3 permit rapid sequential scanning. They are used as dynamic PET blood flow imaging agents to control anti-angiogenic therapy and to determine tumour grade in brain tumours.

Measuring perfusion with $^{15}O_2$-H_2O, has been used as a method to monitor anti-angiogenic therapy (Herbst et al., 2002; Anderson et al., 2003).

Tumour to white matter count and perfusion index measurements can differentiate brain lesions (Zhang et al., 2006a). ^{13}N-NH_3 PET is able to distinguish recurrent astrocytoma from radiation necrosis (Zhang and Chen, 2007).

8.10. Apoptosis imaging

Apoptosis is a physiological process that entails selective programmed cell death. Abnormal control of apoptosis occurs in tumours. Different stimuli such as drugs, radiation, ischaemia can initiate apoptosis through activation of proteolytic enzymes that cause nuclear fragmentation and cell lysis.

Apoptosis imaging can be performed through targeting of extracellular and intracellular products of programmed cell death. A vital step for apoptosis is the externalization on the outer side of cell membranes of phosphatidylserine a phospholipid that is normally present on the internal side of the cell membrane. Annexin V is able to identify extracellular phosphatidylserine and can be used to detect apoptotic cells.

Annexin V, belongs to a family of proteins, the annexins, with anticoagulant properties. The annexin family of calcium/phospholipid-binding proteins includes many members (at least 10 occur in mammals). Most of these proteins have not yet had their functions well characterized. Annexin V is used to detect apoptotic cells since it preferentially binds to negatively charged phospholipids like phosphatidylserine in the presence of Ca^{2+} and shows minimal binding to phosphatidylcholine and sphingomyeline that are normally present on the external side of the cell membrane.

Annexin V labelled with ^{18}F has been developed for apoptosis imaging (Murakami et al., 2004; Yagle et al., 2005). The significantly lower uptake of [^{18}F]annexin V in the liver, spleen and kidneys than that of [^{99m}Tc]annexin V could be an advantage for PET imaging compared to scintigraphy. [^{124}I]annexin V has also been investigated (Keen et al., 2005; Dekker et al., 2005).

Due to its specific internalization properties, annexin V mediated internalization could be a potential therapeutic

platform for targeted drug delivery and cell entry to treat cancer (Kenis et al., 2007).

A new class of intracellular apoptosis imaging agents is being developed, whereby a molecular switch is activated upon recognition of apoptotic cell membrane features, allowing the imaging molecule to bind to the apoptotic cell membrane and enter and accumulate within the cell. This new class of agent detects the apoptotic cell from the start of the apoptotic process and the recognition of the apoptotic cell is universal, irrespective of cell type or apoptotic trigger. Several types of labelling are possible including ^{18}F for PET imaging. An example of this type of molecule is *N*,*N*′-didansyl-L-cystine (DDC) (Cohen et al., 2007).

8.11. *Universal PET imaging agent*

The current universal PET imaging agent for oncology is ^{18}F-FDG but the specificity is compromised due to uptake by inflamed and infected tissues as well as metabolically active tumours. Phospho-lipid ether (PLE) (Weichert et al., 2005) tumour-targeting agents labelled with ^{124}I (half-life 4.2 days) are being investigated as potential alternatives to ^{18}F-FDG as they are not taken up by inflamed and infected tissues.

8.12. *Hormone analogues*

Hormone analogues have been developed as agents for the imaging of breast and prostate cancer. 16α-[^{18}F]Fluoro-17β-oestradiol ([^{18}F]fluoro-oestradiol or ^{18}F-FES) uptake in primary breast cancer has been shown to be proportional to the oestrogen receptor (ER) concentration of the tumour measured by in vitro techniques (Mintun et al., 1988). It has been proposed that by using FES PET for the ER concentration, the in vivo status of the primary cancer can be assessed and that of regional or distant metastatic lesions can be determined avoiding a biopsy of each lesion (Dehdashti et al., 1995). FES PET has been used to predict response to tamoxifen therapy (Linden et al., 2006b).

PET tracers targeting the epidermal growth factor receptor (EGRF) (Abourbeh et al., 2007) and human epidermal growth factor receptor 2 (EGRF2) (Steffen et al., 2005) have been developed with potential use in HER-2 positive breast cancer.

Dihydrotestosterone is produced in the prostate by metabolization of testosterone with 5α-reductase and is a stronger growth factor for prostate cancer than testosterone. Androgen receptor (AR) imaging using the dihydrotestosterone analogue16β-[^{18}F]fluoro-5α-dihydrotestosterone (FDHT) (Dehdashti et al., 2005) has been investigated as a technique for predicting response to hormone therapy for prostate cancer. Uptake of FDHT appears to be a receptor-mediated process as it decreases after androgen-receptor antagonist therapy with flutamide (2-methyl-*N*-[4-nitro-3-(trifluoromethyl)-phenyl]-propanamide). There is a correlation between positive FDHT PET studies and increased PSA levels.

8.13. *Multi-drug resistance imaging*

The over-expression of P-glycoprotein (P-gp), encoded by the *MDR1* gene in humans is one of the main mechanisms causing multi-drug resistance (MDR). P-gp is extensively expressed in the blood–brain barrier and in solid tumour tissue. Over-expression of P-gp on tumour membranes might result in MDR of human tumours. P-gp functionality in tumours can be measured in vivo with PET using different tracers such as [^{11}C]verapamil (Hendrikse and Vaalburg, 2002; Takano et al., 2006), [^{11}C]colchicine (Levchenko et al., 2000) and [^{11}C]loperamide (Passchier et al., 2003).

8.14. *Antibody imaging*

Genetically engineered antibody fragments have been developed for PET (Jain and Batra, 2003) with suitable targeting specificity and systemic elimination properties for the imaging of cancer based on expression of tumour associated antigens. Targeted imaging using antibodies requires longer half-life PET isotopes such as ^{124}I, ^{64}Cu, ^{86}Y and ^{74}As to match the biological half-lives of the antibodies. Pre-clinical imaging has been performed using antibody fragments such as anti-HER-2 labelled with ^{124}I (Robinson et al., 2005) and anti-CEA labelled with ^{124}I (Sundaresan et al., 2003) and ^{64}Cu (Wu et al., 2000).

A ^{74}As labelled chimeric monoclonal antibody that binds to phosphatidylserine expressed on tumour endothelial cells, has been used for the pre-clinical PET imaging of solid tumours (Jennewein et al., 2008).

Future clinical imaging with longer-lived isotopes will require correct patient management to avoid radiation risk to persons coming into contact. Radioimmunotherapy with ^{90}Y monoclonal antibodies (mAbs) has been approved. As ^{90}Y is mainly a β-emitter, ^{86}Y-labelled mAbs are used as surrogates to determine the biodistribution and the dosimetry of ^{90}Y-labelled mAbs in patients (Lövqvist et al., 2001).

8.15. *Pharmacokinetics and microdosing*

PET makes it possible to determine drug distribution and concentration in vivo in man with drugs labelled with a positron-emitting radionuclide that does not change the biochemical properties.

In vivo pharmacokinetic and pharmacodynamic measurements are possible with PET (Gupta et al., 2002). PET imaging is used to measure the efficiency of chemotherapy by evaluating delivery and targeting approaches to maximize drug concentration in tumours relative to normal tissues. PET radiotracers are used to evaluate biodistribution between normal and tumour tissues, metabolism, toxicity, response prediction and dosimetry for radioimmunotherapy.

Several labelled chemotherapy agents have been studied. These include [^{18}F]paclitaxel (Kurdziel et al., 2003), [^{18}F]tamoxifen (Inoue et al., 1996), [^{18}F]fluorouracil (Moehler et al., 1998) and [^{13}N]cisplatin (Ginos et al., 1987).

Pharmacokinetic PET studies with radiolabelled drug candidates have the advantage that they can be performed at very low concentrations of only microgram amounts of unlabelled drug; the potential toxicological risk to human subjects is very limited. This has the potential to reduce or avoid side effects. These studies are known as PET microdosing studies or human phase 0/pre-phase I clinical trials. Accelerator mass spectrometry (AMS) is another technique using radioisotopes that is suitable for microdosing studies

(Sarapa et al., 2005; Boddy et al., 2007). The studies can give important information about the distribution of a novel drug but do not provide data about the safety and tolerability of the drug. The Committee for Human Medicinal Products (CHMP) of the European Agency for the Evaluation of Medicinal Products (EMEA) proposed that a dose of one-hundredth of the pharmacological dose derived from in vitro and animal models could be considered a human microdose (European Agency for the Evaluation of Medicinal Products, 2003). Reviews and guidance for the requirements for PET microdosing have been published (Bergstrom et al., 2003; US Food and Drug Administration, 2006; Marchetti and Schellens, 2007; Bauer et al., 2008). The American College of Clinical Pharmacology has issued a position statement on microdosing (Bertino et al., 2007).

The Food and Drug Administration (FDA) recently introduced the Exploratory Investigational New Drug Guidance to accelerate the clinical evaluation of new therapeutic and imaging agents. Early phase 0 trials performed under this guidance have been initiated at the National Cancer Institute (NCI) to integrate qualified pharmacodynamic biomarker assays into first-in-human cancer clinical trials of molecularly targeted agents. The objective of this integration is to perform molecular proof-of-concept investigations at the earliest stage of cancer drug development. Phase 0 trials do not offer any patient benefit. Intensive, real-time pharmacodynamic and pharmacokinetic analyses of patient tumour samples and/or surrogate tissues are performed to provide data for further trials. Phase 0 studies require a significant investment of resources in assay development early on and do not replace formal phase I drug safety testing. These studies offer the promise of a more rational selection of agents for further, large-scale development. They also can provide molecular identification of potential therapeutic failures early in the development process.

8.16. *Microfluidics*

PET radiochemical syntheses can be miniaturized because these are carried out at levels (micro-nano-molar quantities and micro-litre volumes) that are compatible with microfluidic technology. Microfluidic systems contain micro-reactors and reaction yields, rates and selectivities are enhanced through the use of catalysts. The advantages of microfluidics include ultra-high radiotracer concentration, specific activity and enhanced speed of labelling. Speed is of high importance when dealing with short half-life radionucleotides. Synthesis times of only a few seconds are feasible (Gillies et al., 2006). Other advantages include more efficient use of hot-cell space for production of multiple radiotracers, the use of less non-radioactive precursor for saving expensive material and a reduced separation challenge, highly controlled, reproducible and reliable radiotracer production and cheap, interchangeable, disposable and quality-assured radiochemistry processors.

8.17. *Multi-modality imaging*

Co-registration and automated quantitative assessment of high spatial resolution CT and MR images with molecular and functional images from PET for longitudinal studies of response to chemotherapy will develop further. If the images are acquired in separate systems image registration is simpler for rigid and stationary anatomy like the head. Non-rigid moving anatomy, such as the thorax, creates more difficulty in image registration if the images are not acquired at the same time. In order to overcome this difficulty combined SPECT/CT, PET/CT and PET/MR systems have been developed (Zaidi and Alavi, 2007). Although the concept of a combination of PET/MR was the first to be conceived, SPECT/CT and PET/CT were the first to be commercially available. PET and CT do not have physical constraints precluding the close proximity of the systems. CT also has the advantage of being able to make fast attenuation correction measurements for PET imaging to increase productivity. Photon attenuation in tissues is the most important physical factor degrading PET image quality and quantitative accuracy. Quantitative PET image reconstruction requires an accurate attenuation map of the body under study for the purpose of attenuation compensation. Before the advent of PET/CT, attenuation correction was always calculated using transmission measurements from a γ-ray source such as ^{68}Ge that takes about 20 min compared to about 20 s for CT. PET/CT has demonstrated the advantages of a combined system in oncological imaging especially for staging and radiotherapy planning. Current systems are based on sequential imaging with movement of the patient table between the CT and PET systems. Future systems could be based on the same detector array for PET and CT in order to perform simultaneous imaging. This would imply the development of stationary detector CT with multiple X-ray sources and the development of a detector material sensitive to both X-rays and γ-rays. As MR has better soft-tissue contrast than CT, combined PET/MR systems are being evaluated that can either be used for sequential or simultaneous imaging. Simultaneous PET/MR imaging systems require a ring of PET detectors inside the MR magnet. As magnetic fields interfere with the photomultipliers used in conventional PET systems, their place is being taken by avalanche photodiodes (APTs) (Grazioso et al., 2006). It will be important to have a system of temperature compensation as APTs are sensitive to temperature and MR magnet bores heat up during imaging. MR attenuation correction methods based on proton density measurements and other methods such as inferred information from a stored atlas are being developed (Buzug et al., 2007; Martínez-Möller et al., 2007; Hofmann et al., 2007) to avoid the necessity to use transmission measurements from a ^{68}Ge source. The ^{68}Ge source probably would not fit in the magnet bore and in any case would reduce productivity due to the long acquisition time and make such a system not commercially viable.

8.18. *Dedicated PET systems*

Organ specific PET imaging systems are being developed in order to optimize resolution and allow access for biopsies. A high-resolution, small field of view, positron emission mammography/tomography imaging and biopsy device (called PEM/PET) is being developed (Raylman et al., 2008) to detect and guide the biopsy of suspicious breast lesions. It is hoped this will reduce the amount of negative biopsies.

9. Summary

Multiple biomedical imaging techniques are used in all phases of cancer management. Imaging forms an essential part of cancer clinical protocols and is able to furnish morphological, structural, metabolic and functional information. Integration with other diagnostic tools such as in vitro tissue and fluids analysis assists in clinical decision-making. Hybrid imaging techniques are able to supply complementary information for improved staging and therapy planning. Image guided and targeted minimally invasive therapy has the promise to improve outcome and reduce collateral effects. Early detection of cancer through screening based on imaging is probably the major contributor to a reduction in mortality for certain cancers. Targeted imaging of receptors, gene therapy expression and cancer stem cells are research activities that will translate into clinical use in the next decade. Technological developments will increase imaging speed to match that of physiological processes. Targeted imaging and therapeutic agents will be developed in tandem through close collaboration between academia and biotechnology, information technology and pharmaceutical industries.

REFERENCES

Aberg, P., Nicander, I., Hansson, J., Geladi, P., Holmgren, U., Ollmar, S., 2004. Skin cancer identification using multifrequency electrical impedance – a potential screening tool. IEEE Transactions on Biomedical Engineering 51, 2097–2102.

Aboagye, E.O., Bhujwalla, Z.M., 1999. Malignant transformation alters membrane choline phospholipid metabolism of human mammary epithelial cells. Cancer Research 59, 80–84.

Aboagye, E.O., Bhujwalla, Z.M., Shungu, D.C., Glickson, J.D., 1998. Detection of tumour response to chemotherapy by ^{1}H nuclear magnetic resonance spectroscopy: effect of 5-fluorouracil on lactate levels in radiation-induced fibrosarcoma I tumours. Cancer Research 58, 1063–1067.

Abourbeh, G., Dissoki, S., Jacobson, O., et al., 2007. Evaluation of radiolabeled ML04, a putative irreversible inhibitor of epidermal growth factor receptor, as a bioprobe for PET imaging of EGFR-overexpressing tumors. Nuclear Medicine and Biology 34, 55–70.

Albertoni, P., 2003. Novel antitenascin antibody with increased tumour localisation for pretargeted antibody-guided radioimmunotherapy (PAGRIT). British Journal of Cancer 88, 996–1003.

American College of Radiology, 2004. Breast Imaging Reporting and Data System (BI-RADS), fourth ed. American College of Radiology, Reston, VA.

Anderson, H.L., Yap, J.T., Miller, M.P., et al., 2003. Assessment of pharmacodynamic vascular response in a phase I trial of combretastatin A4 phosphate. Journal of Clinical Oncology 21, 2823–2830.

Anwer, K., et al., 2000. Ultrasound enhancement of cationic lipid mediated gene transfer to primary tumors following systemic administration. Gene Therapy 7, 1833–1839.

Ardenkjaer-Larsen, J.H., et al., 2003. Increase in signal-to noise ratio of >10,000 times in liquid-state NMR. Proceedings of the National Academy of Sciences USA 100, 10158–10163.

Artemov, D., Mori, N., Okollie, B., Bhujwalla, Z.M., 2003. MR molecular imaging of the Her-2/neu receptor in breast cancer cells using targeted iron oxide nanoparticles. Magnetic Resonance in Medicine 49, 403–408.

Ashamalla, H., Rafla, S., Parikh, K., Mokhtar, B., Goswami, G., Kambam, S., et al., 2005. The contribution of integrated PET/CT to the evolving definition of treatment volumes in radiation treatment planning in lung cancer. International Journal of Radiation Oncology Biology Physics 63, 1016–1023.

Atri, M., 2006. New technologies and directed agents for applications of cancer imaging. Journal of Clinical Oncology 24 (20), 3299–3308.

Backer, M.V., et al., 2007. Molecular imaging of VEGF receptors in angiogenic vasculature with single-chain VEGF-based probes. Nature Medicine 13, 504–509.

Bae, U., et al., 2007. Ultrasound thyroid elastography using carotid artery pulsation. Journal of Ultrasound in Medicine 26, 797–805.

Balamugesh, T., et al., 2005. Empyema – a rare complication of transbronchial lung biopsy. Respiratory Medicine Extra 1 (3), 97–99.

Bartella, L., Huang, W., 2007. Proton (^{1}H) MR spectroscopy of the breast. RadioGraphics 27, S241–S252.

Bartella, L., et al., 2007. Enhancing non-mass lesions in the breast: evaluation with proton (^{1}H) MR spectroscopy. Radiology 245, 80–87.

Barthel, H., et al., 2003. 3′-Deoxy-3′-[^{18}F]fluorothymidine as a new marker for monitoring tumor response to antiproliferative therapy in vivo with positron emission tomography. Cancer Research 63, 3791–3798.

Bauer, W., Claudia, C., Langer, O., 2008. Microdosing studies in humans: the role of positron emission tomography. Drugs in R & D 9 (2), 73–81.

Bayford, R.H., 2006. Bioimpedance tomography (electrical impedance tomography). Annual Review of Biomedical Engineering 8, 63–91.

Beck, R., et al., 2007. Pretreatment ^{18}F-FAZA predicts success of hypoxia directed radiochemotherapy using tirapazamine. Journal of Nuclear Medicine 48 (6), 973–980.

Beer, A.J., Haubner, R., Wolf, I., et al., 2006. PET-based human dosimetry of ^{18}Fgalacto- RGD, a new radiotracer for imaging alpha v beta3 expression. Journal of Nuclear Medicine 47, 763–769.

Beheshti, M., et al., 2007. [^{18}F]Fluorocholine PET/CT in the assessment of bone metastases in prostate cancer. European Journal of Nuclear Medicine and Molecular Imaging 34 (8), 1316–1317.

Belfiore, G., Tedeschi, E., Moggio, G., Coffi, R., Cincotti, F.C., Rossi, R., 2004. CT-guided radiofrequency palliative ablation of unresectable lung cancer: clinical and imaging findings at one-year follow-up. Radiology 233, 513. abstract SSK05-06.

Belhocine, T.Z., et al., 2006. Role of nuclear medicine in the management of cutaneous malignant melanoma. Journal of Nuclear Medicine 47, 957–967.

Bergers, G., Song, S., 2005. The role of pericytes in blood-vessel formation and maintenance. Neuro-Oncology 7 (4), 452–464.

Bergland, A., et al., 2001. Metaiodobenzylguanidine (MIBG) scintigraphy and computed tomography (CT) in clinical practice. Primary and secondary evaluation for localization of phaeochromocytomas. Journal of Internal Medicine 249 (3), 247–251.

Bergstrom, M., Grahnen, A., Langstrom, B., 2003. Positron emission tomography microdosing: A new concept with application in tracer and early clinical drug development. European Journal of Clinical Pharmacology 59, 357–366.

Bertino Jr., J.S., Greenberg, H.E., Reed, M.D., 2007. American College of Clinical Pharmacology Position Statement on the Use of Microdosing in the Drug Development Process. Journal of Clinical Pharmacology 47 (4), 418–422.

Beyer, T., Townsend, D.W., Blodgett, T.M., 2002. Dual-modality PET/CT tomography for clinical oncology. Quarterly Journal of Nuclear Medicine 46, 24–34.

Bhattacharyya, M., et al., 2008. Using MRI to plan breast-conserving surgery following neoadjuvant chemotherapy for early breast cancer. British Journal of Cancer 98, 289–293.

Blana, A., Walter, B., Rogenhofer, S., Wieland, W.F., 2004. High-intensity focused ultrasound for the treatment of localized prostate cancer: 5-year experience. Urology 63, 297–300.

Boddy, A.V., et al., 2007. Pharmacokinetic investigation of imatinib using accelerator mass spectrometry in patients with chronic myeloid leukemia. Clinical Cancer Research 13, 4164–4169.

Bohndiek, S.E., et al., 2008. A CMOS active pixel sensor system for laboratory-based x-ray diffraction studies of biological tissue. Physics in Medicine and Biology 53, 655–672.

Bolster, J.M., Vaalburg, W., Paans, A.M., et al., 1986. Carbon-11 labelled tyrosine to study tumor metabolism by positron emission tomography (PET). European Journal of Nuclear Medicine 12, 321–324.

Brasch, R., Turetschek, K., 2000. MRI characterization of tumors and grading angiogenesis using macromolecular contrast media: status report. European Journal of Radiology 34, 148–155.

Brem, R.F., Rapelyea, J.A., Zisman, G., et al., 2005. Occult breast cancer: scintimammography with high-resolution breast-specific gamma camera in women at high risk for breast cancer. Radiology 237 (1), 274–280.

Brem, R.F., et al., 2007. Breast-specific gamma imaging with 99mTc-sestamibi and magnetic resonance imaging in the diagnosis of breast cancer: a comparative study. Breast Journal 13 (5), 465–469.

Brenner, D.J., Elliston, C.D., Hall, E.J., et al., 2002. Estimating cancer risks from pediatric CT: going from the qualitative to the quantitative. Pediatric Radiology 32, 228–231.

Brindle, K.M., 2003. Molecular imaging using magnetic resonance: new tools for the development of tumour therapy. British Journal of Radiology 76, S111–S117.

Brindle, K., 2008. New approaches for imaging tumour responses to treatment. Nature Reviews Cancer 8, 94–107.

Brink, I., Schumacher, T., Mix, M., et al., 2004. Impact of [^{18}F]FDG-PET on the primary staging of small-cell lung cancer. European Journal of Nuclear Medicine and Molecular Imaging 31, 1614–1620.

Brix, G., Lechel, U., Glatting, G., 2005. Radiation exposure of patients undergoing whole-body dual-modality ^{18}F-FDG PET/CT examinations. Journal of Nuclear Medicine 46, 608–613.

Buadu, L.D., et al., 1996. Breast lesions: correlation of contrast medium enhancement patterns on MR images with histopathologic findings and tumor angiogenesis. Radiology 200, 639–649.

Buckley, D.L., et al., 1997. Microvessel density of invasive breast cancer assessed by dynamic Gd-DTPA enhanced MRI. Journal of Magnetic Resonance Imaging 7, 461–464.

Buijs, M., et al., 2007. Assessment of metastatic breast cancer response to chemoembolization with contrast agent enhanced and diffusion-weighted MR imaging. Journal of Vascular and Interventional Radiology 18 (8), 957–963.

Burnside, E., et al., 2007. Differentiating benign from malignant solid breast masses with US strain imaging. Radiology 245 (2), 401–410.

Buzug, T.M., et al., 2007. MRI based attenuation correction for brain PET images. Advances in Medical Imaging 114, 93–97.

Byrne, A., Nadel, H., 2007. Whole body low dose ^{18}F-FDG PET/CT in pediatric oncology. Journal of Nuclear Medicine 48 (suppl. 2), 118. abstract.

Cai, W., et al., 2006. PET of vascular endothelial growth factor receptor expression. Journal of Nuclear Medicine 47, 2048–2056.

Campadelli, P., Casiraghi, I., Artioli, D.A., 2006. Fully automated method for lung nodule detection from postero-anterior chest radiographs. Medical Imaging 25 (12), 1588–1603.

Carrino, J.A., Jolesz, F.A., 2005. MRI-guided interventions. Academic Radiology 12, 1063–1064.

Cascini, G.L., et al., 2006. ^{18}F-FDG PET is an early predictor of pathologic tumor response to preoperative radiochemotherapy in locally advanced rectal cancer. Journal of Nuclear Medicine 47 (8), 1241–1248.

Catane, R., et al., 2007. MR-guided focused ultrasound surgery (MRgFUS) for the palliation of pain in patients with bone metastases – preliminary clinical experience. Annals of Oncology 18, 163–167.

Chan, W.C., Maxwell, D.J., Gao, X., Bailey, R.E., Han, M., Nie, S., 2002. Luminescent quantum dots for multiplexed biological detection and imaging Current Opinion in Biotechnology 13, 40–46.

Chen, W., et al., 2005. Imaging proliferation in brain tumors with ^{18}F-FLT PET: comparison with ^{18}F-FDG. Journal of Nuclear Medicine 46 (6), 945–952.

Chen, X., et al., 2004a. MicroPET imaging of brain tumor angiogenesis with ^{18}F labeled PEGylated RGD peptide. European Journal of Nuclear Medicine and Molecular Imaging 31 (8), 1081–1089.

Chen, X., et al., 2004b. MicroPET imaging of breast cancer alpha(v)-integrin expression with ^{64}Cu-labeled dimeric RGD peptides. Molecular Imaging and Biology 6 (5), 350–359.

Chen, X., et al., 2004c. Pharmacokinetics and tumor retention of (125)I-labeled RGD peptide are improved by PEGylation. Nuclear Medicine and Biology 31 (1), 11–19.

Chen, X., Plasencia, C., Hou, Y., et al., 2005. Synthesis and biological evaluation of dimeric RGD peptide-paclitaxel conjugate as a model for integrin-targeted drug delivery. Journal of Medicinal Chemistry 48, 1098–1106.

Chenevert, T.L., Stegman, L.D., Taylor, J.M.G., Robertson, P.L., Greenberg, H.S., Rehemtulla, A., et al., 2000. Diffusion magnetic resonance imaging: an early surrogate marker of therapeutic efficacy in brain tumors. Journal of the National Cancer Institute 92, 2029–2036.

Cherepenin, V., et al., 2001. A 3D electrical impedance tomography (EIT) system for breast cancer detection. Physiological Measurement 22, 9–18.

Ciernik, I.F., Dizendorf, E., Baumert, B.G., Reiner, B., Burger, C., Davis, J.B., et al., 2003. Radiation treatment planning with an integrated positron emission and computer tomography (PET/CT): a feasibility study. International Journal of Radiation Oncology Biology Physics 57, 853–863.

Civelek, A.C., et al., 2006. Tc-99m sestamibi uptake in the chest mimicking a malignant lesion of the breast. The Breast 15 (1), 111–114.

Cohen, A., et al., 2007. Monitoring of chemotherapy induced cell death in melanoma tumors by N,N′-didansyl-L-cystine. Technology in Cancer Research & Treatment 6 (3), 221–234.

Coover, L.R., Caravaglia, G., Kunh, P., et al., 2004. Scintimammography with dedicated breast camera detects and localizes occult carcinoma. Journal of Nuclear Medicine 45 (4), 553–558.

Czernin, J., Weber, W.A., Herschman, H.R., 2006. Molecular imaging in the development of cancer therapeutics. Annual Reviews of Medicine 57, 99–118.

Damadian, R., 1971. Tumor detection by nuclear magnetic resonance. Science 171, 1151–1153.

Day, S.E., et al., 2007. Detecting tumor response to treatment using hyperpolarized ^{13}C magnetic resonance imaging and spectroscopy. Nature Medicine 13, 1382–1387.

De Boer, R.J., et al., 2002. Carbon-11 tyrosine PET for visualization and protein synthesis rate assessment of laryngeal and

hypopharyngeal carcinomas. European Journal of Nuclear Medicine 29, 1182–1187.
de Geus-Oei, L.-F., et al., 2007. Chemotherapy response evaluation with ^{18}F-FDG PET in patients with non-small cell lung cancer. Journal of Nuclear Medicine 48 (10), 1592–1598.
de Geus-Oei, L.F., et al., 2008. Chemotherapy response evaluation with FDG-PET in patients with colorectal cancer. Annals of Oncology 19 (2), 348–352.
de Torres, J.P., et al., 2007. Assessing the relationship between lung cancer risk and emphysema detected on low-dose CT of the chest. Chest 132, 1932–1938.
Dehdashti, F., et al., 1995. Positron tomographic assessment of estrogen receptors in breast cancer: comparison with FDG-PET and in vitro receptor assays. Journal of Nuclear Medicine 36 (10), 1766–1772.
Dehdashti, F., et al., 2005. Positron tomographic assessment of androgen receptors in prostatic carcinoma. European Journal of Nuclear Medicine and Molecular Imaging 32 (3), 344–350.
Dehghani, H., Pogue, P.W., Poplack, S.P., Paulsen, K.D., 2003. Multiwavelength three-dimensional near-infrared tomography of the breast: initial simulation, phantom, and clinical results. Applied Optics 42, 135–145.
Dekker, B., Keen, H., Lyons, S., et al., 2005. MBP-annexin V radiolabeled directly with iodine-124 can be used to image apoptosis in vivo using PET. Nuclear Medicine and Biology 32, 241–252.
D'Hallewin, M.A., El Khatib, S., Leroux, A., Bezdetnaya, L., Guillemin, F., 2005. Endoscopic confocal fluorescence microscopy of normal and tumor bearing rat bladder. Journal of Urology 174 (2), 736–740.
Diekmann, F., Bick, U., 2007. Tomosynthesis and contrast-enhanced digital mammography; recent advances in digital mammography. European Radiology 17 (12), 3086–3092.
Dobbins, J.T., et al., 2003. Digital x-ray tomosynthesis: current state of the art and clinical potential. Physics in Medicine and Biology 48, R65–R106.
Downey, R.J., Akhurst, T., Ilson, D., et al., 2003. Whole body18-F FDG-PET and the response of esophageal cancer to induction therapy: results of a prospective trial. Journal of Clinical Oncology 21, 428–432.
Downey, R.J., Akhurst, T., Gonen, M., et al., 2004. Preoperative F-18 fluorodeoxyglucose-positron emission tomography maximal standardized uptake value predicts survival after lung cancer resection. Journal of Clinical Oncology 22, 3255–3260.
Dromi, S., et al., 2007. Pulsed-high intensity focused ultrasound and low temperature-sensitive liposomes for enhanced targeted drug delivery and anti-tumor effect. Clinical Cancer Research 13 (9), 2722–2727.
Dugdale, P.E., Miles, K.A., Bunce, I., Kelley, B.B., Leggett, D.A.C., 1999. CT measurement of perfusion and permeability within lymphoma masses and its ability to assess grade, activity, and chemotherapeutic response. Journal of Computer Assisted Tomography 23 (4), 540–547.
Ehman, R.L., et al., 2007. Blueprint for imaging in biomedical research. Radiology 244 (1), 12.
Enquobahrie, A.A., et al., 2007. Automated detection of small pulmonary nodules in whole lung CT scans. Academic Radiology 14 (5), 579–593.
Eriksson, B., et al., 2002. The role of PET in localization of neuroendocrine and adrenocortical tumors. Annals of the New York Academy of Sciences 970, 159–169.
Eschmann, S.M., Paulsen, F., Reimold, M., et al., 2005. Prognostic impact of hypoxia imaging with ^{18}F-misonidazole PET in non-small cell lung cancer and head and neck cancer before radiotherapy. Journal of Nuclear Medicine 46, 253–260.
European Agency for the Evaluation of Medicinal Products, 2003. Evaluation of Medicines for Human Use. Position Paper on Non-Clinical Safety Studies to Support Clinical Trials with a Single Microdose. EMEA, London, pp. 1-4.
Evans, S.F., et al., 2006. ^{18}F EF5 PET imaging with immunohistochemical validation in patients with brain lesions. International Journal of Radiation Oncology Biology Physics 66 (3), S248.
Even-Sapir, E., et al., 2003. Lymphoscintigraphy for sentinel node mapping using a hybrid SPECT/CT system. Journal of Nuclear Medicine 44 (9), 1413–1420.
Fahey, B.J., et al., 2006. Liver ablation guidance with acoustic radiation force impulse imaging: challenges and opportunities. Physics in Medicine and Biology 51, 3785–3808.
Fahey, B.J., et al., 2008. In vivo visualization of abdominal malignancies with acoustic radiation force elastography. Physics in Medicine and Biology 53, 279–293.
Fani, M., et al., 2006. Comparative evaluation of linear and cyclic ^{99m}Tc-RGD peptides for targeting of integrins in tumor angiogenesis. AntiCancer Research 26 (1A), 431–434.
Fermé, C., et al., 2005. Role of imaging to choose treatment. Cancer Imaging 5, S113–S119.
Fogelman, I., et al., 2005. Positron emission tomography and bone metastases. Seminars in Nuclear Medicine 35 (2), 135–142.
Folkman, J., 1992. The role of angiogenesis in tumor growth. Seminars in Cancer Biology 3, 65–71.
Fournier, L., et al., 2007. Dynamic contrast-enhanced CT (DCE-CT) as an early biomarker of response in metastatic renal cell carcinoma (mRCC) under anti-angiogenic treatment. 2007 ASCO Annual Meeting Proceedings Part I. Journal of Clinical Oncology 25 (18S) (abstract 14003).
Franceschini, M.A., et al., 1997. Frequency-domain techniques enhance optical mammography: initial clinical results. Proceedings of the National Academy of Sciences USA 94, 6468–6473.
Frank, R., Hargreaves, R., 2003. Clinical biomarkers in drug discovery and development. Nature Reviews Drug Discovery 2 (7), 566–580.
Front, D., et al., 2000. Aggressive non-Hodgkin lymphoma: early prediction of outcome with ^{67}Ga scintigraphy. Radiology 214, 253–257.
Frush, D.P., Donnelly, L.F., Rosen, N.S., 2003. Computed tomography and radiation risks: what pediatric health care providers should know. Pediatrics 112, 951–957.
Furtado, C.D., et al., 2005. Whole body CT screening: spectrum of findings and recommendations in 1192 patients. Radiology 237 (2), 385–394.
Furusawa, H., Namba, K., Thomasen, S., Akiyama, F., Bendet, A., Tanaka, C., Yasuda, Y., Nakahara, H., 2006. Magnetic resonance-guided focused ultrasound surgery of breast cancer: reliability and effectiveness. Journal of the American College of Surgeons 203 (1), 54–63.
Gangi, A., et al., 1994. Injection of alcohol into bone metastases under CT guidance. Journal of Computer Assisted Tomography 18, 932–935.
Gao, X., Yang, L., Petros, J.A., et al., 2005. In vivo molecular and cellular imaging with quantum dots. Current Opinion in Biotechnology 16, 63–72.
Gao Z, et al. Drug-loaded nano/microbubbles for combining ultrasonography and targeted chemotherapy. Ultrasonics, in press.
GE Senographe, 1999. 2000D FDA PMA submission P990066.
Geddes, L.A., Baker, L.E., 1967. The specific resistance of biological materials: a compendium of data for the biomedical engineer and physiologist. Medical and Biological Engineering 5, 271–293.
Getty D, et al. 2007. Improved accuracy of lesion detection in breast cancer screening with stereoscopic digital mammography. RSNA Meeting 2007 (abstract SSG01–04).
Ghandi, S., et al., 2006. Lipiodol-guided computed tomography for radiofrequency ablation of hepatocellular carcinoma. Clinical Radiology 61 (10), 888–891.

Gianfelice, D., Khiat, A., Boulanger, Y., et al., 2003. Feasibility of magnetic resonance imaging-guided focused ultrasound surgery as an adjunct to tamoxifen therapy in high-risk surgical patients with breast carcinoma. Journal of Vascular and Interventional Radiology 14, 1275–1282.

Gilkeson, R.C., Sachs, P.B., 2006. Dual energy subtraction digital radiography: technical considerations, clinical applications, and imaging pitfalls. classic concepts in thoracic imaging. Journal of Thoracic Imaging 21 (4), 303–313.

Gillies, R.J., Morse, D.L., 2005. In vivo magnetic resonance spectroscopy in cancer. Annual Review of Biomedical Bioengineering 7, 287–326.

Gillies, J.M., et al., 2006. Microfluidic technology for PET radiochemistry. Applied Radiation and Isotopes 64 (3), 333–336.

Ginos, J.Z., Cooper, A.J., Dhawan, V., et al., 1987. [^{13}N]Cisplatin PET to assess pharmacokinetics of intra-arterial versus intravenous chemotherapy for malignant brain tumors. Journal of Nuclear Medicine 28, 1844–1852.

Goel M, et al., 2006. Application of near infrared multi-spectral CCD imager system to determine the hemodynamic changes in prostate tumor. OSA Biomedical Topical Meetings: SH10, Fort Lauderdale, FL.

Golman, K., Petersson, J.S., 2006. Metabolic imaging and other applications of hyperpolarized 13C. Academic Radiology 13, 932–942.

Golman, K., Zandt, R.I., Lerche, M., Pehrson, R., Ardenkjaer-Larsen, J.H., 2006a. Metabolic imaging by hyperpolarized ^{13}C magnetic resonance imaging for in vivo tumor diagnosis. Cancer Research 66, 10855–10860.

Golman, K., Zandt, R.I., Thaning, M., 2006b. Real-time metabolic imaging. Proceedings of the National Academy of Sciences USA 103, 11270–11275.

Grazioso, R., et al., 2006. APD-based PET detector for simultaneous PET/MR imaging. Nuclear Instruments and Methods in Physics Research Section A: Accelerators, Spectrometers. Detectors and Associated Equipment 569 (2), 301–305.

Gromet, M., 2008. Comparison of computer-aided detection to double reading of screening mammograms: review of 231,221 mammograms. AJR American Journal of Roentgenology 190 (4), 854–859.

Grönroos, T., et al., 2004. Comparison of the biodistribution of two hypoxia markers[^{18}F]FETNIM and [^{18}F]FMISO in an experimental mammary carcinoma. European Journal of Nuclear Medicine and Molecular Imaging 31 (4), 513–520.

Grosenick, D., et al., 1999. Development of a time domain optical mammograph and first in vivo applications. Applied Optics 38, 2927–2943.

Grosu, A., et al., 2005. Hypoxia imaging with ^{18}F-FAZA-PET for dose painting using intensity modulated radiotherapy in patients with head and neck cancer. International Journal of Radiation Oncology Biology Physics 63 (Suppl 1), S132–S133.

Gu, X., et al., 2004. Differentiation of cysts from solid tumors in the breast with diffuse optical tomography. Academic Radiology 11 (1), 2094–2107.

Gupta, N., Price, P.M., Aboagye, E.O., 2002. PET for in vivo pharmacokinetic and pharmacodynamic measurements. European Journal of Cancer 38, 2094–2107.

Gusev, V.E., Karabutov, A.A., 1993. Laser Optoacoustics. American Institute of Physics.

Haider, M.A., et al., 2000. Combined T2-weighted and diffusion-weighted MRI for localization of prostate cancer. AJR American Journal of Roentgenology 189, 323–328.

Hainfeld, J.F., Slatkin, D.N., Focella, T.M., Smilowitz, H.M., 2006. Gold nanoparticles: a new X-ray contrast agent. British Journal of Radiology 79, 248–253.

Halter R, Hatrov A, Paulsen KD. High frequency EIT for breast imaging. Sixth Conference on Biomedical Application of Electrical Impedance Tomography, London, UK (2005).

Halter, R.J., Hartov, A., Paulsen, K.D., 2008. A broadband high-frequency electrical impedance tomography system for breast imaging. IEEE Transactions on Biomedical Engineering 55 (2), 650–659.

Harishingani, M.G., et al., 2003. Noninvasive detection of clinically occult lymph-node metastases in prostate cancer. New England Journal of Medicine 348, 2491–2499.

Hayashi, K., et al., 2007. Local therapeutic results of computed tomography-guided transcatheter arterial chemoembolization for hepatocellular carcinoma: results of 265 tumors in 79 patients. Cardiovascular and Interventional Radiology 30, 1144–1155.

He, W., Wang, H.F., Hartmann, L.C., Cheng, J.X., Low, P.S., 2007. In vivo quantitation of rare circulating tumor cells by multiphoton intravital flow cytometry. Proceedings of the National Academy of Sciences USA 104, 11760–11765.

Hehenberger, M., et al., 2007. IT solutions for imaging biomarkers in biopharmaceutical research and development. Information-Based Medicine 46 (1), 183–198.

Heilbrun, M.E., et al., 2007. CT-guided biopsy for the diagnosis of renal tumors before treatment with percutaneous ablation. AJR American Journal of Roentgenology 188 (6), 1500–1505.

Helbich, T.H., Roberts, T.P., Gossmann, A., et al., 2000. Quantitative gadopentetate-enhanced MRI of breast tumors: testing of different analytic methods. Magnetic Resonance in Medicine 44, 915–924.

Hellstrom, M., Svensson, M.H., Lasson, A., 2004. Extracolonic and incidental findings on CT colonography (virtual colonoscopy). AJR American Journal of Roentgenology 182 (3), 631–638.

Hendrikse, N.H., Vaalburg, W., 2002. Dynamics of multidrug resistance: P-glycoprotein analyses with positron emission tomography. Methods 27 (3), 228–233.

Hennings, J., et al., 2006. [^{11}C]Metomidate positron emission tomography of adrenocortical tumors in correlation with histopathological findings. Journal of Clinical Endocrinology and Metabolism 91 (4), 1410–1414.

Henschke, C.I., Yankelevitz, D.F., Libby, D.M., Pasmantier, M.W., Smith, J.P., 2006. Miettinen OS. Survival of patients with stage I lung cancer detected on CT screening. New England Journal of Medicine 355 (17), 1763–1771.

Henschke, C.I., et al., 2007. Survival of patients with clinical stage I lung cancer diagnosed by computed tomography screening for lung cancer. Clinical Cancer Research 13 (17), 4949–4950.

Henschke, C.I., 2007. Computed tomography screening for lung cancer. JAMA 298 (5), 514–515.

Herbst, R.S., Mullani, N.A., Davis, D.W., et al., 2002. Development of biologic markers of response and assessment of antiangiogenic activity in a clinical trial of human recombinant endostatin. Journal of Clinical Oncology 20, 3804–3814.

Herrmann, K., et al., 2007. Early response assessment using 3′-deoxy-3′-[^{18}F]fluorothymidine-positron emission tomography in high-grade non-Hodgkin's lymphoma. Clinical Cancer Research 13 (12), 3552–3558.

Hillman, B.J., 2006. Introduction to the Special Issue on Medical Imaging in Oncology. Journal of Clinical Oncology 24 (20), 3223–3224.

Hillner, B.E., et al., 2007. The National Oncologic PET Registry (NOPR): design and analysis plan. Journal of Nuclear Medicine 48 (11), 1901–1908.

Hindley, J., Gedroyc, W.M., Regan, L., et al., 2004. MRI guidance of focused ultrasound therapy of uterine fibroids: early results. AJR American Journal Roentgenology 183, 1713–1719.

Hirsch, L.R., Halas, N.J., West, J.L., 2003. Nanoshell-mediated near- infrared thermal therapy of tumors under magnetic resonance guidance. Proceedings of the National Academy of Sciences USA 100, 13549–13554.

Ho, C.-L., et al., 2003. ^{11}C-acetate imaging in hepatocellular carcinoma and other liver masses. Nuclear Medicine 44 (2), 213–221.

Hofmann, M., et al., 2007. MR-based PET attenuation correction: method and validation. Proceedings of the 2007 IEEE Nuclear Science Symposium and Medical Imaging Conference (NSS-MIC 2007), 6. IEEE Computer Society, Los Alamitos, CA, USA.

Holdsworth, C.H., et al., 2007. CT and PET: early prognostic indicators of response to imatinib mesylate in patients with gastrointestinal stromal tumor. AJR American Journal of Roentgenology 189, W324–W330.

Hosseinzadeh, K., Schwarz, S.D., 2004. Endorectal diffusion-weighted imaging in prostate cancer to differentiate malignant and benign peripheral zone tissue. Journal of Magnetic Resonance Imaging 20, 654–661.

Hricak, H., 2007. MRI and choline-PET of the prostate, Refresher Course 88 Deutsche RoentgenKongress. Fortschritte der Röntgenstrahlen 179 (Suppl.).

Huang, S.C., 2000. Anatomy of SUV. Nuclear Medicine and Biology 27, 643–646.

Hui, Zhi, et al., 2007. Comparison of ultrasound elastography, mammography, and sonography in the diagnosis of solid breast lesions. Journal Ultrasound in Medicine 26, 807–815.

Hung, S.C., et al., 2005. Mesenchymal stem cell targeting of microscopic tumors and tumor stroma development monitored by noninvasive in vivo positron emission tomography imaging. Clinical Cancer Research 11 (21), 7749–7756.

Husarik, D.B., et al., 2008. Evaluation of [^{18}F]-choline PET/CT for staging and restaging of prostate cancer. European Journal of Nuclear Medicine and Molecular Imaging 35 (2), 253–263.

Hynynen, K., et al., 2005. Local and reversible blood-brain barrier disruption by noninvasive focused ultrasound at frequencies suitable for trans-skull sonications. Neuroimage 24 (1), 12–20.

Iinuma, G., Ushio, K., Ishikawa, T., Nawano, S., Sekiguchi, R., Satake, M., 2000. Diagnosis of gastric cancers comparison of conventional radiography with a 4 million-pixel charge coupled device. Radiology 214 (2), 497.

Ilias, I., et al., 2003. Superiority of 6-[^{18}F]-fluorodopamine positron emission tomography versus [^{131}I]-metaiodobenzylguanidine scintigraphy in the localization of metastatic pheochromocytoma. Journal of Clinical Endocrinology & Metabolism 88 (9), 4083–4087.

Inoue, T., Kim, E.E., Wallace, 1996. S et al. Positron emission tomography using[^{18}F]fluorotamoxifen to evaluate therapeutic responses in patients with breast cancer: preliminary study. Cancer Biotherapy & Radiopharmaceuticals 11, 235–245.

Intenzo, C.M., et al., 2007. Scintigraphic imaging of body neuroendocrine tumors. Radiographics 27, 1355–1369.

Intes, X., 2005. Time-domain optical mammography SoftScan: initial results. Academic Radiology 12 (8), 934–947 (erratum 12(10), 1355).

Itoh, A., Ueno, E., Tohno, E., et al., 2006. Breast disease: clinical application of US elastography for diagnosis. Radiology 239, 341–350.

Itoh, J., Osamura, R.Y., 2007. Quantum dots for multicolor tumor pathology and multispectral imaging. Methods in Molecular Biology 374, 29–42.

Jacobs, A.H., et al., 2005. ^{18}F-Fluoro-L-thymidine and ^{11}C-methyl-methionine as markers of increased transport and proliferation in brain tumors. Journal of Nuclear Medicine 46, 1948–1958.

Jager, P.L., Vaalburg, W., Pruim, J., de Vries, E.G., Langen, K.J., Piers, D.A., 2001. Radiolabeled amino acids: basic aspects and clinical applications in oncology. Journal of Nuclear Medicine 42 (3), 432–445.

Jain, M., Batra, S.K., 2003. Genetically engineered antibody fragments and PET imaging: a new era of radioimmunodiagnosis. Journal of Nuclear Medicine 44 (12), 1970.

Jeffrey, F.M.H., Rajagopal, A., Malloy, C.R., Sherry, A.D., 1991. ^{13}C NMR: a simple yet comprehensive method for analysis of intermediary metabolism. Trends in Biochemical Sciences 16, 5–10.

Jennewein, M., et al., 2008. Vascular imaging of solid tumors in rats with a radioactive arsenic-labeled antibody that binds exposed phosphatidylserine. Clinical Cancer Research 14, 1377–1385.

Jensch, S., et al., 2008. CT colonography with limited bowel preparation: performance characteristics in an increased-risk population. Radiology 247 (1), 122–132.

Joines, W.T., Zhang, Y., Li, C., Jirtle, R.L., 1994. The measured electrical properties of normal and malignant tissues from 50 to 900 MHz. Medical Physics 21, 547–550.

Jolesz, F.A., Hynynen, K., 2002. Magnetic resonance image-guided focused ultrasound surgery. Cancer Journal 8, S100–S112.

Jolesz, F.A., Hynynen, K., McDannold, N., Tempany, C., 2006. MR imaging-controlled focused ultrasound ablation: a noninvasive image guided surgery. Magnetic Resonance Imaging Clinics of North America 13, 545–560.

Jong, R.A., 2003. Contrast-enhanced digital mammography: initial clinical experience. Radiology 228 (3), 842–850.

Jung, K.H., et al., 2006. Favorable biokinetic and tumor-targeting properties of ^{99m}Tc-labeled glucosamino RGD and effect of paclitaxel therapy. Journal of Nuclear Medicine 47 (12), 2000–2007.

Juweid, M.E., Wiseman, G.A., Vose, J.M., et al., 2005. Response assessment of aggressive non-Hodgkin's lymphoma by integrated International Workshop Criteria and fluorine-18-fluorodeoxyglucose positron emission tomography. Journal of Clinical Oncology 23, 4652–4661.

Kamat, P.P., et al., 2008. Hepatic embolization in patients with liver metastases. Cardiovascular and Interventional Radiology 31 (2), 299–307.

Kao, T.J., et al., 2007. A compensated radiolucent electrode array for combined EIT and mammography. Physiological Measurement 28 (7), S291–S299.

Kao, T.J., Isaacson, D., Newell, J.C., Saulnier, G.J., 2006. A 3D reconstruction algorithm for EIT using a handheld probe for breast cancer detection. Physiological Measurement 27 (5), S1–S11.

Kato, T., Tsukamoto, E., Kuge, Y., Takei, T., Shiga, T., Shinohara, N., Katoh, C., Nakada, K., Tamaki, N., 2002. Accumulation of [^{11}C]acetate in normal prostate and benign prostatic hyperplasia: comparison with prostate cancer. European Journal of Nuclear Medicine and Molecular Imaging 29 (11), 1492–1495.

Kato, H., Fukuchi, M., Miyazaki, T., et al., 2007. Prediction of response to definitive chemoradiotherapy in esophageal cancer using positron emission tomography. AntiCancer Research 27, 2627–2633.

Kazuhiro, P., et al., 2006. Classifying pulmonary nodules using dynamic enhanced CT images. IEIC Technical Report (Institute of Electronics, Information and Communication Engineers) 106 (105), 39–43.

Keen, H.G., Dekker, B.A., Disley, L., et al., 2005. Imaging apoptosis in vivo using ^{124}I-annexin V and PET. Nuclear Medicine and Biology 32, 395–402.

Keidar, Z., Haim, N., Guralnik, L., Wollner, M., Bar-Shalom, R., Ben-Nun, A., et al., 2004. PET/CT using FDG in suspected lung cancer recurrence: diagnostic value and impact on patient management. Journal of Nuclear Medicine 45, 1640–1646.

Kemper, J., et al., 2004. MR elastography of the prostate: initial in-vivo application. Rofo 176 (8), 1094–1099.
Kenis, H., et al., 2007. Annexin A5: shifting from a diagnostic towards a therapeutic realm. Cellular and Molecular Life Sciences 64 (22), 2859–2862.
Kent, M.S., Port, J.L., Altorki, N.K., 2004. Current state of imaging for lung cancer staging. Thoracic Surgery Clinics 14, 1–13.
Khalkhali, I., Baum, J.K., Villanueva-Meyer, J., et al., 2002. (99m)Tc sestamibi breast imaging for the examination of patients with dense and fatty breasts: multicenter study. Radiology 222 (1), 149–155.
Kim, S.J., et al., 2008. Computer-aided detection in full-field digital mammography sensitivity and reproducibility in serial examinations. Radiology 246 (1), 71–79.
Kim, Y., et al., 2007. Multiphase contrast-enhanced CT imaging in hepatocellular carcinoma correlation with immunohistochemical angiogenic activities. Academic Radiology 14 (9), 1084–1091.
Kinoshita, M., 2006. Targeted drug delivery to the brain using focused ultrasound. Topics in Magnetic Resonance Imaging 17 (3), 209–215.
Kircher, M.F., Mahmood, U., King, R.S., Weissleder, R., Josephson, L.A., 2003. Multimodal nanoparticle for preoperative magnetic resonance imaging and intraoperative optical brain tumor delineation. Cancer Research 63, 8122–8125.
Kiss, G., Van Cleynenbreugel, J., Thomeer, M., Suetens, P., Marchal, G., 2001. Computer aided diagnosis for virtual colonography. In: MICCAI, Utrecht, The Netherlands. Lecture Notes in Computer Science 2208: 621.
Kob, W.-J., Rasey, J.S., Kvans, M.L., et al., 1992. Imaging of hypoxia in human tumors with [^{18}F] fluoromisonidazole. International Journal of Radiation Oncology Biology Physics 22, 199–212.
Kolb, T.M., et al., 2002. Comparison of the performance of screening mammography, physical examination, and breast US and evaluation of factors that influence them: an analysis of 27,825 patient evaluations. Radiology 225, 165–175.
Kopelman, D., Inbar, Y., Hanannel, A., Dank, G., Freundlich, D., Perel, A., Castel, D., Greenfeld, A., Salomon, T., Sareli, M., Valeanu, A., Papa, M., 2006. Magnetic resonance-guided focused ultrasound surgery (MRgFUS): four ablation treatments of a single canine hepatocellular adenoma. HPB 8, 292–298.
Koukouraki, S., et al., 2006. Evaluation of the pharmacokinetics of ^{68}Ga-DOTATOC in patients with metastatic neuroendocrine tumours scheduled for ^{90}Y-DOTATOC therapy. European Journal of Nuclear Medicine and Molecular Imaging 33 (4), 460–466.
Kruger, R.A., Miller, K.D., Reynolds, H.E., Kiser Jr., W.L., Reinecke, D.R., Kruger, G.A., 2000. Contrast enhancement of breast cancer in vivo using thermoacoustic CT at 434 MHz. Radiology 216, 279–283.
Kruse, S.A., Smith, J.A., Lawrence, A.J., et al., 2000. Tissue characterization using magnetic resonance elastography: preliminary results. Physics in Medicine and Biology 45, 1579–1590.
Kubota, K., Matsuzawa, T., Fujiwara, T., et al., 1989. Differential diagnosis of AH109A tumor and inflammation by radioscintigraphy with L-[methyl-^{11}C]]methionine. Japanese Journal of Cancer Research 80, 778–782.
Kuhl, C.K., Mielcareck, P., Klaschik, S., et al., 1999. Are signal time course data useful for differential diagnosis of enhancing lesions in dynamic breast MR imaging? Radiology 211 (1), 101–110.
Kumar, R., Shamim, S.A., 2004. Radiolabeled metaiodobenzylguanidine (MIBG) in the diagnosis and treatment of neural crest tumors. Journal of the Academy of Hospital Administration 16 (2), 7–12.
Kumar, S., et al., 2006. Biomarkers in cancer screening, research and detection: present and future: a review. Biomarkers 11 (5), 385–405.
Kurdziel, K.A., Kiesewetter, D.O., Carson, R.E., et al., 2003. Biodistribution, radiation dose estimates, and in vivo Pgp modulation studies of ^{18}F-paclitaxel in nonhuman primates. Journal of Nuclear Medicine 44, 1330–1339.
Kurhanewicz, J., et al., 2000. Three dimensional magnetic resonance spectroscopic imaging of brain and prostate cancer. Neoplasia 2 (1-2), 166–189.
Kushner, B.H., et al., 2003. Impact of metaiodobenzylguanidine scintigraphy on assessing response of high-risk neuroblastoma to dose-intensive induction chemotherapy. Journal of Clinical Oncology 21 (6), 1082–1086.
Kwan, A.L.C., et al., 2005. In: Flynn, M.J. (Ed.), Medical Imaging 2005: Physics of Medical Imaging. Proceedings of the SPIE, vol. 5745, pp. 1317–1321.
Långström, B., Itsenko, O., Rahman, O., 2007. [^{11}C]Carbon monoxide, a versatile and useful precursor in labelling chemistry for PET-ligand development. Journal of Labelled Compounds and Radiopharmaceuticals 50 (9-10), 794–810.
Larsen, S.S., et al., 2005. Endoscopic ultrasound guided biopsy versus mediastinoscopy for analysis of paratracheal and subcarinal lymph nodes in lung cancer staging. Lung Cancer 48 (1), 85–92.
Larson, S.M., Erdi, Y., Akhurst, T., et al., 1999. Tumor treatment response based on visual and quantitative changes in global tumor glycolysis using PET-FDG imaging, the visual response score and the change in total lesion glycolysis. Clinical Positron Imaging 2, 159–171.
Larson, S.S., et al., 2002. Endoscopic ultrasound guided biopsy of mediastinal lesions has a major impact on patient management. Thorax 57, 98–103.
Lauterbur, P.C., 1973. Image formation by induced local interactions: examples employing nuclear magnetic resonance. Nature 242, 190–191.
Le Bihan, D., Breton, E., Syrota, A., 1985. Imagerie de diffusion par resonance magnetique nucleaire. Les Comptes rendus de l'Académie des sciences 301, 1109–1112.
Leach, M.O., 2001. Application of magnetic resonance imaging to angiogenesis in breast cancer. Breast Cancer Research 3, 22–27.
Lee, K.S., Jeong, Y.J., Han, J., Kim, B.T., Kim, H., Kwon, O.J., 2004. T1 non-small cell lung cancer: imaging and histopathologic findings and their prognostic implications. Radiographics 24, 1617–1636.
Lehman, C.D., et al., 2007. Cancer yield of mammography, MR, and US in high-risk women: prospective multi-institution breast cancer screening study. Radiology 244 (2), 381–388.
Lehtio, K., Oikonen, V., Gronroos, T., et al., 2001. Imaging of blood flow and hypoxia in head and neck cancer: initial evaluation with [(15)O]H(2)O and[(18)F]fluoroerythronitroimidazole PET. Journal of Nuclear Medicine 42, 1643–1652.
Lehtio, K., et al., 2003. Quantifying tumour hypoxia with fluorine-18 fluoroerythronitroimidazole ([^{18}F]FETNIM) and PET using the tumour to plasma ratio. European Journal of Nuclear Medicine Molecular Imaging 30 (1), 101–108.
Lerman, H., et al., 2007. Improved sentinel node identification by SPECT/CT in overweight patients with breast cancer. Journal of Nuclear Medicine 48 (2), 201–206.
Lerner, R.M., Huang, S.R., Parker, K.J., 1990. ''Sonoelasticity'' images derived from ultrasound signals in mechanically vibrated tissues. Ultrasound in Medicine & Biology 16, 231–239.
Levchenko, A., Mehta, B.M., Lee, J.B., et al., 2000. Evaluation of ^{11}C-colchicine for PET imaging of multiple drug resistance. Journal of Nuclear Medicine 41, 493–501.

Lewin, J.M., et al., 2003. Dual-energy contrast enhanced digital subtraction mammography: feasibility. Radiology 229 (1), 261.
Li, H., Dai, H., Xing, L., Sinclair, R., 2006. Characterization of AuFe-C core-shell nanoparticles. Microscopy and Microanalysis 12, 524–525.
Li, K.C.P., Pandit, S.D., Guccione, S., Bednarski, M.D., 2004. Molecular imaging applications in nanomedicine. Biomedical Microdevices 6, 113–116.
Liapi, E., et al., 2008. Functional MRI evaluation of tumor response in patients with neuroendocrine hepatic metastases treated with transcatheter arterial chemoembolization. AJR American Journal of Roentgenology 190 (1), 67–73.
Liberman, L., Mason, G., Morris, E.A., et al., 2006. Does size matter? Positive predictive value of MRI-detected breast lesions as a function of lesion size. AJR American Journal of Roentgenology 186 (2), 426–430.
Linden, H.M., et al., 2006a. Monitoring targeted therapy: is fluorodeoxyglucose uptake a marker of early response? Clinical Cancer Research 12 (19), 5608–5610.
Linden, H.M., Stekhova, S.A., Link, J.M., et al., 2006b. Quantitative fluoroestradiol positron emission tomography imaging predicts response to endocrine treatment in breast cancer. Journal of Clinical Oncology 24, 2793–2799.
Liu, J., Levine, A., Mattoon, J., Yamaguchi, M., Lee, R., Pan, X., Rosol, T.J., 2006. Nanoparticles as image enhancing agents for ultrasonography. Physics in Medicine and Biology 51, 2179–2189.
Liu, J., Li, J., Rosol, T.J., Pan, X., Voorhees, J.L., 2007. Biodegradable nanoparticles for targeted ultrasound imaging of breast cancer cells in vitro. Physics in Medicine and Biology 52, 4739–4747.
Liu, S., 2007. Evaluation of a (99m)Tc-labeled cyclic RGD tetramer for noninvasive imaging integrin alpha(v)beta3-positive breast cancer. Bioconjugate Chemistry 18 (2), 438–446.
Liu, Y., Wang, H., 2007. Nanotechnology tackles tumours. Nature Nanotechnology 2 (1), 20–21.
Lo, W.K., van Sonnenberg, E., Shankar, S., Morrison, P.R., Silverman, S.G., Tuncali, K., Rabin, M., 2006. Percutaneous CT-guided radiofrequency ablation of symptomatic bilateral adrenal metastases in a single session. Journal of Vascular and Interventional Radiology 17, 175–179.
Lorenz, A., et al., 2000. Ultrasound elastography of the prostate. A new technique for tumor detection. Ultraschall in der Medizin 21 (1), 8–15.
Lövqvist, A., et al., 2001. PET imaging of ^{86}Y-labeled anti-Lewis Y monoclonal antibodies in a nude mouse model: comparison between ^{86}Y and ^{111}In radiolabels. Journal of Nuclear Medicine 42 (8), 1281–1286.
Luo, J., et al., 2006. Elasticity reconstruction for ultrasound elastography using a radial compression: an inverse approach. Ultrasonics 44 (Suppl. 1), e195–e198.
Machulla, H.J., Blocher, A., Kuntzsch, M., Piert, M., Wei, R., Grierson, J.R., 2000. Simplified labeling approach for synthesizing 39-deoxy-39-[^{18}F]fluorothymidine ([^{18}F]FLT). Journal of Radioanalytical and Nuclear Chemistry.,243, 843–846.
MacMahon, H., 2003. Dual-energy and temporal subtraction digital chest radiography. In: Samei, E., Flynn, M.J. (Eds.), Syllabus: Advances in Digital Radiography: RSNA Categorical Course in Diagnostic Radiology Physics. RSNA Publications, pp. 181–188.
Manohar, S., Kharine, A., van Hespen, J.C.G., Steenbergen, W., van Leeuven, T.G., 2005. The Twente photoacoustic mammoscope: system overview and performance. Physics in Medicine and Biology 50, 2543–2557.
Manohar, S., Vaartjes, S.E., van Hespen, J.C.G., Klaase, J.M., van den Engh, F.M., Steenbergen, W., van Leeuwen, T.G., 2007. Initial results of in vivo non-invasive cancer imaging in the human breast using near-infrared photoacoustics. Optics Express 15 (19), 12277–12285.
Mar, M.V., et al., 2007. Evaluation and localization of lymphatic drainage and sentinel lymph nodes in patients with head and neck melanomas by hybrid SPECT/CT lymphoscintigraphic imaging. Journal of Nuclear Medicine Technology 35 (1), 10–16.
Marchetti, S., Schellens, J.H., 2007. The impact of FDA and EMEA guidelines on drug development in relation to Phase 0 trials. British Journal of Cancer 97, 577–581.
Mardor, Y., 2003. Proceedings of the American Association for Cancer Research 41 (abstract 2547).
Mariani, G., et al., 2001. Radioguided sentinel lymph node biopsy in breast cancer surgery. Journal of Nuclear Medicine 42, 1198–1215.
Martínez-Möller, A., et al., 2007. An approach for MR-based attenuation correction for combined MR/PET: effects of ignoring bones. Journal of Nuclear Medicine 48 (Suppl. 2), 156P.
Maskell, N., Gleeson, F., Davies, R., 2003. CT-guided biopsy for diagnosis of malignant disease in pleural effusions. Lancet 362, 174.
Masuzaki, R., et al., 2007. Assessing liver tumor stiffness by transient elastography. Hepatology International 1 (3), 394–397.
Matoba, M., et al., 2007. Lung carcinoma: diffusion-weighted MR imaging – preliminary evaluation with apparent diffusion coefficient. Radiology 243 (2), 570–577.
Matsuki, M., et al., 2007a. Diffusion-weighed MR imaging of pancreatic carcinoma. Abdominal Imaging 32 (4), 481–483.
Matsuki, M., et al., 2007b. Diffusion-weighted MR imaging for urinary bladder carcinoma: initial results. European Radiology 17 (1), 201–204.
McDannold, N., Moss, M., Killiany, R., et al., 2003. MRI-guided focused ultrasound surgery in the brain: tests in a primate model. Magnetic Resonance in Medicine 49 (6), 1188–1191.
McDermott, G.M., Welch, A., Staff, R.T., et al., 2007. Monitoring primary breast cancer throughout chemotherapy using FDG-PET. Breast Cancer Research and Treatment 102, 75–84.
McGee, K.P., Hubmayr, R.D., Ehman, R.L., 2007. MR elastography of the lung with hyperpolarized ^{3}He. Magnetic Resonance in Medicine 59 (1), 14–18.
McKnight, A.L., et al., 2002. MR elastography of breast cancer: preliminary results. AJR American Journal of Roentgenology 178, 1411–1417.
Melodelima, D., et al., 2006. Using intraluminal ultrasound for the treatment of esophageal tumors: first clinical results. Ultrasonics Symposium 2006 IEEE, 740–743.
Mercadante, S., et al., 2002. CT-guided neurolytic splanchnic nerve block by an anterior approach. Journal of Pain and Symptom Management 23 (4), 268–270.
Meyer, B., et al., 2007. Contrast-enhanced abdominal angiographic CT for intra-abdominal tumor embolization: a new tool for vessel and soft tissue visualization. Cardiovascular and Interventional Radiology 30, 743–749.
Miller, J.C., Pien, H.H., Sahani, D., Sorensen, A.G., Thrall, J.H., 2005. Imaging angiogenesis: applications and potential for drug development. Journal of the National Cancer Institute 97, 172–187.
Minami, K., 2001. Computerized characterization of contrast enhancement patterns for classifying pulmonary nodules. Proceedings of 2001 International Conference on Image Processing vol. 2, 897–900.
Min-Ho, Lee, Nammalvar, V., Gobin, A., Barton, J., West, J., Drezek, R., 2006. Nanoshells as contrast agents for scatter-based optical imaging. In: 3rd IEEE International Symposium on Biomedical Imaging: Nano to Macro, pp. 371–374.
Mintun, M.A., Welch, M.J., Siegel, B.A., et al., 1988. Breast cancer: PET imaging of estrogen receptors. Radiology 169, 45–48.
Miyanaga, N., Akaza, H., Yamakawa, M., Oikawa, T., Sekido, N., Hinotsu, S., Kawai, K., Shimazui, T., Shiina, T., 2006. Tissue

elasticity imaging for diagnosis of prostate cancer: a preliminary report. International Journal of Urology 13 (12), 1514–1518.
Moehler, M., Dimitrakopoulou-Strauss, A., Gutzler, F., et al., 1998. ^{18}F-labeled fluorouracil positron emission tomography and the prognoses of colorectal carcinoma patients with metastases to the liver treated with 5-fluorouracil. Cancer 83, 245–253.
Moffat, B.A., et al., 2005. Functional diffusion map: a noninvasive MRI biomarker for early stratification of clinical brain tumor response. Proceedings of the National Academy of Sciences USA 102, 5524–5529.
Morris, E., 2006. Breast cancer. In: Edelman, R., Hesselink, J., Zlatkin, M. (Eds.), Clinical Magnetic Resonance Imaging. Elsevier Publishing, Philadelphia, PA, pp. 2426–2454.
Mulder, W.J.M., et al., 2006. Quantum dots with a paramagnetic coating as a bimodal molecular imaging probe. Nano Letters 6, 1–6.
Murakami, Y., et al., 2004. ^{18}F labeled annexin V: a PET tracer for apoptosis imaging. European Journal of Nuclear Medicine and Molecular Imaging 31 (4), 469–474.
Muthupillai, R., Lomas, D.J., Rossman, P.J., Greenleaf, J.F., Manduca, A., Ehman, R.L., 1995. Magnetic resonance elastography by direct visualization of propagating acoustic strain waves. Science 269, 1854–1857.
Narayan, P., et al., 1995. The role of transrectal ultrasound-guided based-staging, preoperative prostate serum antigen, and biopsy Gleason score in prediction of final pathologic diagnosis of prostate cancer. Urology 46 (2), 205–212.
Nelson, E.D., Slotoroff, C.B., Gomella, L.G., Halpern, E.J., 2007. Targeted biopsy of the prostate: the impact of color Doppler imaging and elastography on prostate cancer detection and Gleason score. Urology 70 (6), 1136–1140.
Nelson, J.L., Roeder, B.L., Carmen, J.C., Roloff, F., Pitt, W.G., 2002. Ultrasonically activated chemotherapeutic drug delivery in a rat model. Cancer Research 62, 7280–7283.
Nelson, S.J., et al., 1997. Volume MRI and MRSI techniques for the quantitation of treatment response in brain tumors: presentation of a detailed case study. Journal of Magnetic Resonance Imaging 7 1164–1152.
Neuwalt, E.A., et al., 2004. Imaging of iron oxide nanoparticles with MR and light microscopy in patients with malignant brain tumors. Neuropathology and Applied Neurobiology 5, 456–471.
Neves, A.A., Brindle, K.M., 2006. Assessing responses to cancer therapy using molecular imaging. Biochimica Biophysica Acta 1766, 242–261.
Ning, R., et al., 2006. In: Flynn, M.J., Hsieh, J. (Eds.), Medical Imaging 2006: Physics of Medical Imaging. Proceedings of the SPIE, vol. 6142, pp. 348–356.
Nomori, H., et al., 2005. ^{11}C-acetate positron emission tomography imaging for lung adenocarcinoma 1 to 3 cm in size with ground-glass opacity images on computed tomography. Annals of Thoracic Surgery 80, 2020–2025.
Ntziachristos, V., Yodh, A.G., Schnall, M.D., Chance, B., 2002. MRI-guided diffuse optical spectroscopy of malignant and benign breast lesions. Neoplasia 4 (4), 347–354.
Nunes, L.W., 2001. Architectural-based interpretations of breast MR imaging. Magnetic Resonance Imaging Clinics of North America 9 (2), 303–320.
O'Connor, M.K., Phillips, S.W., Hruska, C.B., et al., 2007. Molecular breast imaging: advantages and limitations of a scintimammographic technique in patients with small breast tumors. Breast Journal 13 (1), 3–11.
Ohtani, T., Kurihara, H., Ishiuchi, S., Saito, N., Oriuchi, N., Inoue, T., Sasaki, T., 2001. Brain tumour imaging with carbon-11 choline: comparison with FDG PET and gadolinium-enhanced MR imaging. European Journal of Nuclear Medicine 28, 1664–1670.
Okada, A., Murakami, T., Mikami, K., Onishi, H., Tanigawa, N., Marukawa, T., 2006. Nakamura H. A case of hepatocellular carcinoma treated by MR guided focused ultrasound ablation with respiratory gating. Magnetic Resonance in Medical Sciences 5 (3), 167–171.
Oraevsky, A.A., et al., 2002. Optoacoustic imaging of blood for visualization and diagnostics of breast cancer. Proc. SPIE 4618, 81–94.
Oyama, N., Miller, T.R., Dehdashti, F., Siegel, B.A., Fischer, K.C., Michalski, J.M., Kibel, A.S., Andriole, G.L., Picus, J., Welch, M.J., 2003. ^{11}C-acetate PET imaging of prostate cancer: detection of recurrent disease at PSA relapse. Journal of Nuclear Medicine 44 (4), 549–555.
Paajanen, H., 2006. Increasing use of mammography improves the outcome of breast cancer in Finland. The Breast Journal 12 (1), 88–90.
Padhani, A.R., Leach, M.O., 2005. Antivascular cancer treatments: functional assessments by dynamic contrast enhanced MRI. Abdominal Imaging 30, 324–341.
Padhani, A.R., et al., 2000a. . Changes in tumour vascular permeability with antiangiogenesis therapy: observations on histogram analysis. In: Proceedings of the Eighth International Society of Magnetic Resonance in Medicine, April 3–7, 2000. Denver. ISMRM, Berkeley, CA 108.
Padhani, A.R., et al., 2000b. Response of breast carcinoma to chemotherapy: MR permeability changes using histogram analysis. In: Proceedings of the Eighth International Society of Magnetic Resonance in Medicine, April 3–7, 2000. Denver. ISMRM, Berkeley, CA, p. 2160.
Paganelli, G., et al., 2007. IART®: Intraoperative avidination for radionuclide treatment. A new way of partial breast irradiation. The Breast 16, 17–26.
Paliwal, S., Sundaram, J., Mitragotri, S., 2005. Induction of cancer-specific cytotoxicity towards human prostate and skin cells using quercetin and ultrasound. British Journal of Cancer 92 (3), 499–502.
Pallwein, L., Mitterberger, M., Struve, P., Pinggera, G., Horninger, W., Bartsch, G., Aigner, F., Lorenz, A., Pedross, F., Frauscher, F., 2007. Real-time elastography for detecting prostate cancer: preliminary experience. BJU International 100 (1), 42–46.
Palmeri, M., et al., 2004. Acoustic radiation force impulse (ARFI) imaging of the gastrointestinal tract. Ultrasonics Symposium 2004 IEEE vol. 1, 744–747.
Pappo, I., Horne, T., Weissberg, D., Wasserman, I., Orda, R., 2000. The usefulness of MIBI scanning to detect underlying carcinoma in women with acute mastitis. Breast Journal 6, 126–129.
Passchier, J., Lawrie, K., Bender, D., Fellows, I., Gee, A., 2003. [^{11}C]Loperamide as highly sensitive PETprobe for measuring changes in P-glycoprotein functional. Journal of Labelled Compounds and Radiopharmaceuticals 46, S403.
Pech, M., et al., 2004. Synchronous CT-guided brachytherapy in patients at risk for incomplete interstitial laser ablation of liver malignancies. Medical Laser Application 19 (2), 78–32.
Pham, C., Roberts, T., van Bruggen, N., Melnyk, O., Mann, J., Ferrara, N., et al., 1998. Magnetic resonance imaging detects suppression of tumor vascular permeability after administration of antibody to vascular endothelial growth factor. Cancer Investigation 16, 225–230.
Piao, D., et al., 2007. Near-infrared optical tomography: endoscopic imaging approach. Proc. SPIE 6431 643103–1-643103-10.
Pierce, D.A., Shimizu, Y., Preston, D.L., et al., 1996. Studies of the mortality of atomic bomb survivors: report 12, Part 1 – Cancer: 1950–1990. Radiation Research 146, 1–27.

Pineda, A.R., et al., 2006. Optimization of a tomosynthesis system for the detection of lung nodules. Medical Physics 33 (5), 1372–1379.
Pisano, E.D., et al., 2005. Digital Mammographic Imaging Screening Trial (DMIST) investigators group. Diagnostic performance of digital versus film mammography for breast-cancer screening. New England Journal of Medicine 353 (17), 1773–1783.
Plewes, D.B., Bishop, J., Samani, A., Sciarretta, J., 2000. Visualization and quantification of breast cancer biomechanical properties with magnetic resonance elastography. Physics in Medicine and Biology 45, 1591–1610.
Pogue, B.W., Poplack, S.P., McBride, T.O., Wells, W.A., Osterman, K.S., Osterberg, U.L., Paulsen, K.D., 2001. Quantitative hemoglobin tomography with diffuse near-infrared spectroscopy: pilot results in the breast. Radiology 218, 261–266.
Poplack, S.P., et al., 2004. Electromagnetic breast imaging: average tissue property values in women with negative clinical findings. Radiology 231 (2), 571–580.
Poplack, S.P., et al., 2007. Electromagnetic breast imaging: results of a pilot study in women with abnormal mammograms. Radiology 243 (2), 350–359.
Provenzale, J.M., Wang, G.R., Brenner, T., Petrella, J.R., Sorensen, A.G., 2002. Comparison of permeability in high-grade and low-grade brain tumors using dynamic susceptibility contrast MRI. AJR American Journal of Roentgenology 178, 711–716.
Provenzale, J.M., Mukundan, S., Barboriak, D., 2006. Diffusion-weighted and perfusion MR imaging for brain tumor characterization and assessment of treatment response. Radiology 239, 632–649.
Rabin, O., Manuel Perez, J., Grimm, J., et al., 2006. An X-ray computed tomography imaging agent based on long-circulating bismuth sulphide nanoparticles. Nature Materials 5, 118–122.
Rafferty, A.E., 2007. Digital mammography: novel applications. Radiologic Clinics of North America 45 (5), 831–843.
Rago, T., et al., 2007. Elastography: new developments in ultrasound for predicting malignancy in thyroid nodules. Journal of Clinical Endocrinology & Metabolism 92 (8), 2917–2922.
Rajendran, J.G., et al., 2006. Hypoxia imaging-directed radiation treatment planning. European Journal of Nuclear Medicine and Molecular Imaging 33 (Suppl. 1), 44–53.
Rallan, D., Dickson, M., Bush, N.L., Harland, C.C., Mortimer, P., Bamber, J.C., 2006. High-resolution ultrasound reflex transmission imaging and digital photography: potential tools for the quantitative assessment of pigmented lesions. Skin Research and Technology 12 (1), 50–59.
Rapoport, N.Y., Christensen, D.A., Fain, H.D., Barrows, L., Gao, Z., 2004. Ultrasound-triggered drug targeting of tumors in vitro and in vivo. Ultrasonics 42, 943–950.
Rapoport, N., et al., 2007. Multifunctional nanoparticles for combining ultrasonic tumor imaging and targeted chemotherapy. Journal of the National Cancer Institute 99 (14), 1095–1106.
Raylman, R.R., et al., 2008. The positron emission mammography/tomography breast imaging and biopsy system (PEM/PET): design, construction and phantom-based measurements. Physics in Medicine and Biology 53, 637–653.
Reeves, A.P., 2007. The Lung Image Database Consortium (LIDC): a comparison of different size metrics for pulmonary nodule measurements. Academic Radiology 14 (12), 1475–1485.
Rhodes, D.J., O'Connor, M.K., Phillips, S.W., et al., 2005. Molecular breast imaging: a new technique using technetium Tc 99m scintimammography to detect small tumors of the breast. Mayo Clinic Proceedings 80 (1), 24–30.
Ricke, J., et al., 2004. CT-guided interstitial brachytherapy of liver malignancies alone or in combination with thermal ablation: phase I–II results of a novel technique. International Journal of Radiation Oncology Biology Physics 58 (5), 1496–1505.
Rinneberg, H., et al., 2005. Scanning time-domain optical mammography: detection and characterization of breast tumors in vivo. Technology in Cancer Research & Treatment 4 (5), 483–496.
Rizk, N., Downey, R.J., Akhurst, T., et al., 2006. Preoperative [^{18}F]-fluorodeoxyglucose positron emission tomography standardized uptake values predict survival after esophageal adenocarcinoma resection. Annals of Thoracic Surgery 81, 1076–1081.
Ro, R.J., et al., 2006. Assessing angiogenesis in murine glioma and breast tumor models with contrast enhanced ultrasound imaging. Ultrasonics Symposium 2006 IEEE, 416–419.
Robbins, R.J., Wan, Q., Grewal, R.K., et al., 2006. Real-time prognosis for metastatic thyroid carcinoma based on 2-[^{18}F]fluoro-2-deoxy-D-glucose-positron emission tomography scanning. Journal of Clinical Endocrinology and Metabolism 91, 498–505.
Robinson, M.K., et al., 2005. Quantitative immuno-positron emission tomography imaging of HER2-positive tumor xenografts with an iodine-124 labeled anti-HER2 diabody. Cancer Research 65 (4), 1471–1478.
Rogers, W.J., Meyer, C.H., Kramer, C.M., 2006. Technology insight: in vivo cell tracking by use of MRI. Nature Clinical Practice. Cardiovascular Medicine 3 (10), 554–562.
Ross, R.J., Thompson, J.S., Kim, K., Bailey, R.A., 1982. Nuclear magnetic resonance imaging and evaluation of human breast tissue: preliminary clinical trials. Radiology 143, 195–205.
Rossi, C.R., et al., 2006. The impact of lymphoscintigraphy technique on the outcome of sentinel node biopsy in 1,313 patients with cutaneous melanoma: an Italian multicentric study (SOLISM-IMI). Journal of Nuclear Medicine 47, 234–241.
Rousseau, C., Devillers, A., Sagan, C., et al., 2006. Monitoring of early response to neoadjuvant chemotherapy in stage II and III breast cancer by [^{18}F]fluorodeoxyglucose positron emission tomography. Journal of Clinical Oncology 24, 5366–5372.
Săftoiu, A., Vilman, P., 2006. Endoscopic ultrasound elastography – a new imaging technique for the visualization of tissue elasticity distribution. Journal of Gastrointestinal and Liver Diseases 15 (2), 161–165.
Salomir, R., et al., 2006. Image-based control of the magnetic resonance imaging-guided focused ultrasound thermotherapy. Topics in Magnetic Resonance Imaging 17 (3), 139–151.
Samei, E., et al., 2007. Multiprojection correlation imaging for improved detection of pulmonary nodules. AJR American Journal of Roentgenology 188, 1239–1245.
Sampalis, F.S., Denis, R., Picard, D., et al., 2003. International prospective evaluation of scintimammography with technetium sestamibi. American Journal of Surgery 185, 544–549.
Sandblom, G., et al., 2006. Positron emission tomography with C11-acetate for tumor detection and localization in patients with prostate-specific antigen relapse after radical prostatectomy. Urology 67 (5), 996–1000.
Sarapa, N., Hsyu, P.-H., Lappin, G., Garner, R.C., 2005. The application of accelerator mass spectrometry to absolute bioavailability studies in humans: simultaneous administration of an intravenous microdose of ^{14}C-Nelfinavir mesylate solution and oral Nelfinavir to healthy volunteers. Journal of Clinical Pharmacology 45, 1198–1205.
Sarkeala, T., et al., 2008. Breast cancer mortality with varying invitational policies in organised mammography. British Journal of Cancer 98, 641–645.
Schellenberger, E.A., et al., 2002. Annexin V-CLIO: a nanoparticle for detecting apoptosis by MRI. Molecular Imaging 1, 102–107.

Schoder, H., Noy, A., Gonen, M., et al., 2005. Intensity of 18-F fluorodeoxyglucose uptake in positron emission tomography distinguishes between indolent and aggressive non-Hodgkin's lymphoma. Journal of Clinical Oncology 23, 4643–4651.

Scholz, M., et al., 2005. Vibrography during tumor neurosurgery. Journal of Ultrasound in Medicine 24, 985–992.

Shah, S.K., 2005. Computer aided characterization of the solitary pulmonary nodule using volumetric and contrast enhancement features. Academic Radiology 12 (10), 1310–1319.

Shim, S.S., Lee, K.S., Kim, B., Lee, E.J., Choi, J.Y., Chung, M.J., 2004. Accuracy of integrated PET/CT using fluorodeoxyglucose in preoperative staging on non-small cell lung cancer: a prospective comparison with standalone CT. Radiology 233, 383. abstract SSE04-02.

Shulkin, B.L., Wienland, D.M., Shapiro, B., Sisson, J.C., 1995. PET epinephrine studies of pheochromocytoma. Journal of Nuclear Medicine 36, 229P.

Shulkin, B.L., et al., 1998. Current concepts on the diagnostic use of MIBG in children. Journal of Nuclear Medicine 39, 679–688.

Silverman, S.G., et al., 2000. MR imaging-guided percutaneous cryotherapy of liver tumors: initial experience. Radiology 217, 657–664.

Simon, C., Dupuy, D., 2006. Percutaneous minimally invasive therapies in the treatment of bone tumors: thermal ablation. Seminars in Musculoskeletal Radiology 10, 137–144.

Sinkus, R., Lorenzen, J., Schrader, D., Lorenzen, M., Dargatz, M., Holz, D., 2000. High-resolution tensor MR elastography for breast tumour detection. Physics in Medicine and Biology 45, 1649–1664.

Slovis, T.L., 2002. Conference on the ALARA (as low as reasonably achievable) concept in pediatric CT: intelligent dose reduction. Pediatric Radiology 32, 217–218.

Smith, J.J., Sorensen, A.G., Thrall, J.H., 2003. Biomarkers in imaging: realizing radiology's future. Radiology 227 (3), 633–638.

Sorger, D., Patt, M., Kumar, P., et al., 2003. [^{18}F]fluoroazomycinarabinofuranoside (^{18}FAZA) and [^{18}F]fluoromisonidazole (^{18}FMISO): a comparative study of their selective uptake in hypoxic cells and PET imaging in experimental rat tumors. Nuclear Medicine and Biology 30, 317–326.

Souvatzoglou, M., Grosu, A.L., Roper, B., et al., 2007. Tumour hypoxia imaging with[(18)F]FAZA PET in head and neck cancer patients: a pilot study. European Journal of Nuclear Medicine Molecular Imaging 34, 1566–1575.

Srinivas, P.R., Barker, P., Srivastava, S., 2002. Nanotechnology in early detection of cancer Laboratory Investigation 82, 657–662.

Stadnik, T., et al., 2006. Breast imaging. Preoperative breast cancer staging: comparison of USPIO- enhanced MR imaging and ^{18}F-fluorodeoxyglucose (FDG) positron emission tomography (PET) imaging for axillary lymph node staging – initial findings. European Radiology 16 (10), 2153–2160.

Stattaus, J., et al., 2007. CT guided biopsy of small liver lesions: visibility, artifacts and corresponding diagnostic accuracy. Cardiovascular and Interventional Radiology 30 (5), 928–935.

Steffen, A.C., Wikman, M., Tolmachev, V., et al., 2005. In vitro characterization of a bivalent anti-HER-2 affibody with potential for radionuclide-based diagnostics. Cancer Biotherapy & Radiopharmaceuticals 20, 239–248.

Stroobants, S., et al., 2003. (18)FDG-Positron emission tomography for the early prediction of response in advanced soft tissue sarcoma treated with imatinib mesylate (Glivec). European Journal of Cancer 39, 2012–2020.

Su, H., Bodenstein, C., Dumont, R., et al., 2006. Monitoring tumor glucose utilization by positron emission tomography for the prediction of treatment response to epidermal growth factor receptor kinase inhibitors. Clinical Cancer Research 12, 5659–5667.

Su, M.Y., et al., 1998. Tumor characterization with dynamic contrast-enhanced MRI using MR contrast agents of various molecular weights. Magnetic Resonance in Medicine 39 (2), 259–269.

Su, M.-Y., Taylor, J.A., Villarreal, L.P., Nalcioglu, O., 2000. Prediction of gene therapy-induced tumor size changes by the vascularity changes measured using dynamic contrast-enhanced MRI. Magnetic Resonance Imaging 18, 311–317.

Suh, Y., Weiss, E., Keall, P., 2007. A deliverable 4D IMRT planning method for DMLC tumor tracking delivery. International Journal of Radiation Oncology Biology Physics 69 (3), S190–S191.

Sun, H., et al., 2005. Imaging DNA synthesis with [^{18}F]FMAU and positron emission tomography in patients with cancer. European Journal of Nuclear Medicine Molecular Imaging 32 (1), 15–22.

Sundaresan, G., Yazaki, P.J., Shively, J.E., et al., 2003. ^{124}I-labeled engineered anti-CEA minibodies and diabodies allow high-contrast, antigen-specific small-animal PET imaging of xenografts in athymic mice. Journal of Nuclear Medicine 44, 1962–1969.

Suyash, K., et al., 2008. Percutaneous computed tomography-guided core biopsy for the diagnosis of mediastinal masses. Annals of Thoracic Medicine 3 (1), 13–17.

Suzuki, K., Li, F., Sone, S., Doi, K., 2005. Computer-aided diagnostic scheme for distinction between benign and malignant nodules in thoracic low-dose CT by use of massive training artificial neural network. Medical Imaging 24 (9), 1138–1150.

Sweeney, K.J., Sacchini, V., 2007. Is there a role for magnetic resonance imaging in a population-based breast cancer screening program? Breast Journal 13 (6), 543–544.

Swensen, S.J., 2000. Functional CT: Lung nodule evaluation. RadioGraphics 20, 1178–1181.

Swensen, S.J., et al., 2003. Lung cancer screening with CT: Mayo Clinic experience. Radiology 226 (3), 756–761.

Tachibana, K., et al., 2000. Enhanced cytotoxic effect of Ara-C by low intensity ultrasound to HL-60 cells. Cancer Letters 149, 189–194.

Takano, A., Kusuhara, H., Suhara, T., et al., 2006. Evaluation of in vivo P-glycoprotein function at the blood–brain barrier among MDR1 gene polymorphisms by using ^{11}C-verapamil. Journal of Nuclear Medicine 47, 1427–1433.

Takayoshi, U., et al., 2007. Dynamic contrast enhanced screening of microcalcifications in the breast. Is there any value? Breast Cancer Research and Treatment 103 (3), 269–281.

Tam, A., Ahra, K., 2007. Palliative interventions for pain in cancer patients. Seminars in Interventional Radiology 24 (4), 419–429.

Tardivon, A.A., Ollivier, L., El Khoury, C., Thibault, F., 2006. Monitoring therapeutic efficacy in breast carcinomas. European Radiology 16, 2549–2558.

Tata, D.B., et al., 1997. Selective clinical ultrasound signals mediate differential gene transfer and expression in two human prostate cancer cell lines: LnCap and PC-3. Biochemical and Biophysical Research Communications 234 (1), 64–67.

Tatum JL, Hoffman JM. Congressional update-report from the biomedical imaging program of the National Cancer Institute—imaging drug development. Academic Radiology 7: 1007-1008 (2000).

Taylor, S., et al., 2008. CT colonography: investigation of the optimum reader paradigm by using computer-aided detection software. Radiology 246 (2), 463–471.

Tedeschi, G., et al., 1997. Increased choline signal corresponding to malignant degeneration of cerebral gliomas: a serial proton magnetic resonance spectroscopy imaging study. Journal of Neurosurgery 87, 516–524.

Teeuwisse, W.M., et al., 2001. Patient and staff dosage during CT guided biopsy, drainage and coagulation. British Journal of Radiology 74 (884), 720.

Therasse, P., Arbuck, S.G., Eisenhauer, E.A., Wanders, J., Kaplan, R.S., Rubinstein, L., Verweij, J., Van Glabbeke, M., van Oosterom, A.T., Christian, M.C., Gwyther, S.G., 2000. New guidelines to evaluate the response to treatment in solid tumors. Journal of the National Cancer Institute 92 (3), 205–216.

Thorwarth, D., Eschmann, S.M., Paulsen, F., et al., 2005. A kinetic model for dynamic [^{18}F]-FMISO PET data to analyse tumour hypoxia. Physics in Medicine and Biology 50, 2209–2224.

Tillmann, L., et al., 2004. Transrectal ultrasound guided biopsy of the prostate: random sextant versus biopsies of sono-morphologically suspicious lesions. World Journal of Urology 22 (5), 357–360.

Trampal, C., et al., 2004. Pheochromocytomas detection hydroxyephedrine PET with ^{11}C. Radiology 230 (2), 423–428.

Tromberg, B.J., et al., 2000. Noninvasive in vivo characterization of breast tumors using photon migration spectroscopy. Neoplasia 2, 26–40.

Tromberg, B.J., et al., 1997. Non-invasive measurements of breast tissue optical properties using frequency-domain photon migration. Philosophical Transactions of the Royal Society of London B 352, 661–668.

Tsutsumi, M., Miyagawa, T., Matsumura, T., Kawazoe, N., Ishikawa, S., Shimokama, T., Shiina, T., Miyanaga, N., Akaza, H., 2007. The impact of real-time tissue elasticity imaging (elastography) on the detection of prostate cancer: clinicopathological analysis. International Journal of Clinical Oncology 12 (4), 250–255.

Turetschek, K., Preda, A., Floyd, E., et al., 2003. MRI monitoring of tumor response following angiogenesis inhibition in an experimental human breast cancer model. European Journal of Nuclear Medicine and Molecular Imaging 30, 448–455.

US Food and Drug Administration, 2006. Guidance for Industry, Investigators, and Reviewers. Exploratory IND Studies. Center for Drug Evaluation and Research. US Department of Health and Human Services, Washington, DC, 1–16.

van der Ploeg, I.M.C., et al., 2007. The additional value of SPECT/CT in lymphatic mapping in breast cancer and melanoma. Journal of Nuclear Medicine 48 (11), 1756–1760.

van Wamel, A., Bouakaz, A., Bernard, B., ten Cate, F., de Jong, N., 2004. Radionuclide tumour therapy with ultrasound contrast microbubbles. Ultrasonics 42, 903–906.

Velikyan, I., Beyer, G.J., Langstrom, B., 2004. Microwave-supported preparation of ^{68}Ga bioconjugates with high specific radioactivity. Bioconjugate Chemistry 15, 554–560.

Vielvoye-Kerkmeer, A.P.E., 2002. CT guided neurolytic splanchnic nerve block. Journal of Pain and Symptom Management 24 (5), 455.

Virmani, S., et al., 2007. Effect of C-arm angiographic CT on transcatheter arterial chemoembolization of liver tumors. Journal of Vascular and Interventional Radiology 18 (10), 1305–1309.

Vogl, T.J., 2007. Prostate cancer: MR imaging-guided galvanotherapy – technical development and first clinical results. Radiology 245 (3), 895–902.

Volterrani, L., et al., 2006. Three-dimensional analysis of pulmonary nodules by MSCT with Advanced Lung Analysis (ALA1) software. La Radiologia medica 111 (3), 343–354.

von Rahden, B., Sarbia, M., Stein, H., 2006. Combined FDG-PET/CT and CT-guided biopsy in diagnosing oesophageal cancer recurrence. Journal of the New Zealand Medical Association 119, 1228.

Vormola, R., et al., 2007. Correlation of ^{11}C-choline PET and PSA values in patients with prostate cancer and biochemical relapse after primary treatments. 2007 ASCO Annual Meeting Proceedings. Journal of Clinical Oncology 25 (18S), 5073.

Wadsak, W., et al., 2006. [^{18}F]FETO for adrenocortical PET imaging: a pilot study in healthy volunteers. European Journal of Nuclear Medicine and Molecular Imaging 33 (6), 669–672.

Wald, L.L., et al., 1997. Serial proton magnetic resonance spectroscopy imaging of glioblastoma multiforme after brachytherapy. Journal of Neurosurgery 87, 525–534.

Wallace, M.J., 2007. C-arm computed tomography for guiding hepatic vascular intervention. Techniques in Vascular and Interventional Radiology 10 (1), 79–86.

Wallace, M.J., et al., 2007. Impact of C-arm CT on hepatic arterial interventions for hepatic malignancies. Journal of Vascular and Interventional Radiology 18 (12), 1500–1507.

Wang, L.V., Wu, H.I., 2007. Biomedical Optics. Wiley-Interscience.

Weichert, J., et al., 2005. Radioiodinated NM404 – a universal tumor imaging agent? Academic Radiology 12 (5), S58–S59.

Weller, G.E.R., et al., 2005. Ultrasonic imaging of tumor angiogenesis using contrast microbubbles targeted via the tumor-binding peptide arginine-arginine-leucine. Cancer Research 65, 533–539.

Wells, P., West, C., Jones, T., et al., 2004. Measuring tumor pharmacodynamic response using PET proliferation probes: the case for 2-[(11)C]-thymidine. Biochimica Biophysica Acta 1705, 91–102.

Wheatley, M.A., Forsberg, F., Dube, N., Patel, M., Oeffinger, B.E., 2006. Surfactant-stabilized contrast agent on the nanoscale for diagnostic ultrasound imaging. Ultrasound in Medicine & Biology 32, 83–93.

Wieder, H.A., et al., 2007. Prediction of tumor response by FDG-PET: comparison of the accuracy of single and sequential studies in patients with adenocarcinomas of the esophagogastric junction. European Journal of Nuclear Medicine and Molecular Imaging 34 (12), 1925–1932.

Wiegel T. ^{11}C-choline PET-CT for diagnosis of local recurrence following PSA increase after radical prostatectomy: implications for radiotherapy. ASCO 2007 Prostate Cancer Symposium, abstract 178.

Willemsen, A.T., van-Waarde, A., Paans, A.M., et al., 1995. In vivo protein synthesis rate determination in primary or recurrent brain tumors using L-[1-^{11}C]-tyrosine and PET. Journal of Nuclear Medicine 36, 411–419.

Williams, D.B., et al., 1999. Endoscopic ultrasound guided fine needle aspiration biopsy: a large single centre experience. Gut 44, 720–726.

Win, Z., et al., 2007. ^{68}Ga-DOTATATE PET in neuroectodermal tumours: first experience. Nuclear Medicine Communications 28 (5), 359–363.

Wong, C.Y., Schmidt, J., Bong, J.S., et al., 2007. Correlating metabolic and anatomic responses of primary lung cancers to radiotherapy by combined F-18 FDG PET-CT imaging. Radiation Oncology 2, 18.

Wong SH, et al. Capacitive micromachined ultrasonic transducers for high intensity focused ablation of upper abdominal tumors. Ultrasonics Symposium 2006 IEEE, pp. 841–844 (2006).

Wong, T.Z., et al., 2005. ProstaScint (capromab pendetide) imaging using hybrid gamma camera-CT technology. AJR American Journal of Roentgenology 184 (2), 676–680.

Wu, A.M., Yazaki, P.J., Tsai, S., et al., 2000. High-resolution microPET imaging of carcinoembryonic antigen-positive xenografts by using a copper-64-labeled engineered antibody fragment. Proceedings of the National Academy of Sciences USA 97, 8495–8500.

Wu, F., et al., 2007. Expression of tumor antigens and heat-shock protein 70 in breast cancer cells after high-intensity focused ultrasound ablation. Annals of Surgical Oncology 14, 1237–1242.

Tian, Xiaobing, et al., 2004. External imaging of CCND1 cancer gene activity in experimental human breast cancer xenografts

with ^{99m}Tc-peptide-peptide nucleic acid-peptide chimeras. Journal of Nuclear Medicine 45, 2070–2082.
Xiong, T., et al., 2005. Incidental lesions found on CT colonography: their nature and frequency. British Journal of Radiology 78, 22–29.
Xu, M., Wang, L.V., 2006. Photoacoustic imaging in biomedicine. Review of Scientific Instruments 77 (041101).
Xu, Y., Wang, L.V., 2006. Rhesus monkey brain imaging through intact skull with thermoacoustic tomography. IEEE Transactions on Ultrasonics. Ferroelectrics and Frequency Control 53, 542–548.
Xydeas, T., et al., 2005. Magnetic resonance elastography of the breast: correlation of signal intensity data with viscoelastic properties. Rofo 40 (7), 412–420.
Yagle, K.J., Eary, J.F., Tait, J.F., et al., 2005. Evaluation of ^{18}F-annexin V as a PET imaging agent in an animal model of apoptosis. Journal of Nuclear Medicine 46, 658–666.
Yamagami, T., et al., 2002. Management of pneumothorax after percutaneous CT-guided lung biopsy. Chest 121, 1159–1164.
Yao, Y.F., et al., 2007. Immunoscintigraphy of local recurrent rectal cancer with ^{99m}Tc- labeled anti-CEA monoclonal antibody CL58. World Journal of Gastroenterology 13 (12), 1841–1846.
Ye, G., et al., 2006. A 3D EIT system for breast cancer imaging. In: 3rd IEEE International Symposium on Biomedical Imaging: Nano to Macro, pp. 1092–1095.
Yee, J., et al., 2001. Colorectal neoplasia: performance characteristics of CT colonography for detection in 300 patients. Radiology 219 (3), 685–692.
Yeung, D.K.W., et al., 2002. Breast cancer: in vivo proton MR spectroscopy in the characterization of histopathologic subtypes and preliminary observations in axillary node metastases. Radiology 225, 190–197.
Yu, T., Huang, X., Hu, K., Bai, J., Wang, Z., 2004. Treatment of transplanted adriamycin-resistant ovarian cancers in mice by combination of adriamycin and ultrasound exposure. Ultrasonics Sonochemistry 11, 287–291.
Yuan, H., et al., 2006. Intertumoral differences in hypoxia selectivity of the PET imaging agent ^{64}Cu(II)-diacetyl-bis(N^4-methylthiosemicarbazone). Journal of Nuclear Medicine 47 (6), 989–998.
Yuan, L., et al., 2007. Preliminary assessment of one-dimensional MR elastography for use in monitoring focused ultrasound therapy. Physics in Medicine and Biology 52 (19), 5909–5919.
Zagoria, R.J., Hawkins, A.D., Clark, P.E., et al., 2004. Percutaneous CT-guided radiofrequency ablation of renal neoplasms: factors influencing success. AJR American Journal of Roentgenology 183, 201–207.
Zaidi, H., Alavi, A., 2007. Current trends in PET and combined (PET/CT and PET/MR) systems design. PET Clinics 2, 109–123.
Zeisel, S.H., 1993. Choline phospholipids: signal transduction and carcinogenesis. FASEB J 7, 551–557.
Zhang, E., Laufer, J., Beard, P., 2008. Backward-mode multiwavelength photoacoustic scanner using a planar Fabry–Perot polymer film ultrasound sensor for high- resolution three-dimensional imaging of biological tissues. Applied Optics 47 (4), 561–577.
Zhang, H.F., et al., 2006. In vivo volumetric imaging of subcutaneous microvasculature by photoacoustic microscopy. Optics Express 14 (20), 9317–9322.
Zhang, X., Cheng, X., 2007. Preparation and characterization of ^{99m}Tc(CO)$_3$-BPy-RGD complex as $\alpha_v\beta_3$ integrin receptor-targeted imaging agent. Applied Radiation and Isotopes 65 (1), 70–78.
Zhang, X., et al., 2006a. PET imaging of cerebral astrocytoma with ^{13}N-ammonia. Journal of Neuro-Oncology 78 (2), 145–151.
Zhang, X., et al., 2006b. Quantitative PET imaging of tumor integrin $\alpha_v\beta_3$ expression with^{18}F-FRGD2. Journal of Nuclear Medicine 47 (1), 113–120.
Zhang, X., Chen, W., 2007. Differentiation of recurrent astrocytoma from radiation necrosis: a pilot study with ^{13}N-NH_3 PET. Journal of Neurooncology 82, 305–311.
Zhao, M., Beauregard, D.A., Loizou, L., Davletov, B., Brindle, K.M., 2001. Non-invasive detection of apoptosis using magnetic resonance imaging and a targeted contrast agent. Nature Medicine 7, 1241–1244.
Zhi, H., et al., 2007. Comparison of ultrasound elastography, mammography, and sonography in the diagnosis of solid breast lesions. Journal of Ultrasound in Medicine 26, 807–815.
Zippel, D.B., Papa, M.Z., 2005. The use of MR imaging guided focused ultrasound in breast cancer patients: a preliminary phase one study and review. Breast Cancer 12, 32–38.
Zudaire, I., et al., 2008. Molecular characterization of small peripheral lung tumors based on the analysis of fine needle aspirates. Histology and Histopathology 23 (1), 33–40.